Spring 5-17-2010

Mechanical Stiffness and Dissipation in Ultrananocrystalline Diamond Films

Vivek P. Adiga
University of Pennsylvania, adiga@seas.upenn.edu

Mechanical Stiffness and Dissipation in Ultrananocrystalline Diamond Films

Abstract
Tetragonal sp3-bonded diamond has the highest known atomic density. The nature of the bond and its high density enable diamond to have superior physical properties such as the highest Young's modulus and acoustic velocity of all materials, and excellent tribological properties. Recently, conformal thin diamond films have been grown at CMOS-compatible temperatures in the form known as ultrananocrystalline diamond (UNCD). These make diamond promising for high frequency micro/nanomechanical devices. We have measured the Young's modulus (E), Poisson's ratio and the quality factors (Q) for microfabricated overhanging ledges and fixed-free beams composed of UNCD films grown at lower temperatures. The overhanging ledges exhibited periodic undulations due to residual stress. This was used to determine a biaxial modulus of 838 ± 2 GPa. Resonant excitation and ring down measurements of the cantilevers were conducted under ultra high vacuum (UHV) conditions on a customized atomic force microscope to determine E and Q. At room temperature we found E = 790 ± 30 GPa, which is ~20 % lower than the theoretically predicted value of polycrystalline diamond, an effect attributable to the high density of grain boundaries in UNCD. From these measurements, Poisson's ratio for UNCD is estimated for the first time to be 0.057±0.038.

We also measured the temperature dependence of E and Q in these cantilever beams from 60 K to 450 K. Mechanical stiffness of these cantilevers increased linearly with the reduction in temperature until ~160 K where it then saturates. Reduction in the modulus of the film with temperature is slightly higher than that of single crystal diamond(averaged over all directions). We measured extremely low temperature coefficient of resonant frequency and results are promising for applications in MEMS and NEMS wireless devices and biosensors. The room temperature Q varied from 5000 to 16000 and showed a moderate increase as the cantilevers were cooled below room temperature followed by a characteristic low temperature plateau. Overall, results show that grain boundaries of UNCD films play a key role in determining its thermomechanical stability and mechanical dissipation. These results are extremely useful in understanding and controlling the dissipation in nanocrystalline materials.

Degree Type
Dissertation

Degree Name
Doctor of Philosophy (PhD)

Graduate Group
Materials Science & Engineering

First Advisor
Robert W Carpick

Keywords
elastic properties, poisson's ratio, mechanical dissipation, quality factor, ultrananocrystalline diamond films, temperature dependence of elastic properties and dissipation, resonator, MEMS, NEMS

Subject Categories
Condensed Matter Physics | Other Materials Science and Engineering

MECHANICAL STIFFNESS AND DISSIPATION IN ULTRANANOCRYSTALLINE DIAMOND FILMS

Vivekananda P Adiga

A DISSERTATION

in

Materials Science and Engineering

Presented to the Faculties of the University of Pennsylvania

in

Partial Fulfillment of the Requirements for the

Degree of Doctor of Philosophy

2010

Supervisor of Dissertation

Signature _____

Robert W Carpick, Professor, Mechanical Engineering

Graduate Group Chairperson

*Signature*_____

Ju Li, Professor of Materials Science and Engineering

Dissertation Committee

John L Bassani, Professor
Gianluca Piazza, Assistant Professor
Vaclav Vitek, Professor

MECHANICAL STIFFNESS AND DISSIPATION IN ULTRANANOCRYSTALLINE DIAMOND FILMS

This thesis is dedicated to my parents, my family and my friends

Acknowledgements

I would like to thank

…….. my advisor Rob Carpick for inspiration and support during the course of this thesis. It has been a great journey and his insights and open attitude towards science kept me going for last four years. I greatly appreciate his patience and help.

……..my collaborators Sampath Suresh, Arindom Datta (Innovative Micro technologies), John Carlisle (Advanced diamond Technologies), Anirudha Sumant and Orlando Auciello (Argonne National Lab), for all the help with UNCD growth and fabrication of the devices.

…….My collaborators Chris Torres, Pattrick Heaney, Frank Pfefferkorn (UW-Madison) Saahil Sanon, Sina Ghassemi (UPenn) and Chuck Goldsmith (Memtronics) for their help with an ongoing research on adhesion of aluminum on diamond.

……George Lengel (Nanonis, Natick, MA) and Rachel Cannara (NIST, Gaithersburg, MD) for their support during the initial stages of my experiments with RHK UHV AFM.

…….Zhouhang Wang, Ken Kollins (RHK Technologies, Troy, Michigan), Dennis Clark (Nanotech Scientific Inc), my lab members Glauber Mosqueira and Matt Hamilton (now at Exactech, Gainesville, Florida) for their support during the installation of the new RHK system and surface science chamber.

……Andy Konicek for the help with interpreting NEXAFS spectra of UNCD films

Finally I would like to thank current and former lab members of Carpick group who helped and supported me throughout the course of this research.

ABSTRACT

MECHANICAL STIFFNESS AND DISSIPATION IN ULTRANANOCRYSTALLINE DIAMOND FILMS

Vivekananda Adiga

Advisor: Robert Carpick

Tetragonal sp^3-bonded diamond has the highest known atomic density. The nature of the bond and its high density enable diamond to have superior physical properties such as the highest Young's modulus and acoustic velocity of all materials, and excellent tribological properties. Recently, conformal thin diamond films have been grown at CMOS-compatible temperatures in the form known as ultrananocrystalline diamond (UNCD). These make diamond promising for high frequency micro/nanomechanical devices. We have measured the Young's modulus (E), Poisson's ratio and the quality factors (Q) for microfabricated overhanging ledges and fixed-free beams composed of UNCD films grown at lower temperatures. The overhanging ledges exhibited periodic undulations due to residual stress. This was used to determine a biaxial modulus of 838 ± 2 GPa. Resonant excitation and ring down measurements of the cantilevers were conducted under ultra high vacuum (UHV) conditions on a customized atomic force microscope to determine E and Q. At room temperature we found E = 790 ± 30 GPa, which is ~20 % lower than the theoretically predicted value of polycrystalline diamond, an effect attributable to the high density of grain boundaries in UNCD. From these

measurements, Poisson's ratio for UNCD is estimated for the first time to be 0.057±0.038.

We also measured the temperature dependence of *E* and *Q* in these cantilever beams from 60 K to 450 K. Mechanical stiffness of these cantilevers increased linearly with the reduction in temperature until ~160 K where it then saturates. Reduction in the modulus of the film with temperature is slightly higher than that of single crystal diamond(averaged over all directions). We measured extremely low temperature coefficient of resonant frequency and results are promising for applications in MEMS and NEMS wireless devices and biosensors. The room temperature Q varied from 5000 to 16000 and showed a moderate increase as the cantilevers were cooled below room temperature followed by a characteristic low temperature plateau. Overall, results show that grain boundaries of UNCD films play a key role in determining its thermomechanical stability and mechanical dissipation. These results are extremely useful in understanding and controlling the dissipation in nanocrystalline materials.

Table of contents

List of Illustrations

Figure. 3.5.3. (a) Interferometric image of the UNCD film with a 255 μm etched overhang. **(b)** Line scan of the section shown in 7a showing a near saturation beyond 160 μm. The apparent jump in the height at the base of the overhang is simply due to the change in reflectivity from the more reflective underlying substrate.

Figure 4.1. Temperature dependence of Young's modulus (the authors have used symbol of *Y* instead of E) of single crystal diamond and tetrahedral amorphous carbon (ta-C)[11]. Melting temperature (T_m) of single crystal diamond is 3820 °K.

Figure 4.2. (a) The temperature dependence of the resonant frequency of UNCD cantilever with no overhang. **(b)** The relative change in the corresponding resonant frequency. Overhangs of the cantilever were reduced by FIB cuts at the cantilever base. These curves include data points taken during both heating and cooling cycles and are reproducible. Heating and cooling rates are approximately 1 K/ min.

Figure 4.4. Temperature dependence of the resonant frequency for cantilevers with overhangs ranging from 0 (no overhang) to 85 μm overhang. The square of resonant frequency is propositional to modulus, and is compared with that of single crystal diamond (averaged over all directions). Above 55 μm of overhang, wrinkles start to form and the temperature dependence of the modulus strongly depends on the length of cantilever and its position on the wrinkles. Levers are numbered from 1 to 4, largest (400 μm) to smallest (100 μm).

Figure 4.4. Thermal expansion coefficient of diamond [21] and silicon [22]. Below 150 K thermal expansion of diamond is negligible and for silicon it reverses the sign.

Figure 4.5 (a) Temperature dependence of Young's modulus of UNCD in comparison with single crystal diamond. Data for single crystal diamond are from references [2] (**) and [1] (*). A comparison with single crystal silicon is provided in **(b)** [7].
Figure 4.6 Map of local bulk moduli in UNCD.[27] Atoms at grain boundaries have higher or lower local bulk moduli compared to bulk of the atoms in the grains depending on coordination number.

Figure 4.7 Specific heat and Debye temperature (above) and the difference in the specific heats (below) of graphite and diamond as a function of temperature [23].

Figure 5.1 (a) Schematic of a cantilever of finite width attached to a base of thickness t_b. Theoretical models assume both the base and the cantilever are made from same material. In our experiments we have UNCD cantilevers attached to a thickness-matching UNCD base (*i.e.*, a continuous film) which is grown on silicon substrate. Some of the cantilevers have no overhang **(b)** and others have finite overhang **(c)** and so the energy can be reflected back to the lever.

Figure. 5.2 (a) Thermal conductivity of crystalline and amorphous silicon dioxide and crystalline KCl with less than 0.1% impurities. Such a small fraction of defects cause KCl's thermal conductivity to be below that of glass (Pure KCl crystal has a thermal conductivity similar to that of crystalline quartz) [21]. **(b)** Internal friction in different

glasses as a function of temperature. At low temperatures most of the amorphous and some crystalline materials with defects show a characteristic plateau which falls within the 10^{-3} and 10^{-4}.

Figure 5.3 A comparison of intrinsic friction in amorphous silicon, silicon dioxide, polycrystalline SiN cantilevers (stress free), and high tensile stress SiN membranes. A tensile stress of 1 GPa in membranes causes the intrinsic friction to drop by 2 orders of magnitude.

Figure 5.4 (a) Thermal conductivity of single crystal diamond as a function of temperature for natural diamond, which contains 1.1% C^{13} (empty circles, filled squares, and pluses) and isotopically enriched diamond containing 0.1% C^{13}. Theoretical prediction of thermal conductivity as a function of temperature and C^{13} isotope concentration is shown in inset. The thermal conductivity peak strongly depends on the isotope concentration [29]. **(b)** Thermal conductivity of polycrystalline diamond as a function of grain size. UNCD has a thermal conductivity of 1.5 - 10 W/mK which is comparable to glass [14].

Figure 5.5. Comparison of thermal conductivity of polycrystalline diamond (grain size, 2 μm) and NCD films (a), and of NCD films grown with different nitrogen content in the plasma (b) as a function of temperature [30]. Authors measured a grain size of 17-26 nm for all of these films and hence these are NCD films and not UNCD films. Our UNCD films have a grain size in the range of 2-5 nm.

Figure 5.6. **(a)** Quality factor of UNCD cantilevers with different lengths. **(b)** Quality factors as a function of resonant frequency.

Figure 5.7. Solid lines: calculated dissipation in UNCD cantilevers (thickness = 1 μm) due to TED and phonon-phonon dissipation as a function of resonance frequency [31]. Data points: measured dissipation for the cantilevers used in this study. Since diamond remains an ideal Grüneisen's solid independent of the pressure [32], a Grüneisen's constant (γ) of 1 has been used in the models.

Figure 5.8. Quality factor of UNCD cantilever beams before and after hydrogen termination.

Figure 5.9. Quality factor of a 350 μm long cantilever as a function of temperature [41]. These measurements are performed under UHV conditions in a liquid nitrogen cooled RHK UHV 350 AFM. The cantilever is attached to an 85 μm overhang at its base. The heating and cooling rates are about 1 K/min. The experiment was started at 300 K, then cooled to 138 K, then heated back to 300 K.

Figure 5.10. Quality factor of two UNCD cantilevers as a function of temperature. Lever 1 has no overhang and lever 2 has an overhang of approximately 30 μm. Data include both heating and cooling measurements. Below 150 K dissipation reaches a plateau characteristic of the amourphous materials and crystalline materials with defects. The value of $Q^{-1} \sim 10^{-4}$ is in agreement with the so-called "universal behavior".

Figure 5.11(a) Dissipation in UNCD/metal composite fixed-fixed beam resonator structures from 5 K down to 0.03 K. [27] The Q values at 5 K for the resonators are ~2500-6600. Below ~5 K, dissipation reduced dramatically with temperature. Lower frequency resonator (5.1 MHz) shows a cross over temperature at 3 K. As discussed in section 5.1.5.1, the crossover temperature, T_{co}, is higher for higher resonant frequencies [22] which were not reached in this experiment due to experimental limitation. The authors do not discuss the low temperature plateau (below 0.2 K) The departure of the dissipation from the T^{β} dependence at lower temperatures (<0.2 K) has been observed before and has been attributed to interactions between different tunneling states or to thermal decoupling from the sample, *i.e.* where the sample is not actually being cooled to the desired temperature since thermal transfer is very challenging at this low temperature [42] (b) Dissipation as a function of temperature for our UNCD cantilevers. We have explored the intrinsic friction at higher temperatures, i.e. the transition from the dissipation plateau to gradually increasing values. As shown in Fig 5.2 (b), this transition temperature depends on the material.

Figure 5.12. Temperature dependence of dissipation for NCD and tetrahedral amorphous carbon (ta-C) resonators. The ta-C films are deposited by pulsed laser deposition under different laser intensities which are indicated in the legend.[25, 43] These also show a plateau below 100 K. For NCD, the observed dissipation is ~2 orders of magnitude lower than many glasses (which show universal behavior) whereas for ta-C it is well within the range of universal behavior.

List of tables

Chapter 1. Introduction

1.1. Nanocrystallinity and Mechanical Properties

Nanocrystalline materials, having grain sizes well below 100 nm, are characterized structurally by a large volume fraction of grain boundaries and have large proportion of atoms at or very close to grain boundaries. These characteristics significantly influence their physical, mechanical, and chemical properties in comparison with conventional coarse-grained polycrystalline materials and also their single crystal counterparts. Mechanical properties of nanocrystalline materials provide us with an excellent opportunity to understand the nature of the solid interfaces which can be tailored to potential technological applications which otherwise would not be possible with much larger grain sizes. However defects present in these interfaces significantly influence the mechanical performance, since they alter the nature of bonds around them. Such effects are particularly critical to consider in the context of ultrastrong, ultrastiff materials as they may lead to undesirable degradation of the mechanical properties, but may also provide the key to utilizing such materials in practical applications. Here we will consider the mechanical behavior of nanocrystalline diamond.

Single crystal tetrahedral diamond has carbon atoms arranged through sp^3 bonding in specific type of cubic lattice known as diamond cubic, giving it highest atomic density. The nature of the bond and its high density enable diamond to have superior mechanical[1], tribological[2], thermal properties[3]. Diamond can be grown as

a conformal thin film on a variety of surfaces in a form known as ultrananocrystalline diamond (UNCD) (grain size 2–5 nm) and nanocrystalline diamond (grain size <100 nm).

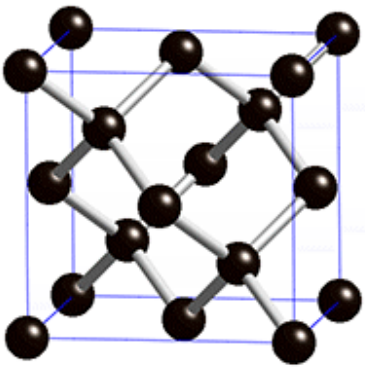

Figure 1.1. Diamond cubic lattice (Courtesy of wikipedia). The diamond has a lattice parameter of 0.357 nm.

These films maintain many of the exceptional properties of diamond despite the presence of large fraction of atoms at or very close to the grain boundaries [4-7]. Understanding the physics governing how the grain boundaries and defects influence the mechanical stiffness is important for device applications in microelectromechanical and nanoelectromechanical systems (MEMS/NEMS), which will be discussed further below. While modest deviations in the elastic properties can be expected due to the polycrystalline nature of the material, mechanical energy dissipation in nanocrystalline materials is far more difficult to predict since mechanical dissipation has a large number of possible sources which are often very sensitive functions of several material parameters. Understanding how defects and grain boundaries absorb long wavelength acoustic phonons is still an ongoing challenge. This thesis will include a particular focus

on the behavior and origins of mechanical dissipation in nanocrystalline diamond thin films.

In pure crystalline solids, the lattice vibrations can be described as collective excitations or waves as explained by Debye [8]. Lattice defects, like impurities, dislocations, vacancies, and stacking faults scatter the thermal phonons. These defects lead to local changes in lattice vibrations, referred to as defect modes, which are specific to the type and concentration of the defects. Their influence on thermal conductivity and specific heat can be seen at low temperatures ($T < 0.1\ \Theta_D$, the Debye temperature), when scattering due to momentum destroying Umklapp processes become negligible. Umklapp processes require that, at least one of the participating phonon in the phonon-phonon scattering process should have energy in the order of debye temperature (Θ_D), chances of which are drastically reduced below $0.1\ \Theta_D$ (Phonon occupation number can be obtained from Bose-Einestein distribution). Diamond has extremely high Debye temperature (1860 K at room temperature) and hence defects can influence the thermal properties even at room temperature [3]. In amorphous solids, a different kind of defect mode referred to as a “two-level system” exists, which leads to characteristic changes in their low-temperature thermal conductivity and specific heat, including short and long-term thermal relaxation, and also in their time dependent elastic and dielectric functions. These properties have been first reported in the 1970’s [9] by Zeller and Pohl, and have been successfully described by a phenomenological model which takes into account the contribution from impurity modes [10, 11]. In this so-called *tunneling model*, it is postulated that some atoms or groups of atoms have two equilibrium positions between which they can tunnel. These tunneling states lead to a low temperature plateau in

thermal conductivity and acoustic dissipation [12, 13]. In crystalline materials with small number of defects, the spectral distribution of the tunneling states is discrete[14]. However, in amorphous solids it is very broad. In general, the spectral distribution of tunneling states and their coupling energy to the lattice depends on several material parameters, preparation conditions, and the nature of the defects themselves [15, 16]. In nanocrystalline materials, impurities and defects at grain boundaries can contribute to the dissipation of low energy acoustic phonons. Due to the large fraction of grain boundaries, the spectral distribution of the tunneling states can be broad.

Measuring the temperature dependence of mechanical properties and mechanical dissipation are necessary to understand the influence of defects and under coordinated atoms at grain boundaries on the mechanical behavior in nanocrystalline materials. Low temperature changes in the mechanical properties give an accurate estimate of the Debye temperature, the temperature dependence of the specific heat and material parameters including the Grüneisen parameter [17-19]. Low temperature measurements of dissipation of acoustic phonons will be helpful in understanding the influence of defects in absorbing the energy from low frequency mechanical vibrations. Literature on the low temperature mechanical stiffness of single crystal diamond is rare. This is due to the fact that the changes in mechanical stiffness are extremely small. Temperature dependent measurements of mechanical stiffness of UNCD films did not exist prior to this work. These measurements extremely important for device applications in MEMS and NEMS systems as mentioned above, and discussed further below.

In this study, we have characterized UNCD films grown at 680 ºC using the hot filament chemical vapor deposition (HFCVD) technique[20]. The Young's modulus of

the films is determined by measuring the resonant frequency of microfabricated UNCD cantilever structures. The Quality factor at the resonance is determined either by measuring the full width at half maximum of the fundamental flexural resonance, or by stopping the mechanical excitation of the resonator and curve-fitting the ensuing damped oscillations. A detailed discussion on measuring tools and methods are discussed in **Chapter 2**. We find that the measured Young's modulus of the UNCD films is somewhat lower than that of the theoretically predicted value for randomly oriented polycrystalline diamond grains [21], and also lower than experimentally-determined values for UNCD films grown under different, previously-established conditions (*i.e.,* using microwave plasma chemical vapor deposition technique (MPCVD) [22] at 800°C). The origins of this difference will be discussed. Biaxial modulus is determined by measuring the amplitude and wavelength of the fully relaxed substrate free, overhanging portion of film using Zygo white light scanning interferometer. From these measurements Poisson's ratio is estimated. We find that the Poisson's ratio is comparable to that of polycrystalline diamond, assuming comparable mass densities. A detailed discussion of these measurements is provided in **Chapter 3.**

We measured the temperature dependence of the resonant frequency and quality factor of stress-free cantilever structures to eliminate the influence from changes in thermal stresses. The measured temperature coefficient of frequency and hence the temperature dependence elastic modulus was found to be slightly higher than that found theoretically [23] and experimentally [24] for single crystal diamond. We attribute this to a slightly higher temperature dependence of specific heat due to the presence of broken bonds at grain boundaries.[18] **Chapter 4** discusses the measurements of the

temperature dependence of the mechanical stiffness of UNCD films grown at 680 °C. Further modeling of specific heat as a function of temperature for UNCD films is needed to characterize the true nature of temperature dependence of modulus in UNCD films.

Dissipation in UNCD micro-cantilevers mainly arises due to the presence of large number of defects at the grain boundaries and the surfaces. The dissipation observed is much higher than single crystal silicon cantilevers and microcrystalline diamond cantilevers [25, 26]. Quality factor has been marginally increased as the temperature is reduced from 450 K to 60 K. Detailed discussions of factors that contribute to dissipation are provided later in this chapter and experimental results are discussed in **Chapter 5.**

These are the first measurements of low temperature elastic properties of UNCD films. This will be helpful in further understanding the influence of grain boundaries on the observed mechanical behavior of nanocrystalline materials. Dissipation in cantilever structures at a much wider temperature range especially at temperatures well below 10 K will give further insight to the nature of defect transitions. Further studies are needed including the influence of impurity atoms in grain boundaries, grain size and intrinsic stresses on temperature dependent mechanical properties and dissipation.

1.2 Applications for nanocrystalline diamond

MEMS and NEMS offer a smaller, more efficient, and more powerful alternative to conventional electronic systems [27, 28]. Radio frequency (RF) MEMS and NEMS devices find important applications in the components of wireless devices such as filters, oscillators and switches, which increase their utility and shrink the size of currently

available wireless devices [29]. With antenna dimensions becoming smaller, their emitted signal frequency has been pushed up into the GHz range. This requires that oscillators, filters, and switches in the circuit also have to be operated at higher frequencies. Conventional RLC (resistor-inductor-capacitor) band-pass filters or oscillators can still operate at these frequencies. However, their quality factors (Q), a characteristic of a resonator's bandwidth relative to its center frequency, are very low, *i.e.*, well below 100. On the other hand, off the chip piezoelectric resonators are successful in applications such as filters, oscillators in heterodyning transceivers. This is mainly due to the fact that they have very high quality factors and extremely stable resonant frequencies. High quality factors and stable resonant frequencies are necessary to achieve adequate frequency selection (filters) and to realize the low phase noise and stability in oscillators. But off the chip piezo electric devices occupy large space and must be interfaced with integrated electronics at the board level. Higher resonant frequencies require that off-the piezo electric resonators should be scalable down to micrometer and sub-micrometer scale [29] which makes it difficult to integrate these devices. MEMS/NEMS resonators offer a better alternative, where one can design them to have very high resonant frequencies and quality factors and they are scalable. They can be fabricated with processes that are compatible with conventional complementary metal–oxide–semiconductor (CMOS) circuits and hence can be completely integrated with CMOS. An example is the radial disk resonator, which operates at GHz frequency range with a quality factor close to 7000 even in air [30]. This, together with the possibility of creating vacuum cavities for achieving high Q resonant structures in many different geometries [31], has increased the possibility of actual application of these devices. Similarly high

frequency and high quality factor MEMS/NEMS resonators find application in resonant mass sensors provided they have very good thermal stability [28]. High frequency and high quality factors are desirable to detect small changes in resonant frequency associated with added mass [32].

However there are challenges in achieving high resonant frequencies without compromising quality factors [33, 34] and frequency stability. Smaller dimensions are required to achieve high resonant frequencies. This means that surface effects will dominate the mechanical behavior of the structural materials used. Understanding the influence of defects and under coordinated atoms on elastic properties, thermomechanical stability, and mechanical dissipation are crucial in achieving commercially-viable MEMS/NEMS devices, *i.e.,* devices with stable, high resonant frequencies with low mechanical dissipation (high Q). Such materials must have extremely stable, inert surfaces. Diamond is one such exceptional material which meets these requirements. Diamond is an attractive material for several applications in MEMS and NEMS devices such as RF MEMS resonators, switches, and biosensors [35-40]. This is due to the superior physical properties of diamond such as high modulus, high acoustic velocity (for high frequency resonators), its stable and inert surface (for high Q resonators) with correspondingly low adhesion to other materials (for MEMS contact switches), as well as good tribological behavior (for RF-MEMS switches and other MEMS actuators, positioners, and any other device with sliding interfaces) [41-43]. Functionalized diamond surfaces are more stable compared to other MEMS materials [40, 44], and the temperature stability of its mechanical properties [17] is useful in applications such as resonant biosensors.

Commercially successful synthesis of diamond was first achieved using the high temperature, high pressure process developed by Tracy Hall at GE in 1950's. Using a "belt" press capable of producing pressures above 10 GPa and temperatures above 2000 °C in pyrophyllite container, he dissolved graphite in the presence of molten nickel, cobalt or iron to turn it into diamond. These metals acted both as a solvent for carbon and catalyst for its conversion into diamond [45]. This led to applications of diamond in cutting tools, heat sinks, and other macroscopic applications. However, the extreme pressures (> 3.5 GPa) and temperatures (> 2500 K) required, and the inability to grow diamond over large areas limited the use of synthetic diamonds in devices or wear-resistant coatings until new growth processes involving chemical vapor deposition (CVD) were discovered in mid 60's[46]. These required much lower temperatures and pressures. Uniform large area (>4" wafer) growth of diamond films remained a challenge, since it is difficult to control the initial nucleation of the diamond on most substrates. This was achieved by pre-seeding the substrate with diamond nanoparticles and by controlling the growth chemistry to achieve a conformal thin film in a form known as ultrananocrystalline diamond (UNCD) and nanocrystalline diamond (NCD), [5, 22, 47, 48] producing films with smooth surfaces [47]. UNCD films have shown mechanical properties that are in the vicinity of single crystal diamond [22] despite the presence of a high volume fraction of grain boundaries and impurities, particularly hydrogen [49]. A comparison of properties of MEMS materials is given is table 1.1. Figure 1.2.shows a transmission electron microscope (TEM) image of a typical ultrananocrystalline diamond film. It has grain sizes in the range of 3-5 nm and atomically-abrupt grain boundaries. UNCD films have been traditionally grown using a microwave plasma

chemical vapor deposition process (MPCVD) [4, 5] and more recently by commercially viable hot filament CVD process (HFCVD) at temperatures well above 700°C.

Properties	UNCD/NCD	SiC	Si
Young's Modulus GPa	825-980	400-700	160
Hardness (GPa)	98	30-40	5-10
Self-mated friction coefficient (air)	0.01	-	0.1
Self-mated adhesion energy (mJ/m^2)	10	-	110
Fracture toughness ($MPa \cdot m^{1/2}$)	4	1.2	2
Acoustic velocity (m/s)	15000	11800	8800
Thermal conductivity (W/m•K)	15-400	120	130

Table 1.1.: A comparison of UNCD properties with other important MEMS materials.

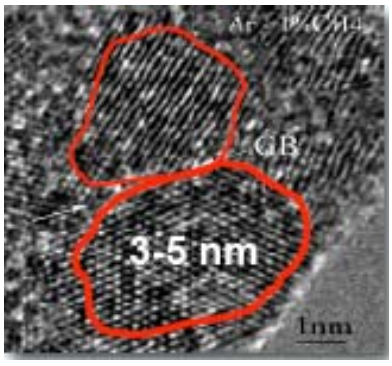

Figure 1.2. A cross sectional high resolution TEM image of a MPCVD-grown UNCD film grown on tungsten[5]

However, there are significant challenges to integrating diamond devices with conventional CMOS electronics. The most crucial are the high growth temperature of conventional UNCD, and the limited ability to grow uniform films over large areas. In recent years, uniform, conformal UNCD films have been grown over large areas (> 6" wafers) at CMOS-compatible temperatures (≤ 400 °C) [11] using both the HFCVD and MPCVD processes, which is close to the threshold temperature CMOS circuits can withstand. In order to fully exploit the true potential of low temperature grown UNCD films in high frequency MEMS devices, it is important to characterize the mechanical properties of these newly-developed UNCD films. While the overall chemical composition and bonding appears to be similar between all the growth processes mentioned, subtle difference in grain size, grain boundary structure, and defect structure and density may have significant consequences. In fact, the mechanical properties of these low temperature UNCD films had not yet been measured prior to this work, and the Poisson's ratio of any UNCD had never been reported at all. Measurements of mechanical dissipation (quality factor) in these films were also lacking. Similarly, the temperature stability of elastic properties of UNCD films had not yet been reported. Understanding the factors that influence these properties will be helpful for applicability of these films in stable frequency oscillators, filters and resonant mass sensors. As mentioned earlier in this chapter, the mechanical performance of low temperature grown UNCD films and the influence of the nanostructure on these properties is the primary topic of this thesis.

References:

[1] J. Philip, P. Hess, T. Feygelson, J. E. Butler, S. Chattopadhyay, K. H. Chen, and L. C. Chen, "Elastic, mechanical, and thermal properties of nanocrystalline diamond films," *Journal of Applied Physics,* vol. 93, pp. 2164-2171, 2003.

[2] A. V. Sumant, D. S. Grierson, J. E. Gerbi, J. Birrell, U. D. Lanke, O. Auciello, J. A. Carlisle, and R. W. Carpick, "Toward the ultimate tribological interface: Surface chemistry and nanotribology of ultrananocrystalline diamond," *Advanced Materials,* vol. 17, pp. 1039-+, Apr 2005.

[3] L. Wei, P. K. Kuo, R. L. Thomas, T. R. Anthony, and W. F. Banholzer, "Thermal conductivity of isotopically modified single crystal diamond," *Physical Review Letters,* vol. 70, p. 3764, 1993.

[4] O. Auciello, J. Birrell, J. A. Carlisle, J. E. Gerbi, X. C. Xiao, B. Peng, and H. D. Espinosa, "Materials science and fabrication processes for a new MEMS technoloey based on ultrananocrystalline diamond thin films," *Journal of Physics-Condensed Matter,* vol. 16, pp. R539-R552, Apr 2004.

[5] O. Auciello, S. Pacheco, A. V. Sumant, C. Gudeman, S. Sampath, A. Datta, R. W. Carpick, V. P. Adiga, P. Zurcher, M. Zhenqiang, Y. Hao-Chih, J. A. Carlisle, B. Kabius, J. Hiller, and S. Srinivasan, "Are Diamonds a MEMS' Best Friend?," *Microwave Magazine, IEEE,* vol. 8, pp. 61-75, 2007.

[6] V. P. Adiga, A. V. Sumant, S. Suresh, C. Gudeman, O. Auciello, J. A. Carlisle, and R. W. Carpick, "Mechanical stiffness and dissipation in ultrananocrystalline diamond microresonators," *Physical Review B (Condensed Matter and Materials Physics),* vol. 79, pp. 245403-8, 2009.

[7] H. D. Espinosa, B. Peng, B. C. Prorok, N. Moldovan, O. Auciello, J. A. Carlisle, D. M. Gruen, and D. C. Mancini, "Fracture strength of ultrananocrystalline diamond thin films---identification of Weibull parameters," *Journal of Applied Physics,* vol. 94, pp. 6076-6084, 2003.

[8] C. Kittel, *Introduction to solid state physics*, 7th ed.

[9] R. C. Zeller and R. O. Pohl, "Thermal Conductivity and Specific Heat of Noncrystalline Solids," *Physical Review B,* vol. 4, p. 2029, 1971.

[10] W. A. Phillips, "Tunneling states in amorphous solids," *Journal of Low Temperature Physics,* vol. 7, pp. 351-360, 1972.

[11] P. w. Anderson, B. I. Halperin, and c. M. Varma, "Anomalous low-temperature thermal properties of glasses and spin glasses," *Philosophical Magazine,* vol. 25, pp. 1 - 9, 1972.

[12] J. Jackle, "ULTRASONIC ATTENUATION IN GLASSES AT LOW-TEMPERATURES," *Zeitschrift Fur Physik,* vol. 257, pp. 212-223, 1972.

[13] W. A. Phillips, "Two-level states in glasses," *Reports on Progress in Physics,* vol. 50, p. 1657, 1987.

[14] V. Narayanamurti and R. O. Pohl, "Tunneling States of Defects in Solids," *Reviews of Modern Physics,* vol. 42, p. 201, 1970.

[15] D. R. Southworth, R. A. Barton, S. S. Verbridge, B. Ilic, A. D. Fefferman, H. G. Craighead, and J. M. Parpia, "Stress and Silicon Nitride: A Crack in the Universal Dissipation of Glasses," *Physical Review Letters,* vol. 102, p. 4, Jun 2009.

[16] Pohl and et al., "Low-temperature thermal conductivity and acoustic attenuation in amorphous solids," *Reviews of Modern Physics,* vol. 74, p. 991, 2002.

[17] A. Migliori, H. Ledbetter, R. G. Leisure, C. Pantea, and J. B. Betts, "Diamond's elastic stiffnesses from 322 K to 10 K," *Journal of Applied Physics,* vol. 104, pp. 053512-4, 2008.

[18] M. X. Gu, Q. S. Chang, Z. Chen, T. C. A. Yeung, S. Li, C. M. Tan, and V. Nosik, "Size, temperature, and bond nature dependence of elasticity and its derivatives on extensibility, Debye temperature, and heat capacity of nanostructures," *Physical Review B (Condensed Matter and Materials Physics),* vol. 75, p. 125403, 2007.

[19] M. Gu, Y. Zhou, L. Pan, Z. Sun, S. Wang, and C. Q. Sun, "Temperature dependence of the elastic and vibronic behavior of Si, Ge, and diamond crystals," *Journal of Applied Physics,* vol. 102, pp. 083524-4, 2007.

[20] P. W. May and Y. A. Mankelevich, "From Ultrananocrystalline Diamond to Single Crystal Diamond Growth in Hot Filament and Microwave Plasma-Enhanced CVD Reactors: a Unified Model for Growth Rates and Grain Sizes," *The Journal of Physical Chemistry C,* vol. 112, pp. 12432-12441, 2008.

[21] C. A. Klein, "Anisotropy of Young's modulus and Poisson's ratio in diamond," *Materials Research Bulletin,* vol. 27, pp. 1407-1414, 1992.

[22] A. Orlando, B. James, A. C. John, E. G. Jennifer, X. Xingcheng, P. Bei, and D. E. Horacio, "Materials science and fabrication processes for a new MEMS technology based on ultrananocrystalline diamond thin films," *Journal of Physics: Condensed Matter,* p. R539, 2004.

[23] G. Mingxia, Z. Yichun, P. Likun, S. Zhuo, W. Shanzhong, and Q. S. Chang, "Temperature dependence of the elastic and vibronic behavior of Si, Ge, and diamond crystals," *Journal of Applied Physics,* vol. 102, p. 083524, 2007.

[24] H. J. McSkimin and P. Andreatch, Jr., "Elastic Moduli of Diamond as a Function of Pressure and Temperature," *Journal of Applied Physics,* vol. 43, pp. 2944-2948, 1972.

[25] U. Gysin, S. Rast, P. Ruff, E. Meyer, D. W. Lee, P. Vettiger, and C. Gerber, "Temperature dependence of the force sensitivity of silicon cantilevers," *Physical Review B,* vol. 69, p. 045403, 2004.

[26] N. Sepulveda, L. Jing, D. M. Aslam, and J. P. Sullivan, "High-Performance Polycrystalline Diamond Micro- and Nanoresonators," *Microelectromechanical Systems, Journal of,* vol. 17, pp. 473-482, 2008.

[27] K. L. Ekinci and M. L. Roukes, "Nanoelectromechanical systems," *Review of Scientific Instruments,* vol. 76, p. 12, Jun 2005.

[28] H. G. Craighead, "Nanoelectromechanical Systems," *Science,* vol. 290, pp. 1532-1535, November 24, 2000 2000.

[29] C. T. C. Nguyen, L. P. B. Katehi, and G. M. Rebeiz, "Micromachined devices for wireless communications," *Proceedings of the Ieee,* vol. 86, pp. 1756-1768, Aug 1998.

[30] W. Jing, Butler, E. James, Feygelson, Tatyana, Nguyen, and T. C. Clark, *1.51-GHz nanocrystalline diamond micromechanical dish resonator with material-mismatched isolating support*.

[31] J. D. Zook, W. R. Herb, Y. Ahn, and H. Guckel, "Polysilicon sealed vacuum cavities for microelectromechanical systems," in *Papers from the 45th National Symposium of the American Vacuum Society*, Baltimore, Maryland (USA), 1999, pp. 2286-2294.

[32] P. S. Waggoner and H. G. Craighead, "Micro- and nanomechanical sensors for environmental, chemical, and biological detection," *Lab on a Chip,* vol. 7, pp. 1238-1255, 2007.

[33] C. Seoanez, F. Guinea, and A. H. C. Neto, "Surface dissipation in nanoelectromechanical systems: Unified description with the standard tunneling model and effects of metallic

electrodes," *Physical Review B (Condensed Matter and Materials Physics),* vol. 77, p. 125107, 2008.

[34] P. Mohanty, D. A. Harrington, K. L. Ekinci, Y. T. Yang, M. J. Murphy, and M. L. Roukes, "Intrinsic dissipation in high-frequency micromechanical resonators," *Physical Review B,* vol. 66, p. 085416, 2002.

[35] C. F. Wang, Y. S. Choi, J. C. Lee, E. L. Hu, J. Yang, and J. E. Butler, "Observation of whispering gallery modes in nanocrystalline diamond microdisks," *Applied Physics Letters,* vol. 90, p. 081110, 2007.

[36] H. M. Thomas, L. Xiao, H. H. Brian, W. B. Jeffrey, E. B. James, and F. Tatyana, "Low temperature internal friction in nanocrystalline diamond films," *Applied Physics Letters,* vol. 86, p. 081910, 2005.

[37] L. Sekaric, J. M. Parpia, H. G. Craighead, T. Feygelson, B. H. Houston, and J. E. Butler, "Nanomechanical resonant structures in nanocrystalline diamond," *Applied Physics Letters,* vol. 81, pp. 4455-4457, 2002.

[38] A. B. Hutchinson, P. A. Truitt, K. C. Schwab, L. Sekaric, J. M. Parpia, H. G. Craighead, and J. E. Butler, "Dissipation in nanocrystalline-diamond nanomechanical resonators," *Applied Physics Letters,* vol. 84, pp. 972-974, 2004.

[39] G. Alexei, I. Matthias, M. Pritiraj, R. Janet, and W. S. Brian, "High quality factor gigahertz frequencies in nanomechanical diamond resonators," *Applied Physics Letters,* vol. 91, p. 203503, 2007.

[40] J. A. Carlisle, "Diamond films: Precious biosensors," *Nat Mater,* vol. 3, pp. 668-669, 2004.

[41] A. R. Konicek, D. S. Grierson, P. U. P. A. Gilbert, W. G. Sawyer, A. V. Sumant, and R. W. Carpick, "Origin of Ultralow Friction and Wear in Ultrananocrystalline Diamond," *Physical Review Letters,* vol. 100, p. 235502, 2008.

[42] A. V. Sumant, D. S. Grierson, J. E. Gerbi, J. A. Carlisle, O. Auciello, and R. W. Carpick, "Surface chemistry and bonding configuration of ultrananocrystalline diamond surfaces and their effects on nanotribological properties," *Physical Review B (Condensed Matter and Materials Physics),* vol. 76, p. 235429, 2007.

[43] D. S. G. J. E. G. J. B. U. D. L. O. A. J. A. C. R. W. C. A. V. Sumant, "Toward the Ultimate Tribological Interface: Surface Chemistry and Nanotribology of Ultrananocrystalline Diamond," *Advanced Materials,* vol. 17, pp. 1039-1045, 2005.

[44] W. Yang, O. Auciello, J. E. Butler, W. Cai, J. A. Carlisle, J. E. Gerbi, D. M. Gruen, T. Knickerbocker, T. L. Lasseter, J. N. Russell, L. M. Smith, and R. J. Hamers, "DNA-modified nanocrystalline diamond thin-films as stable, biologically active substrates," *Nat Mater,* vol. 1, pp. 253-257, 2002.

[45] H. T. Hall, "ULTRA-HIGH-PRESSURE, HIGH-TEMPERATURE APPARATUS - THE BELT," *Review of Scientific Instruments,* vol. 31, pp. 125-131, 1960.

[46] J. C. Angus, H. A. Will, and W. S. Stanko, "GROWTH OF DIAMOND SEED CRYSTALS BY VAPOR DEPOSITION," *Journal of Applied Physics,* vol. 39, pp. 2915-&, 1968.

[47] N. N. Naguib, J. W. Elam, J. Birrell, J. Wang, D. S. Grierson, B. Kabius, J. M. Hiller, A. V. Sumant, R. W. Carpick, O. Auciello, and J. A. Carlisle, "Enhanced nucleation, smoothness and conformality of ultrananocrystalline diamond (UNCD) ultrathin films via tungsten interlayers," *Chemical Physics Letters,* vol. 430, pp. 345-350, 2006.

[48] A. R. Krauss, O. Auciello, D. M. Gruen, A. Jayatissa, A. Sumant, J. Tucek, D. C. Mancini, N. Moldovan, A. Erdemir, D. Ersoy, M. N. Gardos, H. G. Busmann, E. M. Meyer, and M. Q. Ding, "Ultrananocrystalline diamond thin films for MEMS and moving mechanical assembly devices," *Diamond and Related Materials,* vol. 10, pp. 1952-1961, 2001.

[49] C. Liu, X. C. Xiao, J. Wang, B. Shi, V. P. Adiga, R. W. Carpick, J. A. Carlisle, and O. Auciello, "Dielectric properties of hydrogen-incorporated chemical vapor deposited diamond thin films," *Journal of Applied Physics,* vol. 102, p. 7, Oct 2007.

Chapter 2. Experimental Methods

2.1 Ultra high vacuum atomic force microscopy as a tool for characterizing the resonance behavior of materials

2.1.1 General design and operation of UHV AFM and surface science system

Most of the resonance and quality factor measurements discussed in this thesis are performed using the ultra-high vacuum (UHV) atomic force microscope (AFM, RHK-750) system shown schematically in Fig. 2.1.1, developed by RHK Technology, Inc. (Troy, Michigan). It includes a load-lock system for exchanging samples from the outside, *in situ* sample storage of up to 3 sample or cantilever holders, and a wobble stick

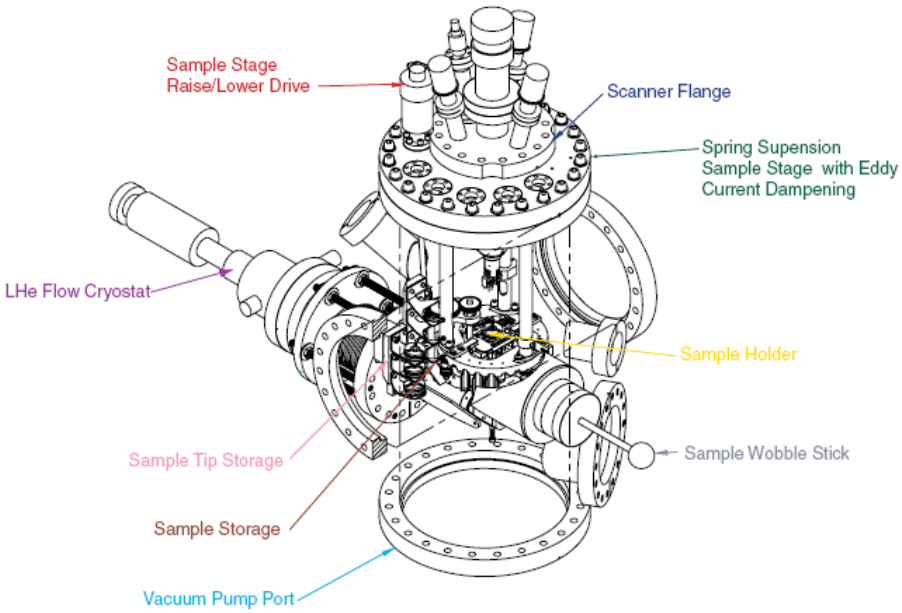

Figure 2.1.1. The cross section of UHV-AFM(750 series) chamber (Courtesy of RHK technology, Troy, Michigan)

fork to facilitate the sample transfer. The sample holder is attached to an eddy current-damped vibration isolation stage. Variable temperature measurements are conducted using a built-in heater filament for heating, with cooling achieved using a liquid helium cryostat which can cool the sample down to approximately 55 K. Also installed on the UHV chamber (but not shown in Fig. 2.1.1) are a mass spectrometer for residual gas analysis and leak testing, ion and convectron gauges for pressure measurement, a 400 L/s turbo pump with a scroll-type roughing pump, a 300 L/s ion pump with titanium sublimation, an *ex situ* video camera to monitor scan-head motion and the alignment of the laser and photo-sensitive detector (PSD), and a leak valve for introducing vapors into the chamber.

The capability of this AFM system is augmented by a connected surface science chamber that we have designed and constructed [Fig. 2.1.2]. *In situ* surface analysis tools include X-ray photoemission spectroscopy (XPS) with a monochromated X-ray source that allows high resolution spectroscopy. A differentially-pumped analyzer column allows for measurements of surface composition in high pressure (up to 100 mTorr) conditions. The surface science chamber also includes low-energy electron diffraction together with Auger electron spectroscopy (LEED/AES) for surface structural and chemical analysis. In addition, a differentially-pumped ion gun is provided for sputtering and charge compensation. Temperature dependent measurements can be performed with a liquid nitrogen cooled VG sample manipulator with a built-in heater that can heat the sample up to 1200 K. This capability is augmented by built-in heating capabilities of a RHK-style sample holder. The system also boasts a mass spectrometer for residual gas analysis, a leak valve for surface chemical modification and a 300 L/s ion

pump with a titanium sublimation pump for UHV operations. The entire system is bolted onto a steel frame supported by laminar-flow vibration isolation air legs to reduce the influence of external mechanical vibrations. These additional tools for *in situ* surface analysis in combination with the AFM will vastly enhance the understanding of surface properties for future nanomechanical and tribological studies performed in this laboratory. While the surface science system was not used for the research results presented here, substantial effort during this thesis was put into the design, assembly, and testing of this system for future use.

Measurements of the resonant frequency shifts and quality factor changes with temperature are performed using both this system (for the later measurements) and by an older RHK 350 AFM system. While both systems are similar in terms of basic operation, they differ in the following ways. First, the RHK 750 AFM can perform non-contact mode AFM as it includes a phase-locked loop electronics system for a non-contact mode known as frequency modulation. Second, the 750 system boasts an internal eddy current damping vibration isolation system, while the 350 systems uses a stack of metal plates separated by Viton rubber. The eddy current system is far better at filtering low-frequency (<1 kHz) mechanical vibrations. Finally, the 750 system has a liquid helium cryostat, while the 350 system has a liquid nitrogen cryostat. Thus, the 750 can cool the sample down to approximately 55 K, while the 350 system can cool it down to approximately 120 K. The basic operation of the system is discussed below for the better understanding of its operation.

The UHV-AFM 750 scan head is based on the "beetle-type" design similar to the one developed by Dai, *et al*. at Lawrence Berkeley National Laboratory.[1] Three piezo

legs control the position of a free-standing scan-head that rests on the sample holder [Fig. 2.1.2, 2.1.3]. This symmetric geometry provides first-order thermal drift compensation in all three axes, with thermal drift less than 1 Å/min. This reduces the need for complex drift compensation software.

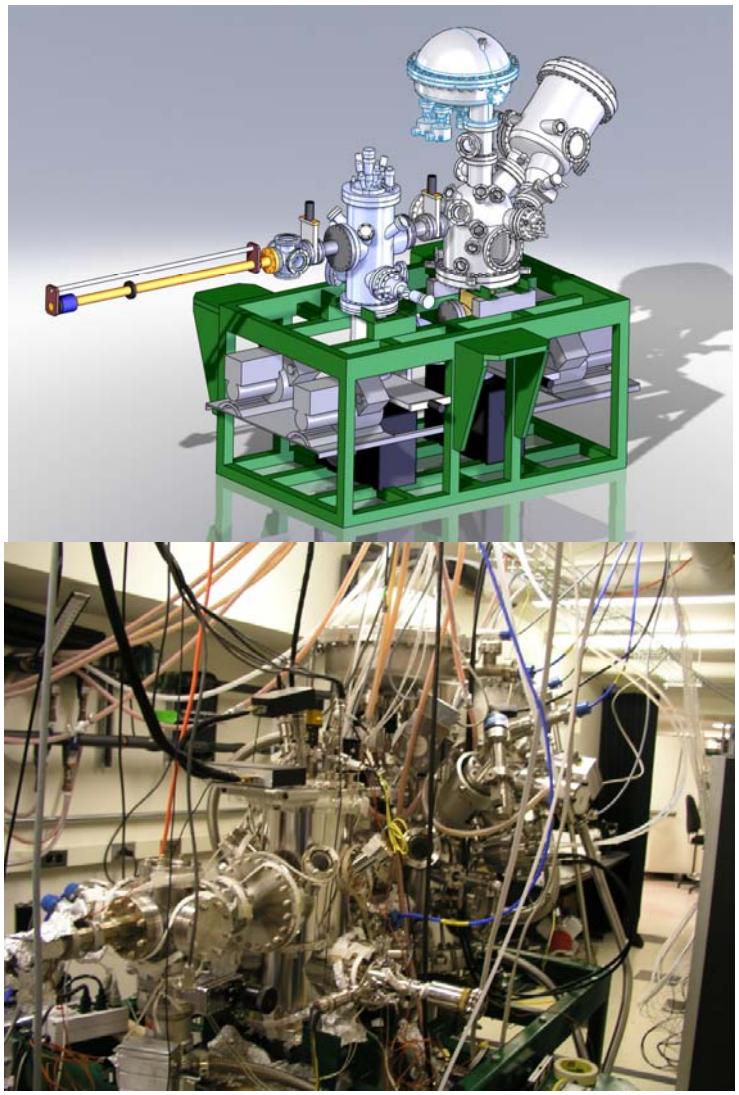

Figure. 2.1.2. (a) Design (using SolidWorks 3-D CAD software) for the combined UHV-AFM (left-hand chamber) and surface science system (right-hand chamber). (b) Actual chamber after construction.

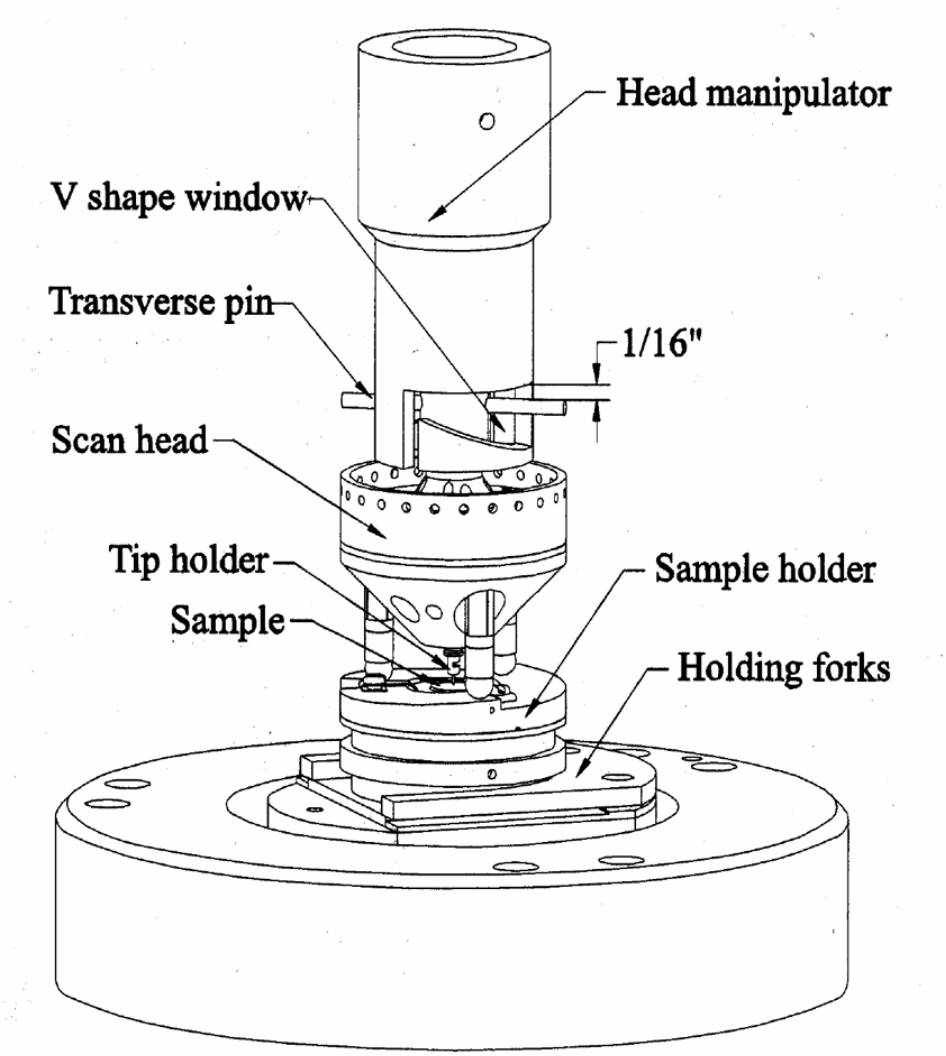

Figure. 2.1.3. Schematic arrangement of the UHV-AFM manipulator, scan head, and sample platform.

With a small mechanical loop from the AFM tip to the sample base, the free-standing scan-head provides greater mechanical stability than larger commercial designs.

Furthermore, the sample platform is static and thus may be outfitted for heating and cooling without affecting the piezoelectric actuator legs used for scanning. The resonant frequency of the scan head is approximately 1.7 kHz and hence higher frequency mechanical noise is filtered out. Each leg consists of a four-quadrant piezo tube for x-y-z scanning.

To achieve the coarse approach motion of the scan head and tip in relation to the sample, a portion of a saw-tooth waveform is applied to each piezo sector so that the scan-head is propelled downward along the three ramps on the sample holder depicted in Fig. 2.1.4b (this is for standard sample holders; a description of the custom-built holders used for this thesis is provided in the next section). While the piezo legs are used for coarse approach / lateral motion of the tip with respect to sample, a z-modulation piezo (not shown here) is attached between the cantilever holder and the rest of the scan head. This is used for tip actuation, or fine z-motion. Hence, there are two ways to control *z*-displacement: using all three legs or the *z*-modulation piezo.

Depending on the sample holder used, samples may be heated up to ~800 K by irradiative heating with the tungsten filament (from below the sample), to >1000 K via electron bombardment (by applying a high voltage between the sample and filament), or to >1200K by direct, resistive heating of the sample itself. Fig. 2.1.4b shows a standard sample holder, which features three titanium nitride-coated ramps at the perimeter for tip approach or retraction, a copper base for greater thermal conductivity while cooling, a thermocouple for temperature measurement, springs and washers for mounting samples securely, and resistive heating leads. In principle, the thermally conductive copper braids that connect the liquid helium cryostat and sample stage permit sample cooling down to

~30 K according to the manufacturer. In practice, we have achieved sample temperatures of ~55-65 K.

To convert PSD output current to voltage, we use a two-stage RHK preamplifier and their PLLPro electronics for processing the PSD signal. The RHK SPM100 electronics unit is used to supply voltage to the piezos and for feedback control for topographic imaging. The output range of the SPM100 is ±130 V. In this configuration, the *x-y* scan range of the UHV-AFM scan-head is 4.9 x 4.9 μm^2. Both the laser spot and the PSD can be positioned for aligning the laser beam with the cantilever, and its reflection with the PSD respectively, by using piezo stepper motors. The RHK750 is capable of both non-contact and contact mode AFM operation. While non-contact mode operation involves detecting minute shifts in the resonant frequency and dissipation of the cantilever, contact mode involves detecting the cantilever deflection in real time.

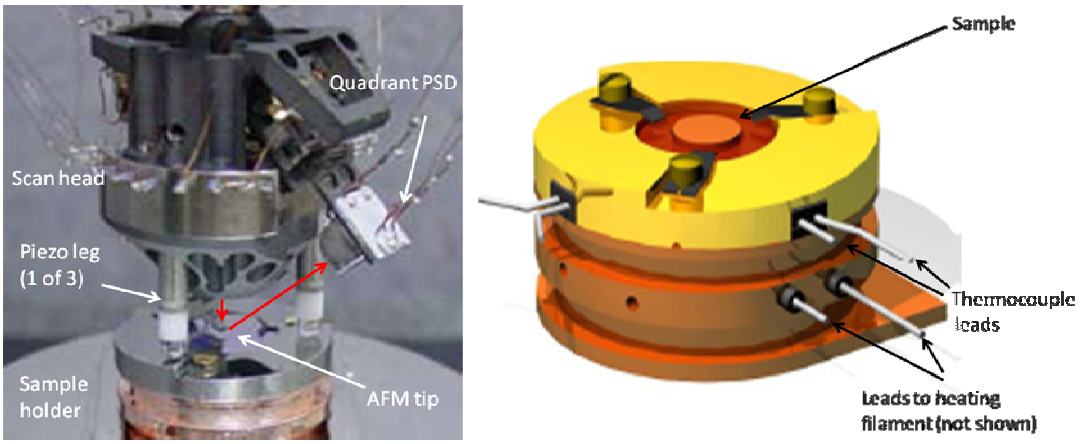

Figure. 2.1.4a UHV-AFM scan-head and residing on the standard sample holder. (*Adapted from drawings, courtesy RHK Technology, Inc., Troy, Michigan*) (b) A standard sample holder with ramps for coarse approach of the AFM tip to the sample. Also seen are the leads to heating filaments underneath the sample.

2.1.2 Design of a low temperature piezo stage for measuring mechanical properties

While the built-in z-modulation piezo is used for actuating the AFM cantilevers, for the temperature dependent measurements cantilevers have to be in the sample side. For normal operation of the AFM, cantilever tips approach the horizontal sample surface at a 22.5° angle. The incident laser beam at an angle of 77.5° (90-22.5°) to the cantilever and is normal to sample surface. In order to ensure normal incidence of the reflected beam from the cantilever to PSD, this tilt angle is necessary. This tilt also prevents reflections from sample surface reaching the detector. In order to achieve reflection from sample side, sample holders have to be tilted at the same angle as shown in Figure 2.1.5. Thus, there are several challenges in fabricating a structure for proper measurement when the a cantilever is located where the sample normally resides. The incident laser is a focused beam emerging from a graded index lens. Departure of the reflecting surface from the focal point of the beam increases the beam size (initially 30 μm) by approximately 60 μm / mm. This not only reduces the intensity of the beam and hence the reflected intensity, it increases the reflection from unnecessary structures surrounding the freestanding beams. Considering the fact that we are using ultrananocrystalline diamond (UNCD) cantilevers as a resonant structure, which give much lower reflection compared to silicon, accurate control of the cantilever chip height with respect to focal point of the laser are necessary to achieve sufficient reflected light intensity.

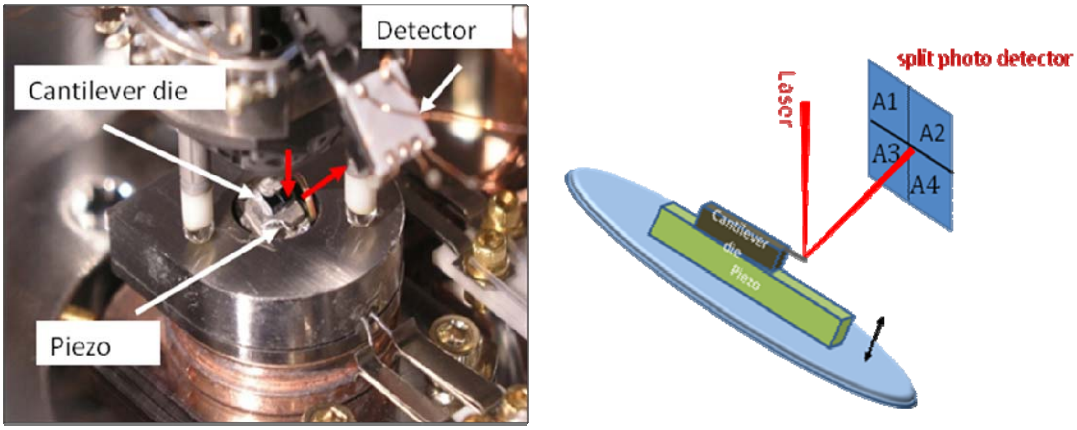

Figure. 2.1.5. (a) Custom built tilted wedge sample holder with an in built piezo actuator. (b) Schematic of the piezo actuation set up. Cantilever die and Piezos are glued after determining the right position for proper reflection into the photodetector. A focused laser beam is reflected off the back of the cantilever onto a four-quadrant photo-sensitive detector (PSD). The amount by which the cantilever bends and twists in response to normal and lateral forces corresponds to variations in the top minus bottom and left minus right signals, respectively.

Fig. 2.1.6 shows a custom wedge holder that I designed and constructed for the purpose of measuring the temperature dependent response of the UNCD cantilevers. The sample platform is tilted by 22.5° with respect to the scanning plane of the microscope. The peizo legs of the AFM head rest on the flat surface surrounding the tilted sample stage. While the piezo legs allow x-y motion of the scan head on the flat sample ramp, z motion is not possible. This fixes the distance between laser source and cantilevers mounted on the piezo actuator. A tilted wedge is made of Invar alloy and is electrically insulated from surrounding platform by an alumina O-ring on the top side and it rests on insulating sapphire ring which has a good low temperature thermal conductivity. The

whole platform and tilted wedge are held together by a set of screws.

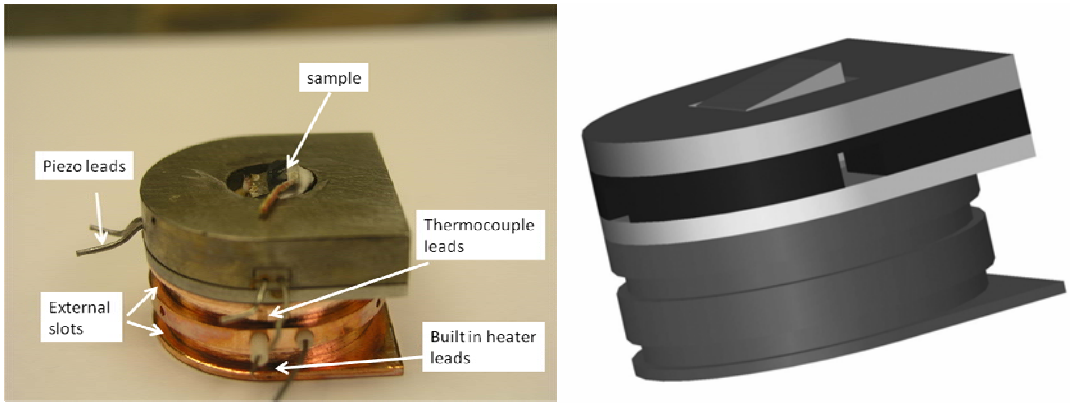

Fig. 2.1.6 (a) Side view of custom built sample holder. 6 lead sample holder, consists of built in heater, piezo leads for actuation of the cantilever mounted on top of the piezo piece. Temperature is measured by type K thermocouple **(b)** Three-dimensional schematic views (using SolidWorks 3-D CAD software) of a wedge-shaped sample holder that is tilted by 22.5°.

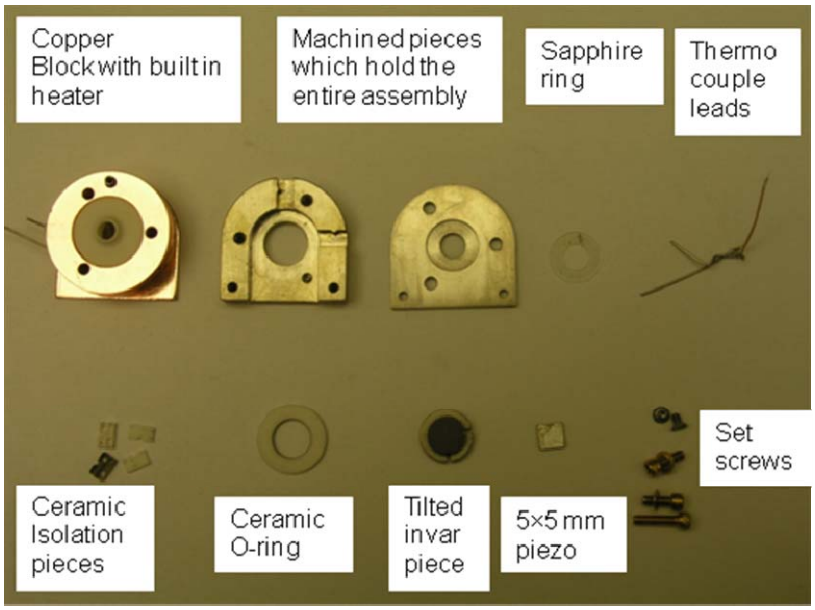

Figure 2.1.7. Individual components of the custom built sample holder.

A 5×5 mm^2 piezo actuator (PZT, z poled, Manufactuer EBL products, Harford, CT)is glued onto the tilted Invar wedge as shown in the schematic 2.6 using a thermally conductive and electrically insulating epoxy, which is compatible with ultra high vacuum conditions and low cryogenic temperatures (T7110, 2 part epoxy, Manufacturer epo-tek, Billerica, MA). Samples are epoxied on top of the piezo actuator and a thermocouple (Type K) is mounted on top of the sample within 2 mm of the cantilever array [2]. This entire assembly is mounted on to a copper holder (for good heat transfer capabilities) with built-in heater to allow high temperature measurements. The external slots on the copper holder facilitate transfer of sample holder between sample stage and sample storage via a wobble stick. Individual components of the custom built sample holder is shown in Figure 2.1.7

2.1.3 Measuring resonant frequency and quality factor

Fig. 2.1.5 shows the arrangement of the cantilever, laser and position-sensitive detector (PSD) in the popular optical-beam-deflection AFM. A focused laser beam reflects off the back of the cantilever and onto the PSD, which consists of four photosensitive sectors quadrants which we label *A1*, *A2*, *A3* and *A4*. Normal or lateral forces applied to the cantilever cause it to bend or twist, respectively. These forces change the angles of reflection of the laser, causing the laser spot on the PSD to displace in the vertical or horizontal direction, respectively. The PSD separately measures the normal and lateral signals, $V_{norm} = (V_{A1}+V_{A2})-(V_{A3}+V_{A4})$ and $V_{lat} = (V_{A1}+V_{A3})-(V_{A2}+V_{A4})$, that vary in proportion to the bending and twisting of the cantilever. At flexural and torsional resonance both V_{norm} *and* V_{lat} reach their maximum respectively. This maximum

can be identified by sweeping the input frequency to the piezo across the expected frequency range for the particular cantilever beam being studied using a function generator and recording the V_{norm} *and* V_{lat} in an oscilloscope.

To determine the quality factor, two approaches can be used. In the first approach, a ring-down measurement is performed whereby the excitation was stopped and the subsequent cantilever motion recorded using a Tektronix 3014B oscilloscope. An exponential fit as shown in Fig 2.1.8 (a) to the ring-down curve gives a measure of dissipation in the fixed-free beams. An equation for the fit is given by

$$A(t) = A_0 e^{\frac{-\pi f_n (t-t_0)}{Q}} \tag{2.1}$$

Where $A(t)$ and A_0 are the time (t) dependent amplitude and initial amplitude respectively. f_n is the resonant frequency of the nth mode and t_0 is the initial time. In the second method, the resonance frequency and the full width half maximum (FWHM) are measured to determine the quality factor. The equation for the quality factor is given by:

$$Q = \frac{2\pi f_n}{\Delta f_n} \tag{2.2}$$

Where f_n is the resonant frequency of the nth mode and Δf_n is the full width at half maximum of the nth mode. To do this, we used the PLL Pro module of the RHK750 AFM which can detect small shifts in resonant frequency and dissipation, and is used to confirm the measured values using oscilloscope. An example is shown in Fig. 2.1.8 (b).

These measurements can be performed independently using XPM Pro software supplied by the vendor and quality factor of this resonator is 10,400.

Measurements are conducted in UHV conditions to avoid condensation of vapor at lower temperatures. There are three thermocouples on the UHV AFM. A solid state thermocouple for the cryostat, a type K thermocouple at the stage and Type K thermocouple glued on top of the chip containing cantilevers. Recent temperature measurements are conducted using a Lakeshore temperature controller (model), which allows one to control the cooling or heating rates through the *in situ* built in heater in the cryostat. Typical heating / cooling rates of the sample are about 1 K/min. The lowest temperature of the sample (measured by the type K thermocouple mounted on top of the cantilever chip) we could reach is approximately 60 K, and the highest temperature reached is 450 K. Even though higher temperatures can be reached, stabilizing the temperature takes much more time due to heat flow from the sample holder to copper foils then to the cryostat. This heat transfer takes place through junction between cryostat and copper block where in a sapphire plate pressed between two indium foil sheets. It is necessary to keep the temperature of the junction less than 150°C in order to prevent the electrical shorting of the stage with the chamber/cryostat. Shorting of the bias voltage to ground prevents the scanning tunneling microscopy imaging capability of the system.

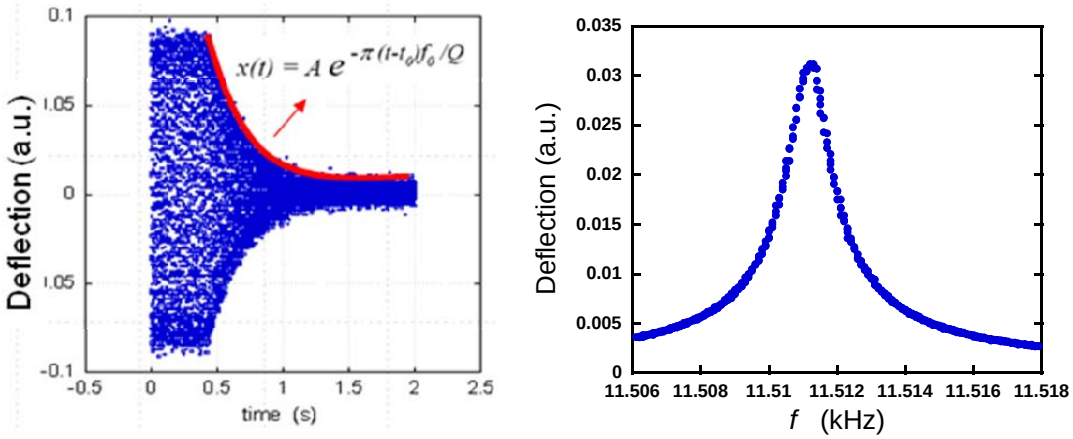

Figure. 2.1.8. a) Typical ringdown measurement of UNCD cantilever acquired using an oscilloscope. b) Resonant excitation of the UNCD cantilever across the fundamental mode using XPM Pro 2.0 software. Both measurements are conducted at room temperature.

2.2 White light interferometry

Zygo white light interferometer is an extremely powerful tool for measuring the topography of the surfaces. While white light interferometry is certainly not new, zygo interferometer offers a combination of rather old white light interferometry techniques with modern electronics, computers, and software to produce extremely powerful measurement tool. It is being manufactured by Zygo Corporation, Middlefield, CT. In our lab, we have 6300 series, which has a dynamic MEMS module, which enables the users to capture the time varying response of MEMS devices. Similarly it enables us to measure the stress gradient of released beams. In this thesis Zygo white light interferometer is used for measuring the amplitude and period of the wrinkles in the overhanging portion of the released UNCD film grown on silicon wafer. A detailed

discussion of this topic is provided in Chapter 3. Here I will briefly discuss the operation of white light interferometer.

Traditionally most interferometry is performed using a laser as the light source. The primary reason for this is that the long coherence length of laser light makes it easy to obtain interference fringes and interferometer path lengths no longer have to be matched as they do if a short coherence length white light source is used. Even though it is easier to obtain these fringes, any stray reflections will also give spurious fringes which can give incorrect measurements. Similarly, It can easily be shown that for laser based phase-shifting interferometry the height difference between two adjacent data points must be less than $\lambda/4$, where λ is the wavelength of the light used. If the slope is greater than $\lambda/4$ per detector pixel then height ambiguities of multiples of half wavelengths can exist [3].

An excellent way of obtaining good height measurements with large steps or rough surfaces is to use a white light source and the coherence peak sensing approach in a vertical scanning interferometer apparatus shown in Figure 2.2.1. In the vertical scanning coherence peak sensing mode of operation a broad spectral width light source is used which has very short coherence length, and good contrast fringes will be obtained only when the two paths of the interferometer are closely matched in length. This is well depicted in Fig. 2.2.1(a) If in the interference microscope the path length of the sample arm of the interferometer is varied using a piezo stack, the height variations across the sample can be determined by looking at the sample position for which the fringe contrast is a maximum. Height ambiguities are eliminated by using this technique, since sample is in focus when the maximum fringe contrast is obtained and there are no focus errors in

the measurement of surface microstructure. The vertical resolution depends on the precision of the mechanical movement measurement which is done through a piezo stack and is well calibrated.

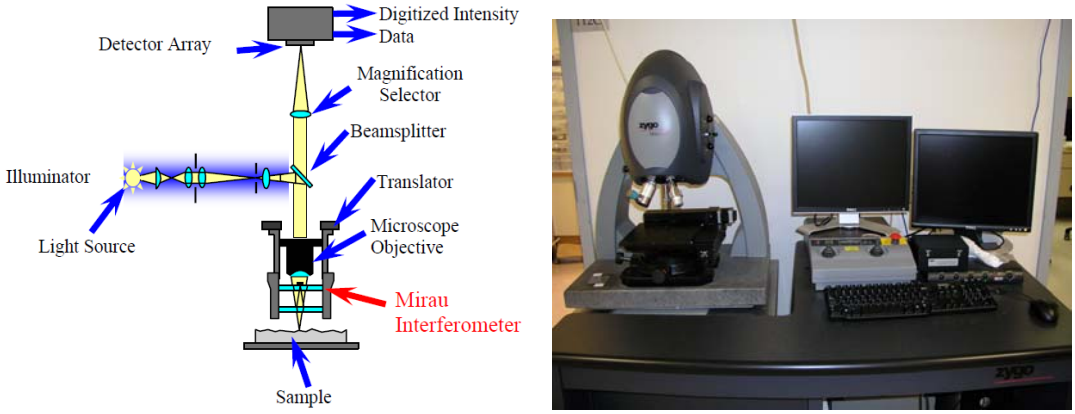

Figure 2.2.1. (a) A schematic showing the operation of white light interferometer.[3] (b) Actual white light interferometer in Carpick research group.

One of the major drawbacks of this type of scanning interferometer measurement is that only a single surface height is being measured at a time. Hence a large number of measurements and calculations are required to determine a large range of surface height values which is performed by the use of modern electronics, computer and software package provided by zygo.

References:

[1] Q. Dai, R. Vollmer, R. W. Carpick, D. F. Ogletree, and M. Salmeron, "VARIABLE-TEMPERATURE ULTRAHIGH-VACUUM ATOMIC-FORCE MICROSCOPE," *Review of Scientific Instruments,* vol. 66, pp. 5266-5271, Nov 1995.

[2] V. P. Adiga, A. V. Sumant, S. Suresh, C. Gudeman, O. Auciello, J. A. Carlisle, and R. W. Carpick, "Mechanical stiffness and dissipation in ultrananocrystalline diamond microresonators," *Physical Review B (Condensed Matter and Materials Physics),* vol. 79, pp. 245403-8, 2009.

[3] J. C. Wyant, "White light interferometry," in *Holography: A Tribute to Yuri Denisyuk and Emmett Leith*, Orlando, FL, USA, 2002, pp. 98-107.

Chapter 3. Elastic properties of UNCD films

3.1 Background

Tetragonal sp^3-bonded diamond has the highest known atomic density (1.77×10^{23} atoms/cm^3). The strong nature of the carbon-carbon bond and the high density of bonds provide diamond with superior mechanical properties such as the highest Young's modulus, hardness, acoustic velocity of any material, and a very low Poisson's ratio. Device applications of diamond are made possible by uniform, large area growth UNCD/NCD films. In general, UNCD and nanocrystalline diamond (grain size ~10 nm-100 nm) thin films exhibit a unique combination of properties suitable for applications in MEMS/NEMS and devices as discussed in Chapter 1. UNCD films were originally grown using microwave plasma chemical vapor deposition (MPCVD) at 800°C. The Young's modulus [1, 2] and hardness[2] of films grown using this well-established recipe have been measured previously.

The mechanical properties of UNCD films grown at low temperatures play an important role in the suitability of these films for applications involving monolithic integration of MEMS/NEMS and CMOS devices. They are rarely reported in the literature. In this chapter, we discuss the experimental results for the Young's modulus and Poisson's ratio of UNCD films grown at 680 °C using the HFCVD technique. We determined the Young's modulus of these films by fabricating UNCD micro-cantilevers and measuring the resonance frequency of the fundamental flexural mode of the cantilevers. Under-etching of the UNCD films was performed to produce overhanging ledges. These overhanging ledges formed periodic wrinkles due to residual compressive

stress in the film. The amplitude and wavelength of the fully relaxed overhanging portion were measured to determine the biaxial modulus of the film and, by comparison with the Young's modulus, Poisson's ratio.

Property	**UNCD [1, 2, 4] (MPCVD grown)**	**Poly Crystalline Diamond – random grain orientation[5]**	**Diamond like carbon[6]**	**Tetrahedral amorphous carbon[3]**
Young's modulus, E (GPa)	860-960 GPa	1143	87±18	662±24
Biaxial modulus (GPa)		1232	101 ± 4	~829
Poisson's ratio, ν		0.069	0.22 ± 0.33	0.202±0.054
Acoustic velocity, V_L (km/s)	14.243	18		~14.7

Table 3.1.1. A comparison of mechanical and acoustic properties of crystalline as well as amorphous forms of carbon.

Table 3.1.1 compares mechanical properties of different carbon films with varying sp^3 content and order. Modest deviations in the elastic properties (modulus, Poisson's ratio) from the values for bulk diamond can be expected due to the polycrystalline nature of the UNCD, due to the presence of a large fraction of the atoms at grain boundaries. These include defects at the grain boundaries such as sp^2 bonds, disordered atoms, and hydrogen atoms. Traditional UNCD films showed Young's

modulus (*E*) values 20 %-30 % lower than that of polycrystalline diamond (averaged over all directions) but Young's modulus values were higher than the amorphous diamond like carbon (DLC) films. The mechanical property of DLC films strongly depends on sp^3 content. Tetrahedral amorphous carbon (ta-C) has the highest modulus (660 GPa,[3]) among the amorphous diamond like carbon (DLC) films since it has very high sp^3 content (80% sp^3, 20% sp^2), while the DLC film quoted in Table 3.3.1 [6] has a much lower modulus. Ultrananocrystalline diamond (which as up to ~5% sp^2 content) has a higher modulus than DLC films but Young's modulus values are lower than nanocrystalline[7] and microcrystalline diamond[8] films due to large fraction of grain boundaries.

3.2 UNCD growth and hydrogen termination

Figure 3.2.1. A hot filament CVD reactor at advanced diamond technologies (ADT).

UNCD films (produced commercially by Advanced Diamond Technologies Inc. and known as **Aqua 25**) were grown using the hot filament chemical vapor deposition (HFCVD) technique at 680°C on silicon wafers (diameter = 150 mm) using a

predominantly methane/hydrogen growth chemistry. Controlling this chemistry is critical to achieve films with ultrananocrystalline grains. Introducing more hydrogen causes the microstructure to evolve from nanocrystalline to microcrystalline [9]. Silicon wafers were ultrasonically seeded with ultradispersive detonation diamond (UDD) powder solution before the growth. The average film thickness was measured by the NANOSPEC thickness measuring tool and found to be 1.002 μm, uniform to within 11% across the wafer, with the thickness greatest at the center. These films exhibited a residual compressive stress of 370 ±1 MPa measured using a Tencor Flexus 2320A stress measurement tool. While we have also characterized microwave plasma CVD grown UNCD films by Argonne National Laboratories, the characterization of resonant structures made from such films was rendered difficult due to the low thickness and high stress of those films. Therefore, discussion of the fabrication and characterization of MPCVD structures will not be described in this thesis. All of the discussion will be on the HFCVD films grown by ADT.

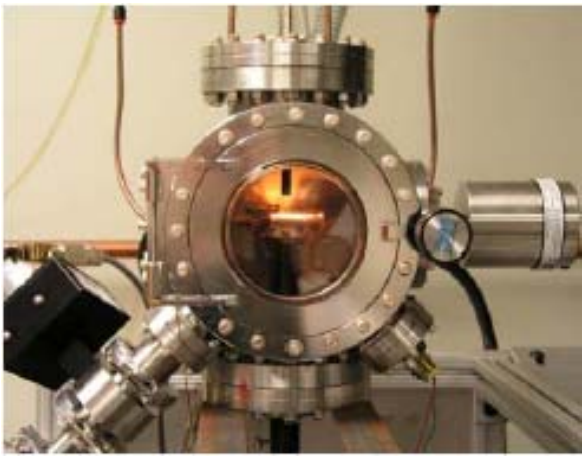

Figure 3.2.2. Hot filament chemical vapor deposition chamber used for hydrogen termination. Hydrogen passed through tungsten filaments after carburization.

In this work, the UNCD films grown by ADT were later H-terminated in the HF-CVD chamber in our laboratory shown in Figure 3.2.2. This is done by flowing H_2 across a carburized tungsten filament at 1800 ºC. Carburization of the tungsten filament is necessary to limit the tungsten contamination during the hydrogen termination. This is done by passing the methane gas (9 sccm, 3 Torr) across the hot filament for about 20 minutes. For hydrogen termination, a sample is placed in close proximity (~ 2 mm) to the carburized filament and the chamber is pumped down to 50 mTorr. Hydrogen gas (100 sccm, 20 Torr) is then passed across the carburized hot filament. At filament temperatures above 1800ºC, H_2 dissociates into atomic hydrogen. The samples are placed within range of the atomic H by mounting them several millimeters below the filament, which also heats the samples to ~700ºC (measured on the sample stage with a type K thermocouple). At this temperature, hydrogen molecules dissociated by the filaments can both bond with the diamond surface and knock off existing hydrogen atoms to form H_2 [10]. After approximately 20 minutes, all of the surface carbon atoms are expected to be H-terminated.[11] If the sample is cooled slowly, then the likelihood of incident hydrogen atoms ejecting (a thermally-activated process) already bonded H is reduced. Therefore, the termination is more complete when sample temperature was slowly decreased at the end of the termination. This is done by progressively lowering of the sample stage until the sample cools to below ~500°C. The filaments are shut off and the sample was allowed to cool under the flow of hydrogen. The UNCD sample was removed from the chamber after cooling and then stored in a dry nitrogen environment for surface characterization.

3.3 Characterization of HFCVD grown UNCD films

Near edge X-ray absorption fine structure (NEXAFS) spectroscopy was used to determine the chemical bonding nature of the films, especially for the presence of sp^3 and sp^2 bonded carbon in the near-surface region (top ~4 nm) of the films.[12] This technique is extremely useful to characterize the local bonding structure of the elements on a sample's surface. Here, monochromated X-rays of sufficient but tunable energy impinge upon a sample and excite core-level (K-shell, for example) electrons above the vacuum level (primary core level electrons) or into unoccupied electronic states above the Fermi level but below the vacuum level. In the case of diamond, it is the excitation from C 1s $\rightarrow\sigma^*$, in the case of graphite, C 1s $\rightarrow\sigma^*$ or C 1s $\rightarrow\pi^*$. When a core-level electron is excited during an X-ray absorption event into unoccupied electronic state, the energized atom will relax by filling the core hole with an electron from a higher electronic state (L-level, for example) and can simultaneously emit an Auger electron or a fluorescent photon from that state.

Emitted Auger electrons from the top few nanometers (Auger electrons have very small ineleastic mean free path only few nanometers) of the surface will then propagate through the material and will either escape from the sample completely or will collide inelastically with other loosely-bound electrons, generating lower energy secondary electrons, which are then ejected from the sample's surface. The Auger and secondary electrons that are ejected from the sample are then collected by an anode and measured as a current as a function of incident X-Ray energy. NEXAFS spectra of different allotropes of carbon are presented in 3.3.1.(a). While ordered graphite shows a much stronger π^* peak, σ^* peaks, single crystal diamond shows much stronger exciton peak at 289.3 eV

(C 1s→σ*) and a dip corresponding to second band gap at 302 eV. Disordered tetrahedral amorphous carbon which has about 80 % sp^3 and 20 % sp^2 content shows peaks corresponding to both transitions, but due to the amorphous nature, peaks are very broad.

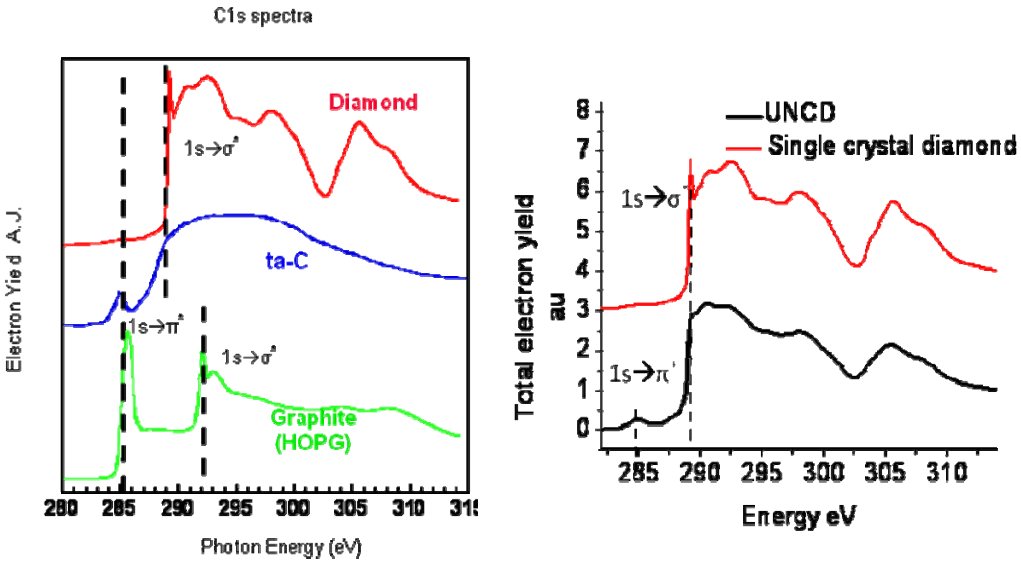

Figure. 3.3.1(a) Comparison of NEXAFS sectra of different carbon allotropes (courtesy of Dr. Dave Grierson and Andy Konicek). (b) NEXAFS spectra from a H-terminated UNCD film and single crystal diamond (offset for clarity). UNCD exhibits a sp^2 peak at 285 eV, a diminished exciton peak at 289 eV, and shallower band gap at 302 eV, all due to the fractional presence of non-diamond bonding

A NEXAFS spectrum taken on the topside of a hydrogen-terminated UNCD film is shown in Fig. 3.3.1.(b)(black curve), where a NEXAFS spectrum from a single crystal diamond is shown for comparison (red curve). Characteristic diamond features observed in Fig. 3.3.1(b) include the exciton peak at 289.3 eV and second band gap at ~302 eV, characteristic of diamond. A small amount of non-diamond bonding in the UNCD film is

revealed by the presence of peak corresponding to sp^2-bonded carbon (C 1s $\rightarrow\pi^*$) centered at 285.0 eV.

Based on these measurements and the corresponding reference spectra obtained on single crystal diamond and HOPG, we estimate the sp^2 content of the films to be 5.8% using the normalization method described by Lenardi *et al* [12]. The sp^2 content observed in the HFCVD UNCD films studied here is on the upper end of the 2-5% sp^2 content typically observed in MPCVD films grown at 800°C. [13] Most of this sp^2-bonded carbon is present at the grain boundaries; some fraction may be due to adsorbates and surface reconstruction. Hydrogen termination[14] of the surface using the hot filament process described above resulted in the reduction of sp^2 content in the near-surface region to 4.3%. Thus, this percentage represents a likely lower bound for the sp^2 content of the bulk of the film assuming a uniform film structure with thickness.

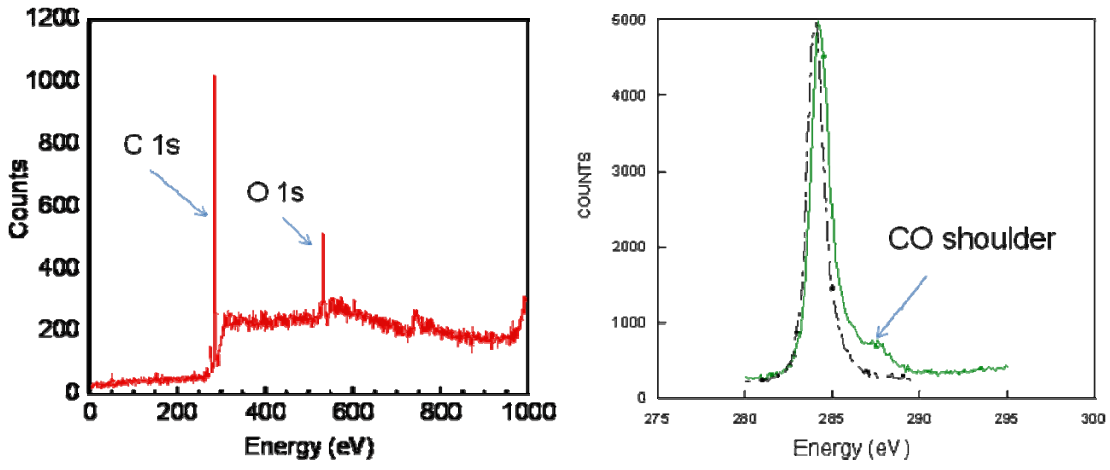

Fig 3.3.2. (a) Normalized XPS survey spectra of HFCVD-grown UNCD (b) Extended high resolution scan of the carbon peak before (green) and after (black) hydrogen termination demonstrates the reduction in C-O shoulder after H-termination.

XPS spectra of the as-received film showed the presence of oxygen at the surface and typical surface composition showed approximately 7-9 % oxygen content at the unterminated HFCVD grown UNCD surface. After hydrogen termination, the oxygen content is drastically reduced as evidenced by reduction in O 1s peak and CO shoulder (Fig 3.3.2 (b)). We have measured the bulk hydrogen content of the films using forward recoil spectroscopy (FRES). In FRES analysis, beam of helium ($^{4}He^{++}$) ions is accelerated to 3 MeV, and are filtered and focused by electro magnets. The sample is mounted at grazing angle (~15°) to the incident ion beam, which knocks out one hydrogen atom per helium ion that collides and embeds in the film. Recoiled hydrogen as well as He ions are passed through 10 μm Mylar filter to suppress the He ions overwhelming the detector. This film is calibrated to take into account the energy loss of both ions of different energy. While the film is very effective in suppressing the energy of the helium ions, the lighter, more energetic hydrogen ions are transmitted. Transmitted hydrogen generates a current (typically 10 nA for our measurements) which is measured by a solid state detector. We count the number of hydrogen ions in a particular energy window and measurements are stopped after a total charge dosage of 10 μC. Each of these energy window corresponds to a depth from which hydrogen is ejected. The typical depth profile resolution is about ~30 nm. Polystyrene on silicon is used as a reference hydrogen-containing film. The small amount of hydrogen in the UNCD film is consistent with previous analyses of UNCD film using FRES [9] which yielded a hydrogen content of approximately 1 to 1.5% depending on growth conditions. We have measured hydrogen content of about 2.5% at the surface and about 1 % in the bulk as shown in Fig 3.3.3. for

the UNCD films grown using HFCVD technique. Higher hydrogen content at the surface is in part due to absorbed water. We also sent out UNCD samples (Aqua 25) to Evans Analytical Group (EAG), Hightstown, NJ, 08520 USA for Secondary Ion Mass Spectrometry (SIMS) analysis. This yielded a hydrogen content of approximately 1.7%.

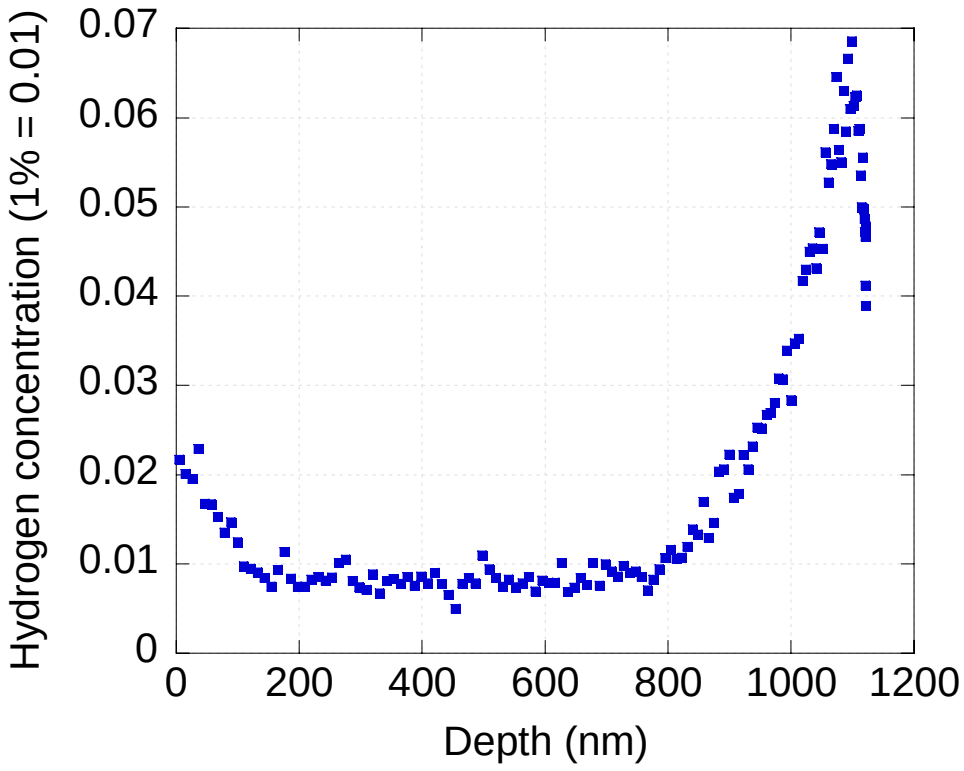

Fig. 3.3.3. FRES data show the hydrogen concentration of the Aqua 25 film as a function of depth from the surface. At higher depths (> 800 nm) low energy He ++ ions overwhelm the signal.

Hydrogen in ultrananocrystalline diamond (UNCD) mainly present in the grain boundaries[9] as evident by the FRES measurements we have done for determining the influence of hydrogen content on the dielectric properties of Microwave plasma CVD

grown UNCD films. Here we found that polycrystalline diamond films containing fine grained diamond had much lower hydrogen content compared to ultrananocrystalline diamond (UNCD) films indicating that hydrogen is present mainly in the grain boundaries.

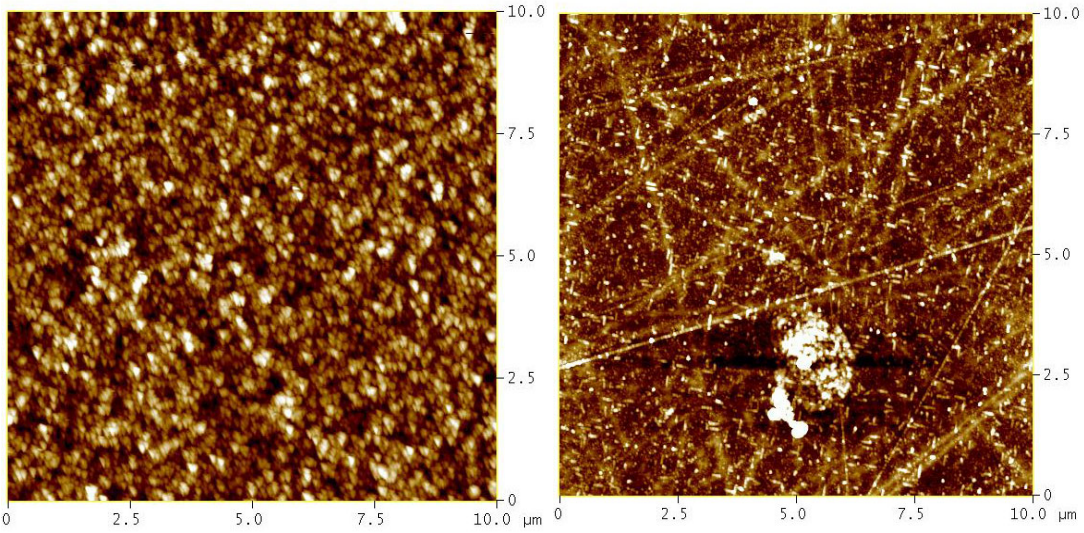

Fig 3.3.4 (a) The UNCD films studied here exhibit an RMS roughness of ~ 10 nm over 10×10 μm^2 area measured by tapping mode AFM imaging. However completely etched underside (b) yielded a much more uniform surface (RMS roughness ~2 nm)

As shown in Figure 3.3.4, RMS roughness of the Aqua 25 UNCD films are typically less than 10 nm over a scan area of 10 ×10 μm^2. After completely removing silicon substrate using wet etching, AFM imaging of the underside of the UNCD film were performed. This yielded a RMS roughness of ~ 2 nm over a scan area of 10 ×10 μm^2. This is initial nucleation side of the film. Earlier studies [15] indicated diamond colonies grow out of single nucleation sites and they coalesce to form pinhole-free films. This is evident by comparing the underside of the UNCD film before and after hydrogen

plasma treatment using AFM. [15] Hydrogen plasma treatment removes the non-diamond carbon present in between the diamond colonies. The initial layer density of the films primarily depends on the initial nucleation density.

UNCD characterization		**Technique/tool**
Surface sp^2 content	4-6 %	NEXAFS
Bulk hydrogen content	1.0 -1.5%	FRES
Surface composition	C 91.5 %, O 8.5 %	XPS
Film stress	-370 ± 1 MPa	Flexus Tencor
Surface roughness (rms)	~5 nm	AFM

Table 3.3.1. Summary of characterization results of UNCD grown by HFCVD technique.

The mass density of Aqua 25 films were examined using X-ray Reflectivity (XRR) measurements. These measurements are performed by Evans Analytical Group, Hightstown, NJ, 08520 USA. This yielded a density of 3.05 g/cm^3 for the UNCD layer and 2.39 g / cm^3 for the low density layer (about 100 nm thick) above silicon substrate (ρ = 2.33 g / cm^3). XRR alone can not determine the composition of this low density layer. We assume it to be either a low density nucleation layer, or an oxide layer on top of silicon, or both. Depth profiling of various elements in UNCD using SIMS (performed by EAG) yielded negligible change in the hydrogen or oxygen content in this region compared to UNCD layer, suggesting that this layer is likely due to silicon oxide. Considering the fact that this is the first measurement of density of UNCD films, for the

following sections we assumed that the density of UNCD to be that of single crystal diamond. Further work is needed to determine the composition and thickness of any initial seed layer in the UNCD. We will discuss the possibility of lower density and its influence on the measured mechanical properties. A summary of the characterization results are shown in Table 3.3.1.

3.4 Fabrication of UNCD devices

For cantilever fabrication, a thick sputtered oxide was deposited on the UNCD surface. This oxide layer is subsequently patterned and etched to expose UNCD. Oxide layer serves as a hard mask for etching the UNCD layer to produce the cantilevers. The UNCD layer was etched using an oxygen-based plasma in a reactive ion etching (RIE) process. The wafers were diced to commercial AFM chip specifications (4.4 mm × 1.6 mm dies) to enable insertion into commercial AFMs for measuring the cantilever properties. Each die contained four cantilevers as shown in the SEM image in Fig. 3.4.1, with the cantilever lengths of 100 μm, 250 μm, 350 μm and 400 μm. The thickness of each cantilever was measured by SEM, and ranged from 820 nm to 1.01 μm. The minor differences in thickness are from thickness variation of the film as deposited or due to subsequent processing. The length-to-width ratio is 7.5 for all the cantilevers. The oxide hard mask and sacrificial oxide were subsequently wet-etched simultaneously, using a 49% (by volume) HF solution.

The Si underside of the cantilevers was further etched with either a SF_6 or a XeF_2 dry etch chemistry to study the effect of overhang on mechanical properties. The substrates were cleaved so that the cantilevers did not have any substrate material

underneath them (Fig. 3.4.2.). This was done to ensure that reflected light was sampled only from the cantilever and not from the more reflective Si substrate. Cantilever dies are further subjected to piranha cleaning and XeF_2 etch process to remove silicon particles after the cleaving process.

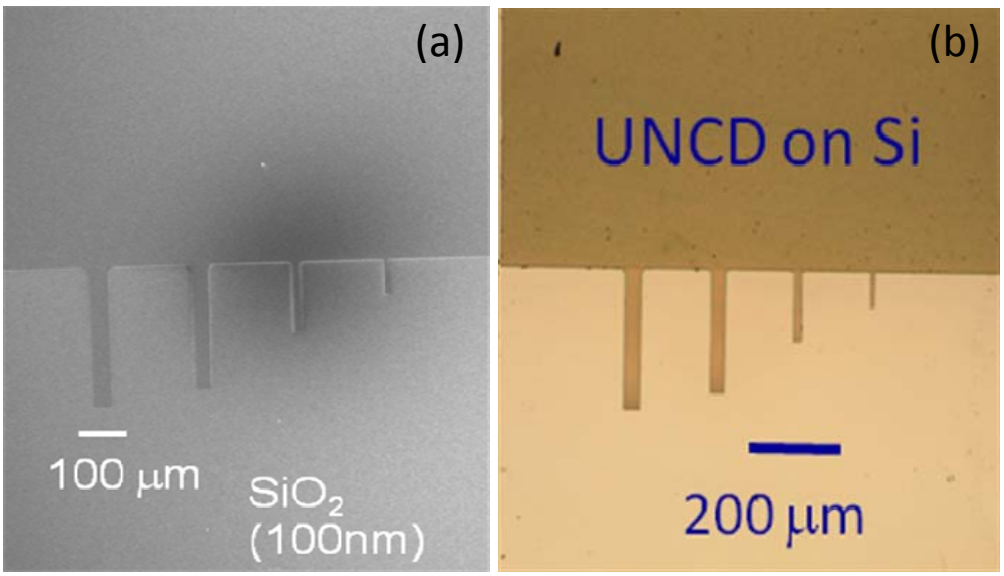

FIG. 3.4.1 (a). SEM image of unreleased UNCD cantilever die which features four different cantilevers with lengths ranging from 100 μm to 400 μm, with a thickness of 1 μm. (b) Optical microscope image of the cantilever die.

In order to fabricate overhang-free cantilevers, we adopted following procedure. After the wet release, cantilever dies are subjected to deep reactive ion etch (DRIE) procedure using SF_6 (Bosch process). This is a highly anisotropic, line of sight process and it etched the silicon between the cantilevers (etch depth is 250μm), leaving the side walls of silicon underneath the levers exposed for isotropic etch. This step is followed by a SF_6 isotropic etch, which removed the remaining silicon underneath the cantilevers and produced an overhang of 30 μm.

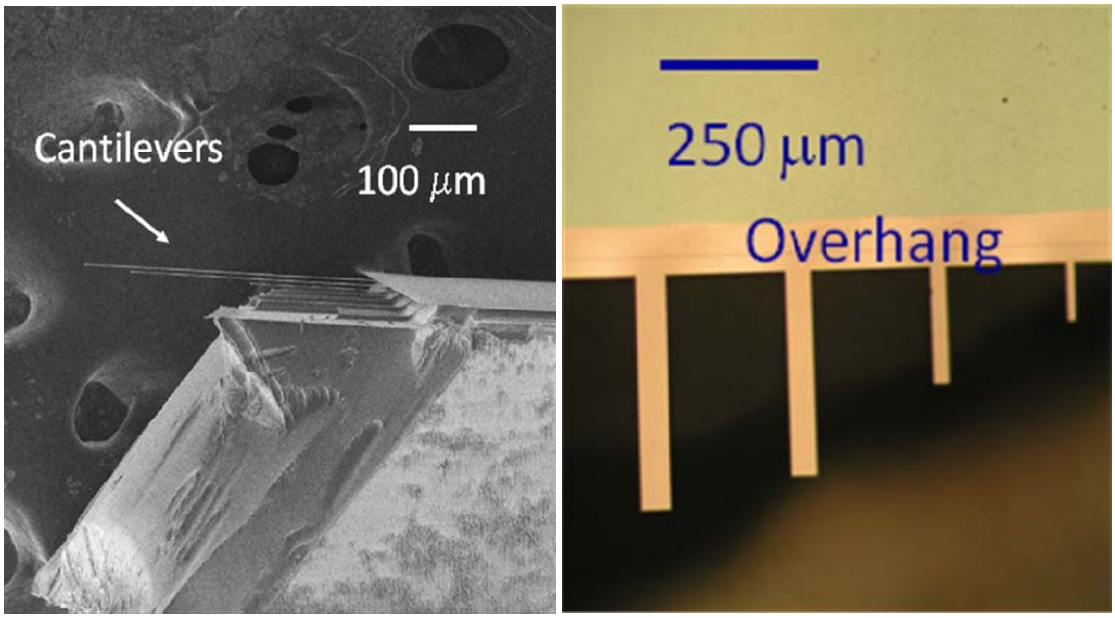

Fig. 3.4.2 (a) SEM image of underside cleaved UNCD cantilevers (b) An optical image of underside cleaved UNCD cantilevers subjected to isotropic etch. Undulating overhang at the cantilever base is due to residual stress.

This procedure ensured that the gap between cantilever and underlying substrate is large (250 μm), so that the laser bouncing of a slightly bent (This curvature is due to residual stress gradient) cantilever can be distinguished by the photosensitive detector (PSD) from light bouncing off from underlying substrate. Similarly, these etch processes resulted in rough substrate surface which limited the reflection from the same. Combination of DRIE and isotropic etch helps to limit the overhang to about 30μm which can be eliminated by focused ion beam milling of both sides of cantilever base as shown in Fig 3.4.3. Dies were then cleaned using a piranha solution (3:1 concentrated sulfuric acid to 30% hydrogen peroxide solution) before being tested under UHV (2×10^{-10}

Torr) conditions on a custom-built AFM stage inserted into a RHK 350 UHV AFM and RHK 750 UHV AFM.

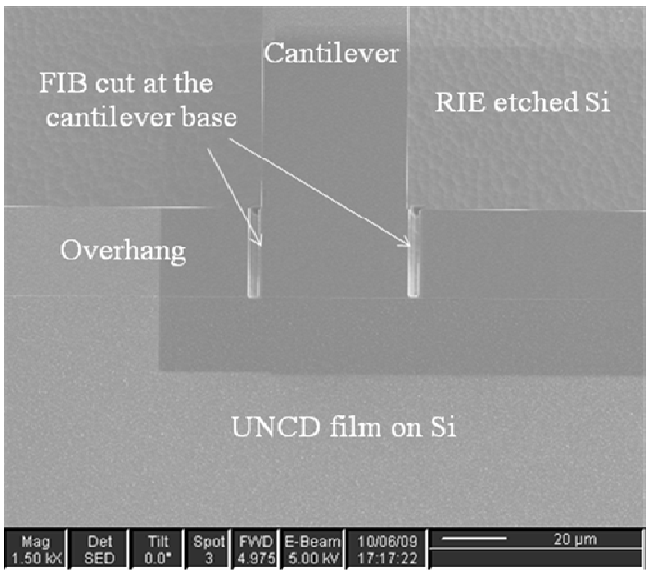

Fig 3.4.3 SEM image of DRIE etched UNCD cantilevers dies after FIB milling the cantilever base to eliminate the overhang.

Dies without cantilevers were also studied to determine the biaxial modulus. XeF_2 dry etching chemistry is used to produce an uninterrupted overhang of UNCD films grown on silicon. This etching method is preferable as the SF_6 reactive ion etch (RIE) also attacks UNCD due to the presence of a small amount of oxygen in the plasma. The amplitude and wavelength of the overhanging portion were measured using a Zygo white light scanning interferometer (NewView 6K). Different overhangs were produced till the film is completely relaxed to determine the biaxial modulus. Zygo interferometer is used to measure the curvature of the released cantilevers. Based on this measurement, we determined that the films have a residual stress gradient of ~75 MPa/μm.

3.5 Elastic properties of UNCD

A. Young's modulus

The measured resonant frequencies of cantilevers of different lengths and overhangs are plotted in Fig. 3.5.1. The resonant frequency for the n^{th} mode of an undamped, freely vibrating cantilever is given by [16]

$$f_n = \frac{\beta_n^2}{2\pi}\frac{t}{L^2}\sqrt{\frac{E}{12\rho}} \tag{3.1}$$

where L and t are the length and thickness of the beam, respectively, and E and ρ are Young's modulus and density, respectively. β_n is a constant equal to ~ 1.875, 4.694, 7.855 for n = 1,2,3 respectively. Therefore, the Young's modulus of the cantilever material can be determined if the mass density and the dimensions are known. Measurements of resonance frequencies *vs.* $1/L^2$ for all cantilevers with overhangs ranging from 5 μm to 85 μm are shown in Fig. 3.5.1(a). In principle, if the mass density is specified, Eq. (3.1) could then be used to determine Young's modulus. However, the presence of an overhang at the cantilever base alters the resonant frequency from the value predicted by Eq. (3.1) by an amount which increases as the lever gets shorter. Therefore, we employed two independent methods to correct for this effect. First, we determined the modulus numerically using the COMSOL multi-physics package (COMSOL Inc. Burlington, MA, USA), accounting for the measured overhang. This yielded a Young's modulus of 790±30 GPa. Second, the Young's modulus was estimated by adding an effective length chosen to give a constant Young's modulus for all the

levers of different lengths.[17] Fig. 4(b) shows such an estimate of the Young's modulus for cantilevers with 85 μm overhang obtained by adding 36 μm to the actual length of the cantilevers. Based on these estimates, we determine the modulus to be 792 ± 38 GPa. There is excellent agreement between the two independent correction methods.

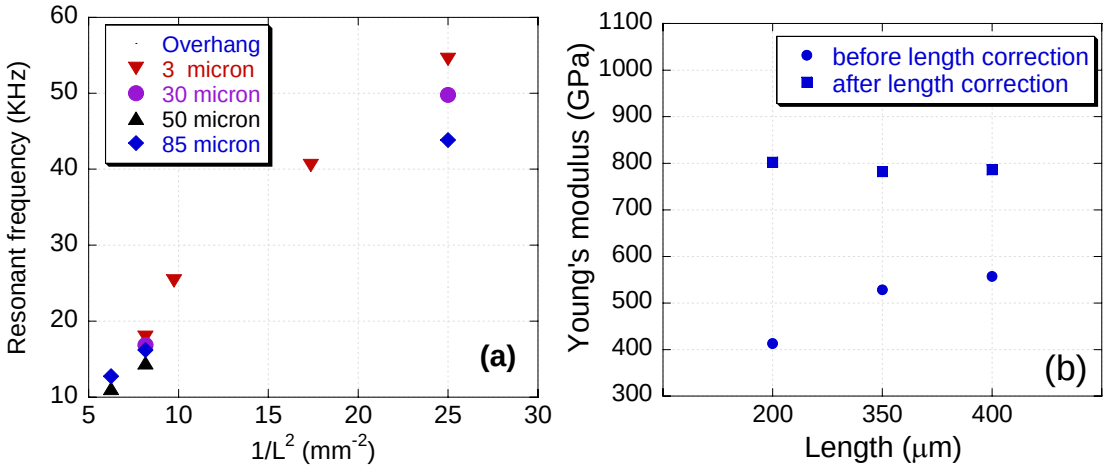

Figure. 3.5.1. (a) First flexural resonance frequency of the cantilevers as a function of the inverse square of the cantilever length. (b) A comparison of the modulus determined from Eq. (3.1) as a function of actual cantilever length, before and after adding an effective length of 30 μm to the actual length of the levers. All three cantilevers were on a single die with an 85 μm overhang.

Both of the calculations of the Young's modulus described above depend linearly of the density of the UNCD films as shown in Eq. 3.1. The density is not known with certainty. For the calculations presented here, the density of the UNCD is assumed to be equal to that of single crystal diamond (3500 kg/m^3). The effect of lower density will be discussed further below. The reported uncertainty of the Young's modulus of individual cantilevers was determined from the accuracy of the thickness of the beams measured in

SEM, which leads to an error of ~ 4% in the measured Young's modulus**.** The Hershey-Kroner-Eshelby averaging procedure for polycrystalline diamond yields a Young's modulus value of 1143 GPa [5]. Thus, the measured Young's modulus is ~20-25% lower than the theoretically calculated value for microcrystalline diamond with randomly oriented grains, [5] and is ~5-15 % lower than the experimentally determined value for the modulus of traditional UNCD films measured using nanoindentation (864 GPa)[2] and beam deflection (916-959 GPa)[1]. However, MPCVD-grown NCD fixed-fixed resonator structures yielded modulus values ranging from 680-980 GPa[18-20], and MPCVD-grown UNCD fixed-fixed resonators grown at 550° C yielded a modulus of 710 GPa.[4] These results are summarized in Table 3.5.1

Film thickness nm	Growth method	Growth temperature (°C)	Grain size (nm)	Young's modulus (GPa)
~1000	HFCVD	680	~5 nm	790 ± 30[21]
870	MPCVD	550	~2-5 nm	710[4]
~500	MPCVD	800	~2-5 nm	916-957[1]
600 - 4100	MPCVD	720	~10-100 nm	500-1120[22]
340	HFCVD	600	~5 nm	440[23]

Table 3.5.1. Comparison of Young's modulus of diamond thin films.

The reasons for the somewhat lower Young's modulus of the UNCD films discussed here compared to traditional MPCVD grown films are not understood at this time. Theoretical studies [24-26] of mechanical properties of UNCD have indicated that the observed Young's modulus strongly depends on the sp^2 content as well as volume

fraction of grain boundaries. Philip *et al*.[22] showed that NCD films (columnar grains, grain size 10-100 nm) can have Young's moduli in the range of 500 GPa – 1120 GPa depending on the initial nucleation densities. UNCD and NCD films all have an initial nucleation layer which can be geometrically irregular, disordered, and lower in density due to voids, and can possess enhanced sp^2 bonding [15, 27]. These factors can reduce the modulus of that layer. Indeed, thinner films of UNCD are reported to have a reduced Young's modulus compared to single crystal diamond, [23] which could be explained by the increased proportion of the level that is composed of this inhomogeneous seed layer.

As mentioned earlier, experimental measurement of density using XRR yielded a value of 3.05 g/cm^3 with the possibility of seeding layer with a much lower density of 2.39 g/cm^3. Taking these into account would produce an even lower Young's modulus for the UNCD. Modeling the cumulative effects of the lower density of the UNCD layer and the seed layer are difficult. This is due to the lack of information about the modulus of seed layer and its structure. In the case of resonator structures which are subjected to fabrication processes, including reactive ion etching, it is challenging to speculate on the nature of the underside, since oxygen present during this process etches both sp^2 and sp^3 carbon at different rates. We have not seen a variation in the modulus of levers that have undergone XeF_2 release and SF_6 RIE release (including for some levers the Deep reactive ion etch process, described earlier in this chapter) or wet etch using hydro fluoric acid (HF).

As well, when the modulus is measured using resonant methods, one should consider the effects of stresses on resonant frequency shifts. Fixed-fixed beams often suffer residual compressive [23] or tensile stresses which can increase or decrease the

resonant frequency. To understand the origins of these differences fully, it is necessary to perform a systematic series of studies comparing UNCD films grown at the same temperature, with similar chemistries, such that both films show similar content of sp^2 and sp^3 bonds, and comparable nanostructures. However, it is reasonable to assume that the different Young's modulus observed for the HFCVD, high temperature (800 °C) grown MPCVD UNCD films, and MCD films may at least partially be attributed to volume fraction of grain boundaries which accommodate some amount of disordered carbon, dangling bonds, hydrogen, seeding method used and initial nucleation densities.

B. Poisson's Ratio

If a compressively-stressed thin film is partially released from its substrate so that it exhibits an overhang, the stress in the film can produce sinusoidal wave-like structures as a means of stress relief. The biaxial modulus, $E/(1-\nu)$, of such compressively-stressed overhanging thin films can be estimated by measuring the period and the amplitude of the sinusoidal waves of the fully relaxed portion of the overhang. This requires that independently measuring the residual compressive stress. As well, the overhanging ledge should be several wavelengths long (in the direction parallel to the edge of the substrate) to avoid boundary effects. [28, 29] To ensure the film is completely relaxed, the film has to be under-etched to produce an overhang until the ratio of amplitude to wavelength does not change with further under-etching. This condition is satisfied when the underetch becomes more than half of the wavelength ($\lambda/2$) of the relaxed overhang. For

the fully relaxed thin films with sinusoidal amplitude A_0 much smaller than thewavelength, the biaxial modulus is given by [28, 30]

$$\frac{E}{1-\nu} \approx \left(\frac{\lambda}{\pi A_0} \right)^2 \sigma_0 \tag{3.2}$$

where σ_0 is the residual compressive stress and ν is the Poisson's ratio of the film. The residual stress was measured using a Tencor profilometer as discussed earlier, and the films were found to have residual compressive stress of 370 ±1 MPa. If the Young's modulus and the residual compressive stress in the film are measured independently, then we can determine the Poisson's ratio ν using:

$$\nu = \frac{E_b - E}{E_b} \tag{3.3}$$

where E_b is the bulk modulus. Residual stress in the film was relieved by underetching the substrate using dry etching as described above. Figure 3.5.2 (a) shows a schematic of periodic wrinkles, and the Zygo interferometric image of the underetched overhang. Figure 3.5.2 (b) shows the ratio of the amplitude of the undulation A_0 to the period λ of the overhanging portion of the film as a function of the overhang length. For overhangs less than 50 μm, periodic undulations are barely observed. Beyond an overhang of 160 μm (~λ/2), the ratio stabilizes to 0.0067. Thus, the film is fully relaxed by this overhang length, and the remaining substrate does not change the stress relaxation behavior of the edge of the film.

Figure 3.5.3 (a) shows the profile of one such overhang taken using the scanning white light interferometer. Figure 3.5.3 (b) shows the line profile of the overhang at the ridge of the sinusoidal undulation. Based on these measurements, we estimate the biaxial modulus to be 838 ± 2 GPa. We assume that biaxial residual stress remains the same throughout the sample. Using the Young's modulus of 790±30 GPa determined using the resonance measurements described earlier, the calculated Poisson's ratio of UNCD is then 0.057±0.038. The large relative error is due to the subtraction of two large, similar values E and E_b to produce a much smaller value.

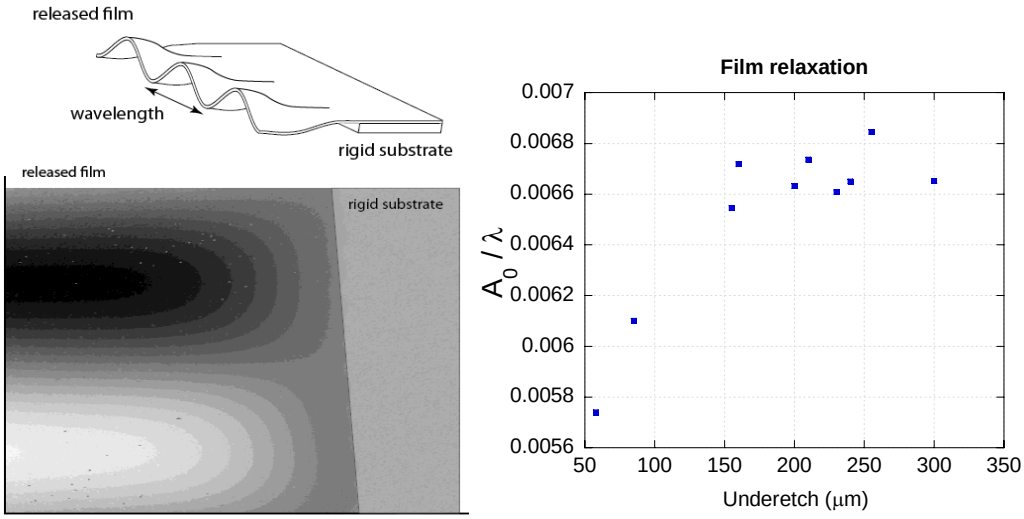

Figure. 3.5.2.(a) A Zygo white light interferometer image of a substrate free overhang and a schematic of the same. (b) Ratio of amplitude to wavelength of the overhang as a function of the overhang length(for several different samples). For overhangs between 50 μm and 160 μm, the UNCD film is not fully relaxed from residual stress present in the substrate. Beyond 160 μm, A_0/λ does not change with further etch depths.

The theoretical value of Poisson's ratio of polycrystalline diamond with randomly oriented grains and ignoring the contribution of grain boundaries is 0.069, based on the Hershey-Kroner-Eshelby averaging method [5]. A low Poisson's ratio is a unique property of sp^3 tetragonal bonded carbon, which shows a higher elastic resistance to bond bending compared to bond stretching. However, for UNCD films, which have a significant proportion of grain boundaries containing sp^2 bonded carbon, the Poisson's ratio may be expected to be higher than the theoretically predicted value for polycrystalline diamond. For example, the Poisson's ratio of tetrahedral amorphous carbon (ta-C) films, which contain much higher sp^2 bonding than UNCD (~20% of the bonds are sp^2 in ta-C) is 0.202±0.054.[31] In comparison with polycrystalline diamond, UNCD grain boundaries are atomically abrupt.[32] The influence of grain size on Poisson's ratio has recently been modeled.

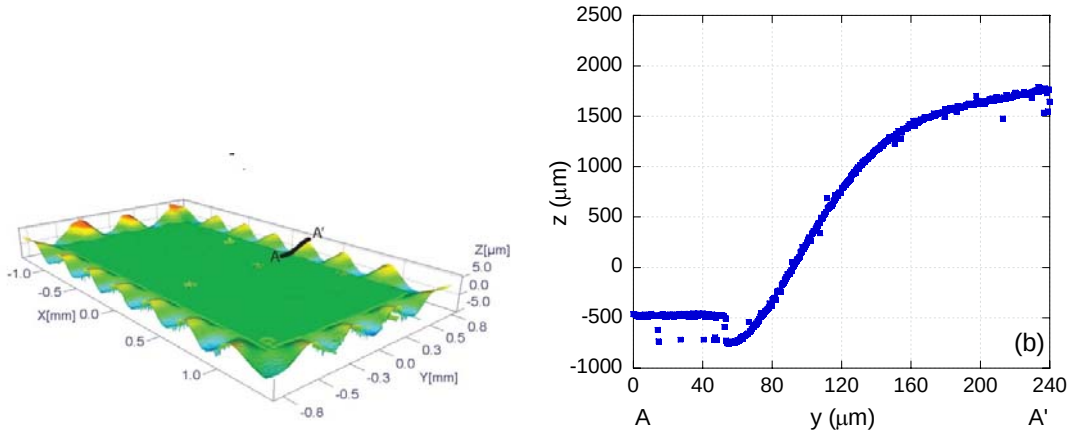

Figure. 3.5.3. (a) Interferometric image of the UNCD film with a 255 µm etched overhang. (b) Line scan of the section shown in 7a showing a near saturation beyond 160 µm. The apparent jump in the height at the base of the overhang is simply due to the change in reflectivity from the more reflective underlying substrate.

A theoretical prediction for Poisson's ratio of UNCD (calculated from Young's modulus and the bulk modulus) yielded a value of 0.07 for a grain size of 4.41 nm. In the modeled material, there was significant (9.12%) non-diamond (sp^2) content [26], which is substantially more than the sp^2 content of 4.3% that we measured for our films using NEXAFS. This suggests that a low Poisson's ratio can still be preserved even with significant sp^2 content. One limitation of this model is that it does not consider effects of the presence of hydrogen in grain boundaries [9]. As well note that the value of Poisson's ratio measured here, like the value for *E,* does depend on the mass density. The mass density could be lower for UNCD as compared to the value single crystal diamond, which we have used in our calculations. A lower density reduces the calculated modulus and hence increases the measured Poisson's ratio. Regardless, overall this model demonstrates that the low Poisson's ratio we have measured is a reasonable finding.

C. Acoustic velocity:

As discussed in Chapter 1, for high frequency resonator structures, one of the most important material parameters is the acoustic velocity. This can be determined accurately by resonance frequency measurements. The longitudinal acoustic velocity can be determined using the following equation,

$$V_L = 6.184 \frac{fL^2}{h} \sqrt{\frac{1-\nu}{(1+\nu)(1-2\nu)}} \tag{3.4}$$

where *f* is the resonant frequency of the beam. Using the measured values of Poisson's ratio and Young's modulus we determined the longitudinal acoustic velocity to be 15.1 ±

0.3 km/s. This compares very well with UNCD films grown with MPCVD technique (Table 3.1.1) [4]. The acoustic velocity of UNCD films measured here is much higher than other thin film MEMS materials such as silicon (8.8 km/s), silicon nitride (11.8 km/s), and aluminum nitride (11.4 km/s), and is only lower than that of theoretically predicted value of polycrystalline diamond (18 km/s) as shown in the bar graph. The values quoted for Si, polycrystalline diamond (Poly-D), and SiC are from ref. [33]. The value for AlN is from ref. [34]. The value for UNCD is from this work. This is a critical advantage for the use of UNCD films in high frequency devices.

References:

[1] H. D. Espinosa, B. C. Prorok, B. Peng, K. H. Kim, N. Moldovan, O. Auciello, J. A. Carlisle, D. M. Gruen, and D. C. Mancini, "Mechanical properties of ultrananocrystalline diamond thin films relevant to MEMS/NEMS devices," *Experimental Mechanics,* vol. 43, pp. 256-268, Sep 2003.

[2] A. V. Sumant, Auciello, A. R. Krauss, D. M. Gruen, D. Ersoy, J. Tucek, A. Jayatissa, E. Stach, N. Moldovan, D. Mancini, H. G. Busmann, and E. M. Meyer, "Fabrication of MEMS Components Based on Ultrananocrystalline Diamond Thin Films and Characterization of Mechanical Properties," *Mater. Res. Soc. Symp. Proc,* vol. 657, 2000.

[3] D. A. Czaplewski, J. P. Sullivan, T. A. Friedmann, and J. R. Wendt, "Temperature dependence of the mechanical properties of tetrahedrally coordinated amorphous carbon thin films," *Applied Physics Letters,* vol. 87, p. 161915, 2005.

[4] O. Auciello, S. Pacheco, A. V. Sumant, C. Gudeman, S. Sampath, A. Datta, R. W. Carpick, V. P. Adiga, P. Zurcher, M. Zhenqiang, Y. Hao-Chih, J. A. Carlisle, B. Kabius, J. Hiller, and S. Srinivasan, "Are Diamonds a MEMS' Best Friend?," *Microwave Magazine, IEEE,* vol. 8, pp. 61-75, 2007.

[5] C. A. Klein, "Anisotropy of Young's modulus and Poisson's ratio in diamond," *Materials Research Bulletin,* vol. 27, pp. 1407-1414, 1992.

[6] C. Sungwoo, C. Ioannis, A. F. Thomas, and P. S. John, "Young's modulus, Poisson's ratio and failure properties of tetrahedral amorphous diamond-like carbon for MEMS devices," *Journal of Micromechanics and Microengineering,* p. 728, 2005.

[7] N. Sepulveda, L. Jing, D. M. Aslam, and J. P. Sullivan, "High-Performance Polycrystalline Diamond Micro- and Nanoresonators," *Microelectromechanical Systems, Journal of,* vol. 17, pp. 473-482, 2008.

[8] F. Szuecs, M. Werner, R. S. Sussmann, C. S. J. Pickles, and H. J. Fecht, "Temperature dependence of Young's modulus and degradation of chemical vapor deposited diamond," *Journal of Applied Physics,* vol. 86, pp. 6010-6017, 1999.

[9] C. Liu, X. C. Xiao, J. Wang, B. Shi, V. P. Adiga, R. W. Carpick, J. A. Carlisle, and O. Auciello, "Dielectric properties of hydrogen-incorporated chemical vapor deposited diamond thin films," *Journal of Applied Physics,* vol. 102, p. 7, Oct 2007.

[10] R. P. Chin, J. Y. Huang, Y. R. Shen, T. J. Chuang, and H. Seki, "Interaction of atomic hydrogen with the diamond C(111) surface studied by infrared-visible sum-frequency-generation spectroscopy," *Physical Review B,* vol. 52, p. 5985, 1995.

[11] C. Su, K. J. Song, Y. L. Wang, H. L. Lu, T. J. Chuang, and J. C. Lin, "Hydrogen chemisorption and thermal desorption on the diamond C(111) surface," *The Journal of Chemical Physics,* vol. 107, pp. 7543-7558, 1997.

[12] C. Lenardi, P. Piseri, V. Briois, C. E. Bottani, A. L. Bassi, and P. Milani, "Near-edge x-ray absorption fine structure and Raman characterization of amorphous and nanostructured carbon films," *Journal of Applied Physics,* vol. 85, pp. 7159-7167, 1999.

[13] A. R. Krauss, O. Auciello, D. M. Gruen, A. Jayatissa, A. Sumant, J. Tucek, D. C. Mancini, N. Moldovan, A. Erdemir, D. Ersoy, M. N. Gardos, H. G. Busmann, E. M. Meyer, and M. Q. Ding, "Ultrananocrystalline diamond thin films for MEMS and moving mechanical assembly devices," *Diamond and Related Materials,* vol. 10, pp. 1952-1961, 2001.

[14] R. J. Cannara, M. J. Brukman, K. Cimatu, A. V. Sumant, S. Baldelli, and R. W. Carpick, "Nanoscale friction varied by isotopic shifting of surface vibrational frequencies," *Science,* vol. 318, pp. 780-783, Nov 2007.

[15] A. V. Sumant, D. S. Grierson, J. E. Gerbi, J. Birrell, U. D. Lanke, O. Auciello, J. A. Carlisle, and R. W. Carpick, "Toward the ultimate tribological interface: Surface chemistry and nanotribology of ultrananocrystalline diamond," *Advanced Materials,* vol. 17, pp. 1039-+, Apr 2005.

[16] A. N. Cleland, *Foundations of Nanomechanics*. Heidelberg, New York: Springer Verlag, 2003.

[17] E. Q. J. Mencik, "Determination of elastic modulus of thin films and small specimens using beam bending methods," in *Journal of Materials Research*. vol. 14, 1999, pp. 2152-2161

[18] L. Sekaric, J. M. Parpia, H. G. Craighead, T. Feygelson, B. H. Houston, and J. E. Butler, "Nanomechanical resonant structures in nanocrystalline diamond," *Applied Physics Letters,* vol. 81, pp. 4455-4457, 2002.

[19] T. H. Metcalf, X. Liu, B. H. Houston, J. W. Baldwin, J. E. Butler, and T. Feygelson, "Low temperature internal friction in nanocrystalline diamond films," *Applied Physics Letters,* vol. 86, pp. 081910-3, 2005.

[20] A. B. Hutchinson, P. A. Truitt, K. C. Schwab, L. Sekaric, J. M. Parpia, H. G. Craighead, and J. E. Butler, "Dissipation in nanocrystalline-diamond nanomechanical resonators," *Applied Physics Letters,* vol. 84, pp. 972-974, 2004.

[21] V. P. Adiga, A. V. Sumant, S. Suresh, C. Gudeman, O. Auciello, J. A. Carlisle, and R. W. Carpick, "Mechanical stiffness and dissipation in ultrananocrystalline diamond microresonators," *Physical Review B (Condensed Matter and Materials Physics),* vol. 79, pp. 245403-8, 2009.

[22] J. Philip, P. Hess, T. Feygelson, J. E. Butler, S. Chattopadhyay, K. H. Chen, and L. C. Chen, "Elastic, mechanical, and thermal properties of nanocrystalline diamond films," *Journal of Applied Physics,* vol. 93, pp. 2164-2171, 2003.

[23] M. Imboden and P. Mohanty, "Evidence of universality in the dynamical response of micromechanical diamond resonators at millikelvin temperatures," *Physical Review B (Condensed Matter and Materials Physics),* vol. 79, pp. 125424-5, 2009.

[24] J. T. Paci, T. Belytschko, and G. C. Schatz, "The mechanical properties of single-crystal and ultrananocrystalline diamond: A theoretical study," *Chemical Physics Letters,* vol. 414, pp. 351-358, Oct 2005.

[25] J. T. Paci, T. Belytschko, and G. C. Schatz, "Mechanical properties of ultrananocrystalline diamond prepared in a nitrogen-rich plasma: A theoretical study," *Physical Review B,* vol. 74, p. 9, Nov 2006.

[26] I. N. Remediakis, G. Kopidakis, and P. C. Kelires, "Softening of ultra-nanocrystalline diamond at low grain sizes," *Acta Materialia,* vol. 56, pp. 5340-5344, 2008.

[27] A. V. Sumant, D. S. Grierson, J. E. Gerbi, J. A. Carlisle, O. Auciello, and R. W. Carpick, "Surface chemistry and bonding configuration of ultrananocrystalline diamond surfaces and their effects on nanotribological properties," *Physical Review B (Condensed Matter and Materials Physics),* vol. 76, p. 235429, 2007.

[28] R. T. Howe and R. S. Muller, "Stress in polycrystalline and amorphous silicon thin films," *Journal of Applied Physics,* vol. 54, pp. 4674-4675, 1983.

[29] P. G. Borden, "A simple technique for determining the stress at the Si/SiO[sub 2] interface," *Applied Physics Letters,* vol. 36, pp. 829-831, 1980.

[30] S.-J. Cho, J.-W. Chung, and K.-R. Lee, "Characterization of the mechanical properties of diamond-like carbon films," *Diamond and Related Materials,* vol. 14, pp. 1270-1276, 2005.

[31] S. Cho, I. Chasiotis, T. A. Friedmann, and J. P. Sullivan, "Young's modulus, Poisson's ratio and failure properties of tetrahedral amorphous diamond-like carbon for MEMS devices," *Journal of Micromechanics and Microengineering,* vol. 15, pp. 728-735, Apr 2005.

[32] O. Auciello, S. Pacheco, A. V. Sumant, C. Gudeman, S. Sampath, A. Datta, R. W. Carpick, V. P. Adiga, P. Zurcher, Z. Ma, H. C. Yuan, J. A. Carlisle, B. Kabius, J. Hiller, and S. Srinivasan, "Are diamonds a MEMS' best friend?," *Ieee Microwave Magazine,* vol. 8, pp. 61-75, Dec 2007.

[33] W. Jing, J. E. Butler, D. S. Y. Hsu, and T. C. Nguyen, "CVD polycrystalline diamond high-Q micromechanical resonators," in *Micro Electro Mechanical Systems, 2002. The Fifteenth IEEE International Conference on*, 2002, pp. 657-660.

[34] M. B. Assouar, O. Elmazria, L. Le Brizoual, and P. Alnot, "Reactive DC magnetron sputtering of aluminum nitride films for surface acoustic wave devices," *Diamond and Related Materials,* vol. 11, pp. 413-417, 2002/6//.

Chapter 4. Thermomechanical stability of UNCD films

4.1 Background

The temperature dependence of the mechanical properties, specifically the elastic constants, of single crystal diamond and polycrystalline diamond films have been measured previously either using acoustic reflection methods [1], by measuring the shift in the resonant frequency of a vibrating beam [2-4], or by independently measuring[5] mechanical properties using dynamical methods. Some of these studies involved Brillouin scattering [6]. However, experimental investigations of the low temperature (< 300K) mechanical properties of single crystal diamond are rare. There are only two articles [1, 2] to date which report measurements of the low temperature mechanical properties of single crystal diamond. This is due to the fact that changes in the modulus of diamond are extremely small (<0.1% from 0 K to 300 K). As well, diamond has an extremely high acoustic velocity (18 km/s) which makes it difficult to detect these changes in acoustical measurements.

The temperature dependence of the mechanical properties is strongly affected by the specific heat, and this will be discussed later in this Chapter. Single crystal diamond has an extremely high Debye temperature (1860 K) and even at room temperature the specific heat follows a T^3 temperature dependence, which is the low-temperature limiting behavior predicted from Debye theory. Hence, the relative reduction in modulus at finite temperature is much lower than many metals and other materials relevant for MEMS, including silicon, silicon nitride, silicon carbide, and aluminum nitride. It is therefore interesting to study whether this stable behavior occurs in UNCD, since the

nanostructure, grain boundaries, and other defects may affect the temperature dependence of the modulus.

To determine the expected minute changes in the modulus, we measured shifts in the resonant frequency of UNCD cantilevers *versus* temperature under UHV conditions. UHV conditions are necessary to limit the condensation of molecular contaminants onto the resonators as the temperature is reduced. In addition, damping due to a surrounding gas, which is what will dominate the damping of these cantilevers at ambient pressure, is eliminated in vacuum. Shifts in the resonant frequency can be correlated with the corresponding change in the modulus according to Eq. 3.1. and is given by:

$$\frac{df}{dT} \propto \frac{1}{2}\frac{dE}{dT} \tag{4.1}$$

The changes in the dimension of the cantilever due to thermal contraction or expansion and changes in the density with temperature together contributes to an error of the order of coefficient of thermal expansion (1×10^{-6} /K for single crystal diamond) and can be neglected. To make a comparison between temperature dependent properties of different materials, a parameter called the temperature coefficient of frequency (TCF) is commonly used. It is defined as

$$TCF = \frac{\Delta f}{f_0 \times \Delta T}(in\ ppm/K) \tag{4.2}$$

where f_0 is the resonant frequency at room temperature, and Δf is the shift in the resonant frequency from 260 K to 320 K (ΔT =60). A low TCF is important for applications in adsorbed mass sensing where thermal fluctuations can overwhelm the change in resonant frequency due to the adsorbed mass. Similarly, it is important for stable high frequency

filters. An *XY*-cut quartz crystal has an extremely stable resonant frequency near room temperature and hence is used commercially as a mass sensor as well for filters in electronic circuits. Therefore, the determination of the TCF for UNCD is interesting scientifically and important technologically. There are only a few measurements of the temperature dependence of the resonant frequency of diamond resonators, and prior to this work, none for low temperature measurements of UNCD.

4.2. Temperature dependence of Young's modulus

The elastic modulus of materials at 0 K strongly depends on atomic bond energy ($E_B(0)$) and the bond length (d_0). At finite temperatures, the atoms absorb thermal energy and vibrate around their mean positions. Within the bond lengths sampled by these oscillations, the potential is harmonic and hence there is no expansion in bond length or reduction in the elastic modulus. Hence at low temperatures, the modulus has negligible temperature dependence. However, as the temperature further rises, the anharmonic character of the potential begins to be sampled by the atoms. In particular, the potential well becomes wider at larger separations. This causes the bonds to expand overall, and become less stiff. As a result, the modulus reduces with temperature [7-9] [10]. At higher temperatures, most materials show a linear reduction in the Young's modulus with increasing temperature. A typical temperature dependence of Young's modulus is shown in Figure 4.1.

The analytical solution to thermally driven softening of the Young's modulus has been a challenge. Wachtman *et al.* [8] developed an empirical solution for temperature dependent modulus:

$$E(T) = E_0 - AT\exp\left(-\frac{T_0}{T}\right) \tag{4.3}$$

where E_0 is the Young's modulus at 0 K. Watchtman assumed that A is a temperature-independent constant related to the Grueneisen parameter γ, and T_0 is characteristic temperature related to the Debye temperature, Θ_D. Later, Anderson *et al.* [9] derived an equation for the temperature-dependent bulk modulus by taking into account anharmonic effects of lattice vibrations:

$$\begin{aligned} B_S(T) &= B_0 - \frac{\gamma\delta}{V_0}U \\ &= B_0 - \frac{\gamma\delta}{V_0}3RT \times H\left(\frac{\Theta_D}{T}\right) \end{aligned} \tag{4.4}$$

where B_0 and V_0 are the bulk modulus and specific volume per average atom at 0 K respectively. U is the thermal energy, R is the ideal gas constant, δ is Anderson-Grueneisen parameter, and $H(x)$ is given by

$$H(x) = \frac{3}{x^3}\int_0^x \frac{x^3}{e^x - 1}dx \tag{4.5}$$

.

We can rewrite this equation in terms of the specific heat c_v:

$$B_S(T) = B_0 - \frac{\gamma\delta}{V_0}\int_0^T c_v dT \tag{4.6}$$

.

This relation assumes that temperature-dependent volume changes are negligible, and γ and δ are temperature-independent [9]. In terms of Young's modulus we can write this relationship as:

$$E_S(T) = E_0 - \frac{\gamma\delta}{3V_0}\int_0^T c_v dT \quad . \tag{4.7}$$

This relation assumes that $E_S \approx 3B_S$ (Poisson's ratio ν << 1) and that ν has negligible temperature dependence. [7] Taking the first derivative with respect to *T*, we obtain:

$$\frac{\partial E_S(T)}{\partial T} \propto c_v \quad . \tag{4.8}$$

At low temperatures specific heat reduces and has a T^3 dependence and is zero at 0 K. Hence at very low temperature, the predicted rate of change of the bulk modulus and Young's modulus with temperature decreases and is zero at 0 K so as to satisfy the Nernst Law [7]. In the high temperature limit, the specific heat saturates (3R) and we see a linear reduction in modulus with temperature. In this high temperature limit, the Debye temperature can be estimated by comparing (4.7) and (4.3). This yields, $A = \frac{R\gamma\delta}{V_0}$ and $T_0 \approx \frac{\Theta_D}{2}$ [9].

4.3 Temperature dependence of elastic properties of diamond and nanocrystalline solids

The temperature dependence of the elastic constants, including Young's modulus, for single crystal diamond has been studied [2, 5, 6] and theoretically predicted previously [11]. As shown in Fig. 4.1, the rate of change of the Young's modulus of single crystal diamond with respect to temperature is dramatically reduced below 150 K.

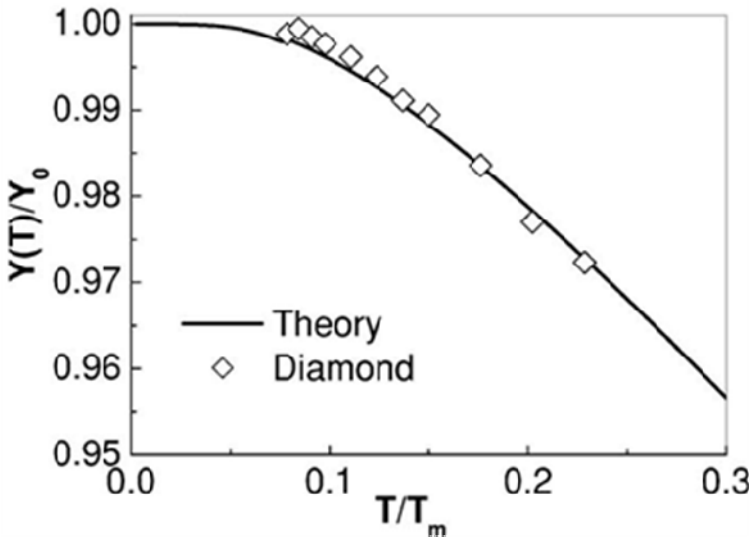

Figure 4.1. Temperature dependence of Young's modulus (the authors have used symbol of *Y* instead of E) of single crystal diamond and tetrahedral amorphous carbon (ta-C)[11]. Melting temperature (T_m) of single crystal diamond is 3820 °K.

However, in nanoscale materials the temperature dependence of the specific heat and the elastic moduli can be substantially different than that of bulk materials. Recent progress [12] has shown that it is possible to correlate changes in the Young's modulus of nanoscale particles (nanoparticles, shells, or rods, as opposed to nanostructured bulk materials) to atomistic parameters [10, 13] by the bond-order-length-strength (BOLS)

correlation, by taking into account the bond nature, bond order, bond length, and bond strength. Broken bonds at the surfaces can make the remaining bonds stronger or weaker, depending on the nature of bond, co-ordination number, and bond length. In metals, a higher fraction of surface atoms results in lower elastic moduli, and a higher temperature dependence of the moduli and specific heat at lower temperatures.[12, 13] However, in silicon, which has much stronger bonds than metals, a higher fraction of surface atoms results in higher moduli and a lower specific heat at low temperature. [12] There exists a core-shell structure, wherein undercoordinated surface atoms can have different local bulk moduli compared to the core. M. X. Gu *et al.* [13] proposed expressions for the size and temperature dependence of Young's modulus and the Debye temperature of nanoscale materials. Gu also showed that the Young's modulus, specific heat, and Debye temperature of nanoscale materials can increase or decrease compared to the bulk depending on the nature of the bonds, size of the nanostructure and temperature [13].

In extended nanocrystalline solids however, we have solid interfaces (grain boundaries), wherein some of the bonds are broken but others are not. Grain boundaries also contain undercoordinated atoms, strained bonds, and impurities. The temperature dependence of the thermal properties of nanocrystalline solids at low temperatures can be significantly different than nanoscale materials, since long wavelength phonons are allowed. Similarly, nanocrystalline solids can have very different thermal properties compared to bulk single crystals, since high frequency phonons are scattered by grain boundaries. The vibrational density of states (VDOS) can be significantly different in nanocrystalline solids compared to bulk crystals or nano crystals which strongly influences the specific heat and it can significantly deviates from the T^3 dependence. We

can expect there to be some degree of size effects at high vibrational frequencies, but at low frequencies the influence of the VDOS will be characterized by the intrinsic properties of the grain boundaries. Recalling that these can account for approximately 30% of the atoms in the solid, these effects may be significant. Thus, measurements of the temperature dependence of the elastic properties will be helpful in understanding the influence of grain boundaries in UNCD and nanocrystalline solids more generally. As mentioned before, such measurements also provide extremely useful and important data for implementing UNCD in high frequency devices. Further discussion on the influence of grain boundaries will provided in later in this chapter in the context of the experimental results we have obtained.

4.4 Experimental results

4.4.1 Temperature dependence of resonant frequency, and influence of overhang

Our measurements of the temperature dependence of the resonance frequency were typically performed from 63 K to 450 K (Fig. 4.2). The upper and lower temperature limits we can reach are determined by heat exchange between the sample stage and the rest of the chamber in the UHV AFM system. Even though it is possible to reach 1000 K with the built-in heater, the Curie temperature of the actuation piezo and the softening temperature of the solder joints limit the maximum attainable temperature to approximately 450 K. The thermocouple on the top of the die is calibrated before mounting it onto the stage. The AFM has three different thermocouples which independently measure the temperature at the cryostat, the sample stage, and on top of the

sample itself. While the cryostat can be cooled to 10 K, the stage and the sample can only be cooled to ~60 K.

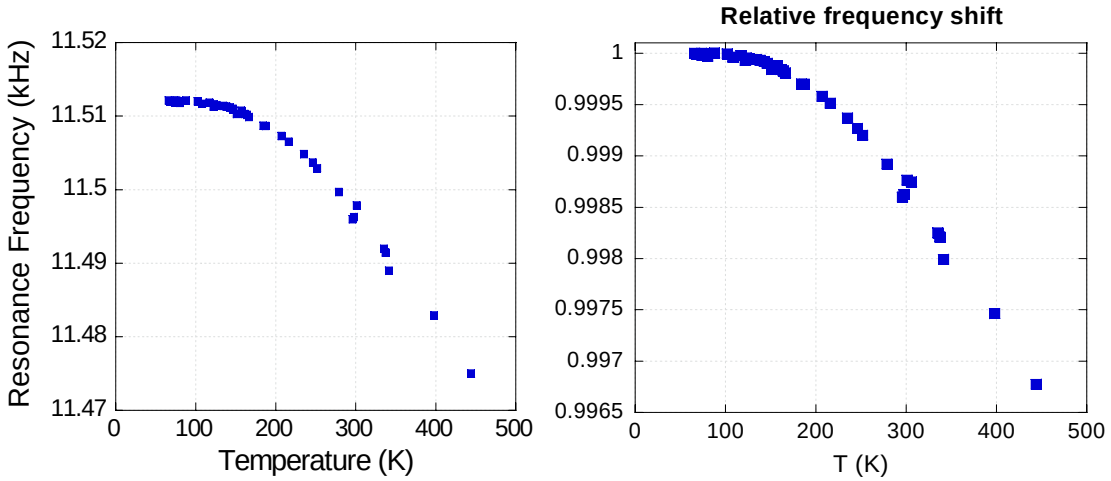

Figure 4.2. (a) The temperature dependence of the resonant frequency of UNCD cantilever with no overhang. (b) The relative change in the corresponding resonant frequency. Overhangs of the cantilever were reduced by FIB cuts at the cantilever base. These curves include data points taken during both heating and cooling cycles and are reproducible. Heating and cooling rates are approximately 1 K/ min.

Fig. 4.2. shows the resonant frequency shift with temperature for a typical, overhang-free UNCD cantilever. For all the measured cantilever beams, we observed little change in the resonant frequency below 160 K, followed by a transition to a nearly linear decrease with frequency. Overall, the resonant frequency reduction is only 0.3% over the whole temperature range. The TCFs of the resonators were approximately ~13.5 ppm/K near room temperature. This is among the lowest measured TCF of all materials (see Table 4.1), and is only 8% higher than the predicted value for single crystal diamond (averaged over all directions) and the measured value nanocrystalline diamond disk resonators.

Table 4.1 lists the TCF for most promising MEMS materials. Except for nanocrystalline diamond and polycrystalline silicon, UNCD has the lowest temperature dependence of resonant frequency. The polycrystalline silicon measurements are reported only once, and the measurements were performed using capacitive technique which requires a metal layer deposited directly onto the Si structure. Hence the resultant shift in the frequency may not be intrinsic.

Material	Type of resonator	TCF (ppm/K)
Silicon	Cantilever	50 [14]
Silicon carbide	Comb drive	22.3 [15]
Aluminum nitride	Contour mode	25 [16]
Polycrystalline diamond (grain size >100 nm)	Disk	12.1 [17, 18]
Polycrystalline silicon	Fixed-fixed	12.5 [19]
UNCD	Cantilever	13.5 - present work
Polycrystalline diamond (grain size ~300 nm)	Cantilever	18.5-25.5 [4]

Table 4.1. A comparison of the TCF of different MEMS materials. Only polycrystalline diamond[17] and polycrystalline silicon (with a metal coating) [19] show a lower TCF than UNCD (present work). Single crystal silicon [7] and silicon carbide[15], aluminum nitride[16, 20], silicon nitride[20] show a much stronger temperature dependence.

Cantilevers are stress-free structures and hence the frequency shifts are intrinsic to the material. However, even though the cantilevers are free of stress, the overhangs at their base are not. Residual compressive stresses in UNCD films result in wrinkles at overhanging cantilever bases, as discussed in Chapter 3. Residual stresses are partly due

to thermal mismatch stresses which change as a function of temperature, as does the period and amplitude of the wrinkles at the cantilever base. A discussion regarding the evolution of this curvature is provided in Chapter 3. Even though changes in the thermal expansion coefficient contribute negligibly to the changes in resonant frequency, the changes in thermal stresses can significantly alter the temperature-dependent response of the resonant frequency for resonators which have wrinkles at their base.

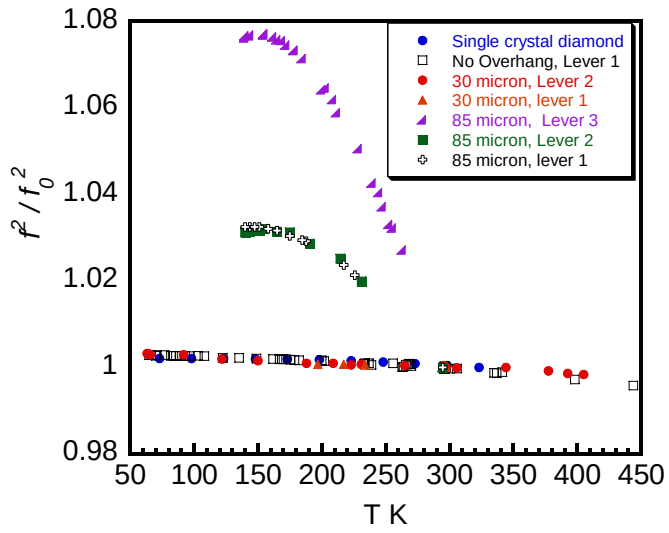

Figure 4.4. Temperature dependence of the resonant frequency for cantilevers with overhangs ranging from 0 (no overhang) to 85 μm overhang. The square of resonant frequency is propositional to modulus, and is compared with that of single crystal diamond (averaged over all directions). Above 55 μm of overhang, wrinkles start to form and the temperature dependence of the modulus strongly depends on the length of cantilever and its position on the wrinkles. Levers are numbered from 1 to 4, largest (400 μm) to smallest (100 μm).

We investigated the effects due to the presence of wrinkles at the cantilever base on the temperature dependence of the resonant frequency for these cantilever beams. For cantilevers with small or negligible overhangs, the shift in the resonant frequency compares very well with that of the single crystal diamond, as shown Figure 4.3. However, for larger overhangs (for overhangs >55 μm, wrinkles form at the base) we observed that smaller cantilever beams had a higher temperature coefficient of frequency compared with larger ones. This indicates that wrinkles strongly influence the observed shifts. The observed frequency shifts were also strongly dependent on the position of the cantilever with respect to the wrinkle feature, *i.e.*, on a trough, a ridge, or in between.

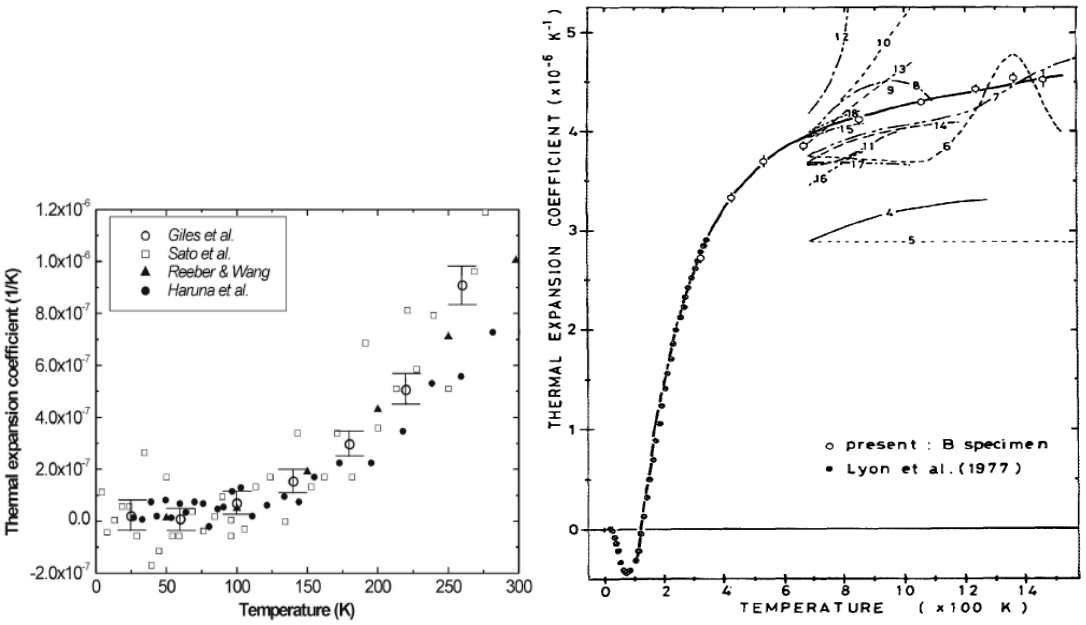

Figure 4.4. Thermal expansion coefficient of diamond [21] and silicon[22]. Below 150 K thermal expansion of diamond is negligible and for silicon it reverses the sign.

We observed a slight increase in the resonant frequency for cantilevers (2 of them) with 85 μm of overhang as we increased the temperature from 138 K to 160 K. Fig. 4.4 shows the thermal expansion coefficient of single crystal diamond (a) and silicon (b) respectively. Thermal mismatch between single crystal diamond and silicon decreases as the temperature is reduced and changes sign below 160 K. A slight increase in the resonant frequency with temperature from 138 K to 160 K could be due to a reduction in the thermal mismatch stress due to the fact that thermal mismatch changes from negative to positive. Further studies are needed to understand the effects of overhang on the shift in the resonant frequency of the beams with temperature. However, since we had structures available with no wrinkling at the base because of a sufficiently short overhang (Fig. 4.2), we are confident that those results represent intrinsic mechanical behavior of UNCD. Clearly, it is critical to use cantilevers with sufficiently low overhangs to investigate the true nature of the resonant frequency shifts and the associated thermo-mechanical properties in materials made of these cantilevers.

4.4.2 Thermomechanical stability of UNCD films

The relative change in the Young's modulus of UNCD in comparison with single crystal diamond and silicon is shown in Figure 4.5. Single crystal diamond values are averaged over all directions using the Voigt-Reuss-Hill approximation. [1, 2] The experimental results for single crystal diamond match theoretical predictions very well. [11, 13, 23-25] UNCD shows a slightly higher temperature dependence than single crystal diamond, but a much lower dependence than that of single crystal silicon. This is an extremely important practical result which demonstrates the suitability of UNCD for variable-temperature resonators and other applications.

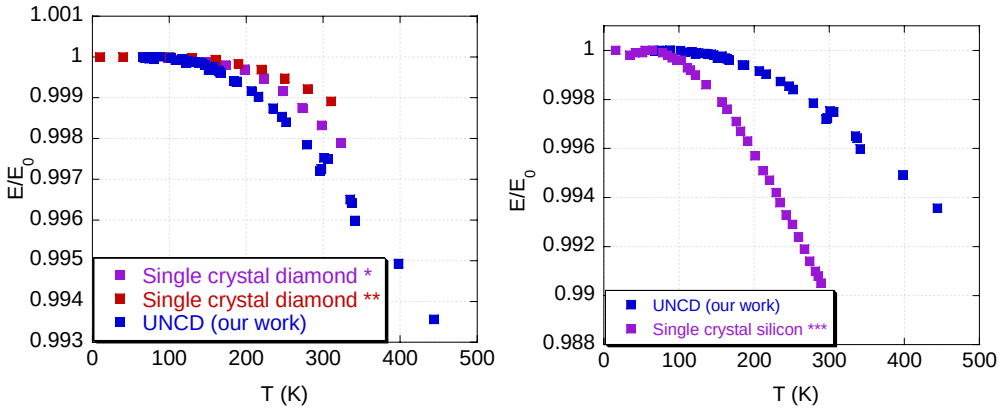

Figure 4.5 (a) Temperature dependence of Young's modulus of UNCD in comparison with single crystal diamond. Data for single crystal diamond are from references [2] (**) and [1] (*). A comparison with single crystal silicon is provided in (b) [7].

In order to understand the temperature-dependent properties of UNCD below 300 K, it is important to consider the contribution from the grain boundaries which account for considerable a volume fraction of UNCD. Grain boundaries are locations of impurities such as hydrogen [14], and defects. Carbon atoms at the grain boundaries may be two-fold (sp^1) and three-fold (sp^2) coordinated, or may form bonds at different lengths or angles from those observed in diamond due to the grain boundary structure. Even though bonds between two-fold coordinated sp^1 atoms or between three-fold coordinated sp^2 atoms are normally stronger than bonds between fourfold coordinated sp^3 atoms, bonds between sp^2 or sp^1 atoms are stabilized by p-bonding, which is very sensitive to the geometry [26]. As a consequence, the local bulk moduli of sp^1 and sp^2 atoms could to be significantly lower than the bulk moduli of sp^3 atoms [27]. Recently, an atomistic model of UNCD was conducted by Remdiakis *et al.* [27] who determined the mechanical

properties of UNCD films as a function of grain size, finding a reduction in modulus with grain size. The simulations were performed using a continuous-space Monte Carlo method using many body Tersoff potential. Figure 4.6 shows a map of local bulk moduli of atoms at grain boundaries compared to atoms within the individual grains [27] which show large fraction of atoms with lower local bulk modulus compared to atoms within the grains. Such weaker bonds will then bend or stretch with greater ease compared to the bonds in the crystalline region, and may have a different (*i.e.*, stronger) temperature dependent behavior.

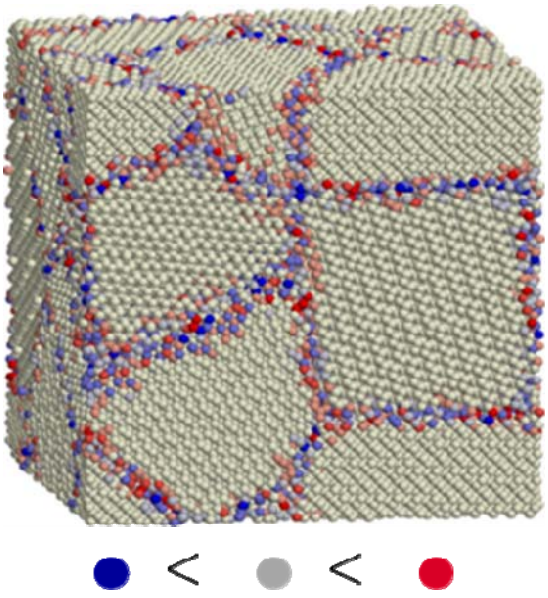

Figure 4.6 Map of local bulk moduli in UNCD.[27] Atoms at grain boundaries have higher or lower local bulk moduli compared to bulk of the atoms in the grains depending on coordination number.

Interestingly, the temperature dependence of Young's modulus for microcrystalline diamond (MCD) films (grain size ~100 μm) has been measured to be much higher compared with either single crystal diamond or UNCD [5]. The measurement was performed using a dynamic mechanical analyzer (DMA) with temperature variation capability. The MCD film exhibited an increase of approximately 3% in modulus compared to less than 0.2% for single crystal diamond (averaged over all directions) as the sample was cooled from room temperature to 150 K, below which the changes were negligible. We do not know the reason for the higher temperature dependence of MCD films. However, it could be due to larger and weaker grain boundaries compared to UNCD (grain boundaries of UNCD films are very abrupt (Figure 1.2)).

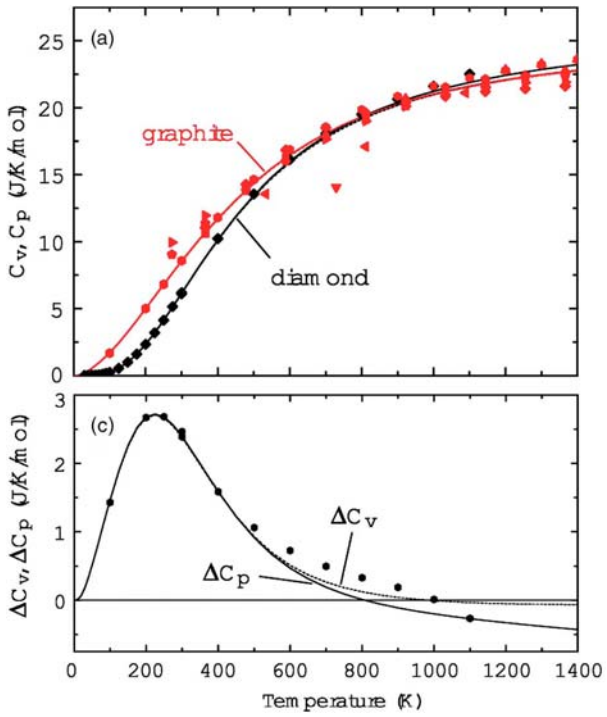

Figure 4.7.Specific heat and Debye temperature (above) and the difference in the specific heats (below) of graphite and diamond as a function of temperature [23].

Elevated temperature (>300 K) measurements of resonant frequency shifts in resonators made from ta-C (Fig 4.1) [28], which contains 80% sp^3 content, and nanocrystalline diamond (grain size 300 nm, TCF of 17 – 25 ppm/K) [4] thin films have demonstrated a slightly higher reduction in Young's modulus with respect to single crystal diamond and UNCD. Some ta-C films show a far more drastic drop in modulus, from 700 to 100 GPa, [29] as the temperature is raised from 250 °C - 400 °C.

The temperature dependence of the modulus depends on the specific heat of UNCD according to equations 4.6 and 4.7. The temperature dependence of the specific heat of single crystal diamond and graphite are shown in Fig. 4.7. Graphite has a slightly higher temperature dependence of the specific heat at lower temperatures compared to diamond [23]. The behavior of graphite cannot be directly related with the behavior attributable to sp^2–bonded carbon in the grain boundaries of UNCD, and therefore a more robust model which considers the phonon density of states for different types of bonding in grain boundaries, nano grains and the structure as a whole is necessary. Modeling the heat capacity of ultrananocrystalline diamond at low temperatures should also take into account the influence of defect transitions by low frequency acoustic phonons (Discussed in Chapter 5). Similarly, contribution from carbon atoms with sp^2 and sp^1 bonding and the presence of impurities like hydrogen and interfacial energy should be taken into consideration. As mentioned earlier, the specific heat of nanocrystalline solids have shown a significant departure from the T^3 temperature dependence at low temperatures [13, 30]. Estimating the temperature dependent specific heat of ultranocrystalline diamond films using theoretical models is necessary in order to understand the

temperature dependence of Young's modulus of UNCD at low temperatures (<300 K). Efforts are underway to determine this through molecular dynamic simulations [31].

In summary, we have seen only a slightly higher temperature dependence of the specific heat of UNCD at low temperatures compared to single crystal diamond, and a much lower dependence than seen for larger grained diamond films. Overall, UNCD films exhibit extremely good thermomechanical stability of compared many potential MEMS materials.

References:

[1] A. Migliori, H. Ledbetter, R. G. Leisure, C. Pantea, and J. B. Betts, "Diamond's elastic stiffnesses from 322 K to 10 K," *Journal of Applied Physics,* vol. 104, pp. 053512-4, 2008.

[2] H. J. McSkimin and P. Andreatch, Jr., "Elastic Moduli of Diamond as a Function of Pressure and Temperature," *Journal of Applied Physics,* vol. 43, pp. 2944-2948, 1972.

[3] V. P. Adiga, A. V. Sumant, S. Suresh, C. Gudeman, O. Auciello, J. A. Carlisle, and R. W. Carpick, "Temperature dependence of mechanical stiffness and dissipation in ultrananocrystalline diamond," in *Micro- and Nanotechnology Sensors, Systems, and Applications*, Orlando, FL, USA, 2009, pp. 731818-9.

[4] N. Sepulveda, L. Jing, D. M. Aslam, and J. P. Sullivan, "High-Performance Polycrystalline Diamond Micro- and Nanoresonators," *Microelectromechanical Systems, Journal of,* vol. 17, pp. 473-482, 2008.

[5] F. Szuecs, M. Werner, R. S. Sussmann, C. S. J. Pickles, and H. J. Fecht, "Temperature dependence of Young's modulus and degradation of chemical vapor deposited diamond," *Journal of Applied Physics,* vol. 86, pp. 6010-6017, 1999.

[6] E. S. Zouboulis, M. Grimsditch, A. K. Ramdas, and S. Rodriguez, "Temperature dependence of the elastic moduli of diamond: A Brillouin-scattering study," *Physical Review B,* vol. 57, p. 2889, 1998.

[7] U. Gysin, S. Rast, P. Ruff, E. Meyer, D. W. Lee, P. Vettiger, and C. Gerber, "Temperature dependence of the force sensitivity of silicon cantilevers," *Physical Review B,* vol. 69, p. 045403, 2004.

[8] J. B. Wachtman, W. E. Tefft, D. G. Lam, and C. S. Apstein, "Exponential Temperature Dependence of Young's Modulus for Several Oxides," *Physical Review,* vol. 122, p. 1754, 1961.

[9] O. L. Anderson, "Derivation of Wachtman's Equation for the Temperature Dependence of Elastic Moduli of Oxide Compounds," *Physical Review,* vol. 144, p. 553, 1966.

[10] G. Mingxia, Z. Yichun, P. Likun, S. Zhuo, W. Shanzhong, and Q. S. Chang, "Temperature dependence of the elastic and vibronic behavior of Si, Ge, and diamond crystals," *Journal of Applied Physics,* vol. 102, p. 083524, 2007.

[11] M. Gu, Y. Zhou, L. Pan, Z. Sun, S. Wang, and C. Q. Sun, "Temperature dependence of the elastic and vibronic behavior of Si, Ge, and diamond crystals," *Journal of Applied Physics,* vol. 102, pp. 083524-4, 2007.

[12] C. Q. Sun, "Size dependence of nanostructures: Impact of bond order deficiency," *Progress in Solid State Chemistry,* vol. 35, pp. 1-159, 2007.

[13] M. X. Gu, Q. S. Chang, Z. Chen, T. C. A. Yeung, S. Li, C. M. Tan, and V. Nosik, "Size, temperature, and bond nature dependence of elasticity and its derivatives on extensibility, Debye temperature, and heat capacity of nanostructures," *Physical Review B (Condensed Matter and Materials Physics),* vol. 75, p. 125403, 2007.

[14] C. Liu, X. C. Xiao, J. Wang, B. Shi, V. P. Adiga, R. W. Carpick, J. A. Carlisle, and O. Auciello, "Dielectric properties of hydrogen-incorporated chemical vapor deposited diamond thin films," *Journal of Applied Physics,* vol. 102, p. 7, Oct 2007.

[15] W. T. Chang and C. Zorman, "Electrical characterization of microelectromechanical silicon carbide resonators," *Sensors,* vol. 8, pp. 5759-5774, Sep 2008.

[16] G. Piazza, P. J. Stephanou, and A. P. Pisano, "Piezoelectric aluminum nitride vibrating contour-mode MEMS resonators," *Journal of Microelectromechanical Systems,* vol. 15, pp. 1406-1418, Dec 2006.

[17] W. Jing, Butler, E. James, Feygelson, Tatyana, Nguyen, and T. C. Clark, *1.51-GHz nanocrystalline diamond micromechanical dish resonator with material-mismatched isolating support*.

[18] W. Jing, J. E. Butler, D. S. Y. Hsu, and T. C. Nguyen, "CVD polycrystalline diamond high-Q micromechanical resonators," in *Micro Electro Mechanical Systems, 2002. The Fifteenth IEEE International Conference on*, 2002, pp. 657-660.

[19] C. T. C. Nguyen and R. T. Howe, "An integrated CMOS micromechanical resonator high-Q oscillator," *Solid-State Circuits, IEEE Journal of,* vol. 34, pp. 440-455, 1999.

[20] R. J. Bruls, H. T. Hintzen, G. de With, and R. Metselaar, "The temperature dependence of the Young's modulus of MgSiN2, AlN and Si3N4," *Journal of the European Ceramic Society,* vol. 21, pp. 263-268, 2001.

[21] C. Giles, "Diamond thermal expansion measurement using transmitted X-ray back-diffraction," *Journal of Synchrotron Radiation,* vol. 12, pp. 349–353, 2005.

[22] Y. Okada, *Journal of Applied Physics,* vol. 56, pp. 314-320, 1984.

[23] T. Tetsuya, K. Akihide, O. Fumiyasu, and T. Isao, "Debye temperature and stiffness of carbon and boron nitride polymorphs from first principles calculations," *Physical Review B (Condensed Matter and Materials Physics),* vol. 73, p. 064304, 2006.

[24] J. T. Paci, T. Belytschko, and G. C. Schatz, "The mechanical properties of single-crystal and ultrananocrystalline diamond: A theoretical study," *Chemical Physics Letters,* vol. 414, pp. 351-358, Oct 2005.

[25] J. T. Paci, T. Belytschko, and G. C. Schatz, "Mechanical properties of ultrananocrystalline diamond prepared in a nitrogen-rich plasma: A theoretical study," *Physical Review B,* vol. 74, p. 9, Nov 2006.

[26] N. R. Ioannis, K. Georgios, and C. K. Pantelis, "Softening of ultra-nanocrystalline diamond at low grain sizes," vol. 56, pp. 5340-5344, 2008.

[27] I. N. Remediakis, G. Kopidakis, and P. C. Kelires, "Softening of ultra-nanocrystalline diamond at low grain sizes," *Acta Materialia,* vol. 56, pp. 5340-5344, 2008.

[28] D. A. Czaplewski, J. P. Sullivan, T. A. Friedmann, and J. R. Wendt, "Temperature dependence of the mechanical properties of tetrahedrally coordinated amorphous carbon thin films," *Applied Physics Letters,* vol. 87, p. 161915, 2005.

[29] J. P. Hirvonen, J. Koskinen, M. Kaukonen, R. Nieminen, and H. J. Scheibe, "Dynamic relaxation of the elastic properties of hard carbon films," *Journal of Applied Physics,* vol. 81, pp. 7248-7254, Jun 1997.

[30] K. N. Shrivastava, "Specific heat of nanocrystals," *Nano Letters,* vol. 2, pp. 21-24, Jan 2002.

[31] S. P. Adiga, "private communication."

5. Dissipation in mechanical resonators

5.1. Loss mechanisms in mechanical resonators

Dissipation in mechanical resonators has many physical origins. These can be generally classified as being of either intrinsic or extrinsic origin. Viscous damping from a surrounding fluid medium (e.g., air), clamping losses (irreversible energy flow from resonator to resonator support), and dissipation due to the measuring system itself are examples of extrinsic losses. Loss mechanisms due to the intrinsic dissipation mechanisms include dissipation at surfaces and interfaces [1], thermoelastic dissipation (TED) [2-4], coupling between acoustic and thermal phonons,[5] and, most importantly for this study, strain-assisted relaxation of defects [6]. In other words, measuring the intrinsic mechanical dissipation can provide a window into the structure and physics of defects in the material, and the understanding gained can be used to help develop materials and structures with desired amounts of dissipation. As mentioned in the introduction to this thesis, low dissipation resonators are particularly crucial for next-generation MEMS and NEMS components including resonators, oscillators, and filters. Experimental results and discussion of the dissipation mechanisms relevant to UNCD cantilever structures will be discussed in the chapter.

Experimentally, dissipation in mechanical resonators is discussed in terms of quality factor. The quality factor is defined as follows:

$$Q = 2\pi \frac{E_{stored\ in\ the\ oscilator}}{E_{energy\ dissipated\ in\ one\ cycle}} \qquad (5.1)$$

From this equation, we can easily derive

$$Q = \frac{\omega}{\Delta\omega} \approx \frac{\omega}{2\gamma} \tag{5.2}$$

where ω is the resonant frequency of the oscillator, $\Delta\omega$ the full width at half maximum, and γ the viscous damping term in the equation for motion of the oscillator. When discussed as a physical quantity, the terms "dissipation" or "internal friction" specifically refers to the quantity Q^{-1}: a high Q structure like a tuning fork has low dissipation and will oscillate for long time before the oscillations are damped out. In particular, for a damped harmonic oscillator, it takes Q cycles for the initial amplitude to reduce to $1/e$ of its original value. Overall the dissipation we measure for a resonator structure is a summation of contributions from individual factors as follows:

$$\frac{1}{Q} = \frac{1}{Q_{\text{intrinsic}}} + \frac{1}{Q_{\text{extrinsic}}}. \tag{5.3}$$

For these experiments, we have conducted measurements in ultra high vacuum (UHV) conditions, and hence air damping can be neglected [7] and this mechanism will not be considered further. We note in passing that the measurement of air damping is used commonly in AFM to calibrate the stiffness of the cantilever [8, 9].

Similarly, we are able to rule out significant contributions to dissipation from the measurement system itself in our experiments. As will be shown below, a lower bound on dissipation from the measuring system was determined by carrying out a measurement of dissipation on a structure known to have a high Q.

Therefore, in this Chapter we fill focus on the extrinsic effect of clamping losses, and intrinsic effects in resonators.

5.1.1. Clamping losses

There are several models for clamping losses [10-12], which we will represent as $Q_{clamping}$, for out-of-plane flexural cantilever resonators attached to supports of different dimensions. A complicating factor here is that not all of these models are in agreement, and there are different assumption made in calculating the clamping losses. One key assumption concerns the dimensions of the base to which the cantilever is attached, specifically its thickness.

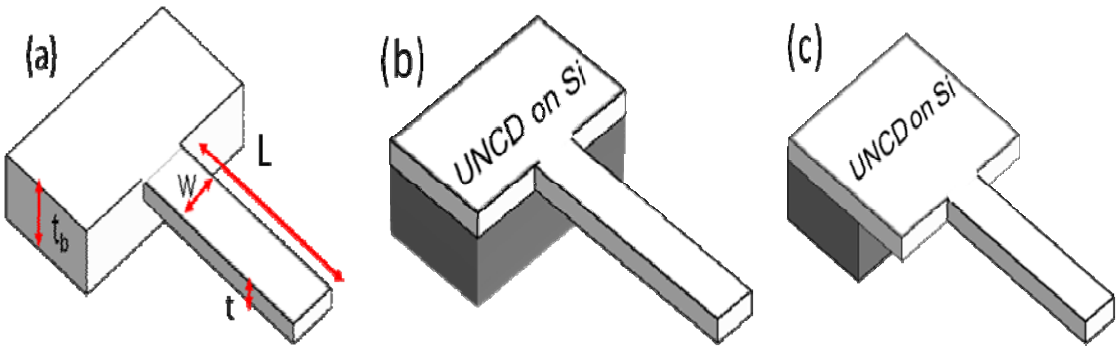

Figure 5.1.(a) Schematic of a cantilever of finite width attached to a base of thickness t_b. Theoretical models assume both the base and the cantilever are made from same material. In our experiments we have UNCD cantilevers attached to a thickness-matching UNCD base (*i.e.*, a continuous film) which is grown on silicon substrate. Some of the cantilevers have no overhang (b) and others have finite overhang (c) and so the energy can be reflected back to the lever.

Jimbo *et al*.[12] predicted the clamping losses of cantilever beam of infinite width attached to a base of semi-infinite thickness to be given by

$$Q_{clamping}^{-1} \propto \left(\frac{L}{t}\right)^{-3} \tag{5.4}$$

where L is the length and t the thickness of the cantilever. However, in many cases, the base thickness is not necessarily much larger than the cantilever thickness.

Correspondingly, Cross *et al*.[10] later proposed equations for dissipation of energy for out-of-plane flexural resonators of finite width attached to a base whose height matches the thickness of the cantilever. For a base thickness (t_b) smaller than the wavelength of the elastic wave in the base (λ_b), dissipation due to clamping losses to the thickness-matching base are inversely proportional to the aspect ratio of the levers (L/w)[10, 11]. However, this model does not take into account the fact that thickness-matching bases can be overhangs attached to thicker substrates, where the energy can be reflected back to the oscillator as shown in Figure 5.1 (c) [10]. Photiadis *et al* [11] developed a model for clamping losses of flexural cantilever resonators with finite ($t_b < \lambda_b$, $t_b \geq t$) and semi-infinite bases ($t_b > \lambda_b$, $t_b \geq t$). For finite base ($t_b < \lambda_b$, $t_b \geq t$), [11]

$$Q_{clamping}^{-1} \propto \frac{w}{L}\left(\frac{t}{t_b}\right)^2 \quad . \tag{5.5}$$

In our experiments we have UNCD cantilevers attached to thickness matching UNCD bases grown on silicon substrate (*i.e.,* a continuous film from which the cantilever was fabricated). Some of the cantilevers have finite overhangs and others do not (Fig 5.1

(b), (c)). None of the models are suitable for determining the clamping losses for this structure. However, equation 5.5 can be used to find approximate upper and lower bounds for the clamping losses. A detailed discussion of this is provided in the experimental section (5.2) .

5.1.2. Surfaces and interfaces

Another important form of intrinsic dissipation occurs at interfaces of high frequency, *e.g.*, RF, resonators, especially at the surfaces of resonators. Dissipation at surfaces could dominate the losses in oscillators that have a high surface-to-volume ratio [1, 13] and could arise from the presence of a large number of defects at the surface, the presence of extraneous material (contamination), defects induced by processing steps such as etching, or simply roughness on the surfaces of the structure. However, for low frequency devices with much lower surface-to-volume ratio dissipation is mainly due to the presence of defects within the films. The specific nature of dissipation due to surfaces is not well understood at present and quantitative models for comparison to experiments are lacking.

5.1.3. Thermoelastic dissipation

Flexural oscillations in resonators cause local volume changes. These volume changes result in a temperature gradient being set up across the thickness of the cantilever. This causes irreversible heat flow across the temperature gradient, resulting in dissipation of the mechanical energy. This is known as thermoelastic dissipation (TED). The relaxation time for such heat flow strongly depends on the thermal diffusivity and thickness of the oscillator. Zener *et al.* [2, 3] developed an approximate equation for TED, which for flexural beams is given by:

$$Q^{-1} = \frac{E\alpha^2 T}{\rho C_P} \frac{\omega\tau_Z}{1+\left(\omega\tau_Z\right)^2} \tag{5.6}$$

where α, C_P, and T are the coefficient of thermal expansion, specific heat, and temperature of the material respectively; ω is the oscillation frequency; and τ_z is the relaxation time for TED given by:

$$\tau_z = \frac{t^2}{\pi^2 D} \tag{5.7}$$

where D is the thermal diffusivity. For UNCD, the thermal diffusivity will be much smaller than single crystal diamond due to the lower thermal conductivity of UNCD [14] caused by the scattering of thermal phonons by the grain boundaries in UNCD. Maximum dissipation occurs when the product $\omega\tau_z = 1$.

TED in polycrystalline materials is discussed by Srikar *et al.* [4] and the essential properties are summarized here. In polycrystalline materials, grains have higher thermal conductivities than the grain boundaries. Hence, relaxation times for heat flow for individual grains (intracrystalline relaxation time) are much smaller than the structure as a whole (Zener relaxation time). This causes the splitting of the dissipation peak, (one at lower frequencies, Zener) and the other at higher frequencies (intracrystalline). Similarly at higher frequencies, there exists a separate dissipation peak due to a characteristic heat flow in the lateral direction. This lateral heat flow arises due to the strain matching conditions at grain boundaries and relaxation times (intercrystalline relaxation times) are determined by the size of the grains and their thermal conductivity.

For low frequency (kHz) UNCD micro-cantilevers, TED due to Zener damping will be much larger than TED due to intracrystalline and intercrystalline damping mechanisms, since these are active at GHz frequencies. This is due to the extremely high thermal conductivity of individual diamond grains and to their nanoscale dimension [4].

Later in this chapter we discuss measurements of the temperature dependence of the quality factor. It is important to remember that the dissipation due to TED is a strong function of temperature and resonant frequency. For diamond, assuming a T^3 dependence for specific heat (which is appropriate for temperatures below 300 K), dissipation due to TED follows the relation:

$$\frac{1}{Q_{TED}} \propto \frac{\alpha^2}{T^2} \quad .$$

Where α is the thermal expansion coefficient of diamond. This was shown as a function of temperature in Figure 4.3. At low temperature thermal expansion coefficient reduces to zero and hence the contribution to dissipation from thermoelastic effects reduces to zero.

5.1.4. Dissipation due to interaction between thermal and acoustic phonons

Another important form of intrinsic dissipation occurs due to the interaction between high frequency thermal phonons and the low frequency acoustic phonons associated with the mechanical oscillations of the resonator. If the wavelength of the acoustic wave is much larger than the mean free path of the thermal phonons, then this low frequency mechanical oscillation locally perturbs the thermal phonon distributions away from equilibrium [6]. Restoring this equilibrium causes dissipation in the oscillating beam. Dissipation produced by such an interaction is given by:

$$Q_{ph-ph}^{-1} = \frac{CT\gamma^2}{\rho v^2} \frac{\omega\tau_{ph}}{1+(\omega\tau_{ph})^2} \tag{5.8}$$

where γ is Grüneisen's constant, v the sound velocity, C the heat capacity per unit volume, and τ_{ph} the phonon relaxation time, which for flexural beams is given by

$$\tau_{ph} = \frac{3\kappa}{Cv_D^2} \tag{5.9}$$

where v_D is the Debye sound velocity which depends of the transverse and longitudinal sound velocities,[6] and κ is the thermal conductivity. Again, it can be seen from equation 5.8 that at low temperatures, dissipation due to phonon-phonon interactions goes to zero since the phonon population reduces with temperature.

5.1.5. Dissipation due to defect transitions

5.1.5.1 "Universality" in the dissipation of glasses and defective materials

Dissipation in most oscillators, including cantilevers, is often dominated by intrinsic dissipation due to the stress-assisted relaxation of defects. When subjected to stress, impurity atoms, dislocations, and other defects at grain boundaries and surfaces may undergo a transition from one state to another state which are separated by an energy barrier. This is often described generically as a two level system, although the detailed configuration of each state is rarely if ever defined. Regardless, dissipation in such systems exhibits certain characteristics which have been widely observed. Specifically, characteristic Debye peaks associated with particular defect transitions are observed, and

they possess a characteristic relaxation time τ which is unique to that transition. The frequency-dependent dissipation in such systems is given by [15]

$$Q_{defect}^{-1} = A\frac{\omega\tau}{1+(\omega\tau)^2} \quad * \tag{5.10}$$

where A is a dimensionless constant which depends on the nature of the defect and the defect concentration (number of defects per unit volume) and τ is the relaxation time which follows the Arrhenius relation given by [15]

$$\frac{1}{\tau} = \frac{1}{\tau_0}\exp\left(-\frac{E_A}{k_B T}\right) \tag{5.11}$$

where E_A is the activation energy for the process, k_B the Boltzmann constant, and τ_0 the characteristic atomic vibration frequency. In UNCD, due to the presence of a large fraction of grain boundaries as well as amorphous carbon in the seeding layer, there is a large number of defect states. Because of the energy barrier between the defect states, the strain assisted defect transitions are aided by the presence of thermal energy at higher temperatures. Temperature-dependent measurements of the quality factor will therefore yield information regarding the defect transitions.[16-18] At lower temperatures we expect to freeze more and more defect transitions.

However, for systems with large fraction of defects, as the temperature is reduced, the dissipation typically reaches a plateau which is then followed by a sharp drop in dissipation below ~1 K (typical tunnel splitting energies are of the order of 1 K) when the transition related to fastest relaxation rate freezes. This is evident in disordered crystals [19], amorphous solids [20], and polymers[20]. The defects states may be separated by an

extremely small activation barrier, and therefore atoms can tunnel from one potential minimum to another in the presence of low frequency acoustic phonons. The study of this behavior has been carried out for decades, but progress has been stymied for quite some time due to a lack of understanding of the defective structures and their dynamics. Here we summarize the understanding developed in this field so far.

In several glasses, evidence of dissipation due to tunneling between two states was determined from low temperature thermal conductivity measurements. The thermal conductivity of crystalline, electrically insulating materials is given by:

$$\kappa = \frac{1}{3} C_D v_D l(T) \tag{5.12}$$

where C_D is the Debye specific heat, v_D the Debye sound velocity, and l the phonon mean free path. At the lowest temperatures, the mean free path is determined by the boundaries or the defects in the crystalline sample and is independent of temperature. Above that, but still at low temperatures, the thermal conductivity shows a cubic temperature dependence because the specific heat of crystalline materials shows a cubic temperature dependence at low temperatures. At higher temperatures, l reduces due phonon-phonon scattering from Ümklapp processes. This reduction in l is more drastic than the increase in specific heat with temperature. Therefore, the thermal conductivity reaches a peak and then begins to fall off (Fig. 5.2(a)).

Initially, many argued that there should be little difference in the low temperature thermal conductivity of amorphous and crystalline materials. This was based on the

argument that the low temperature thermal properties are dominated by long wavelength

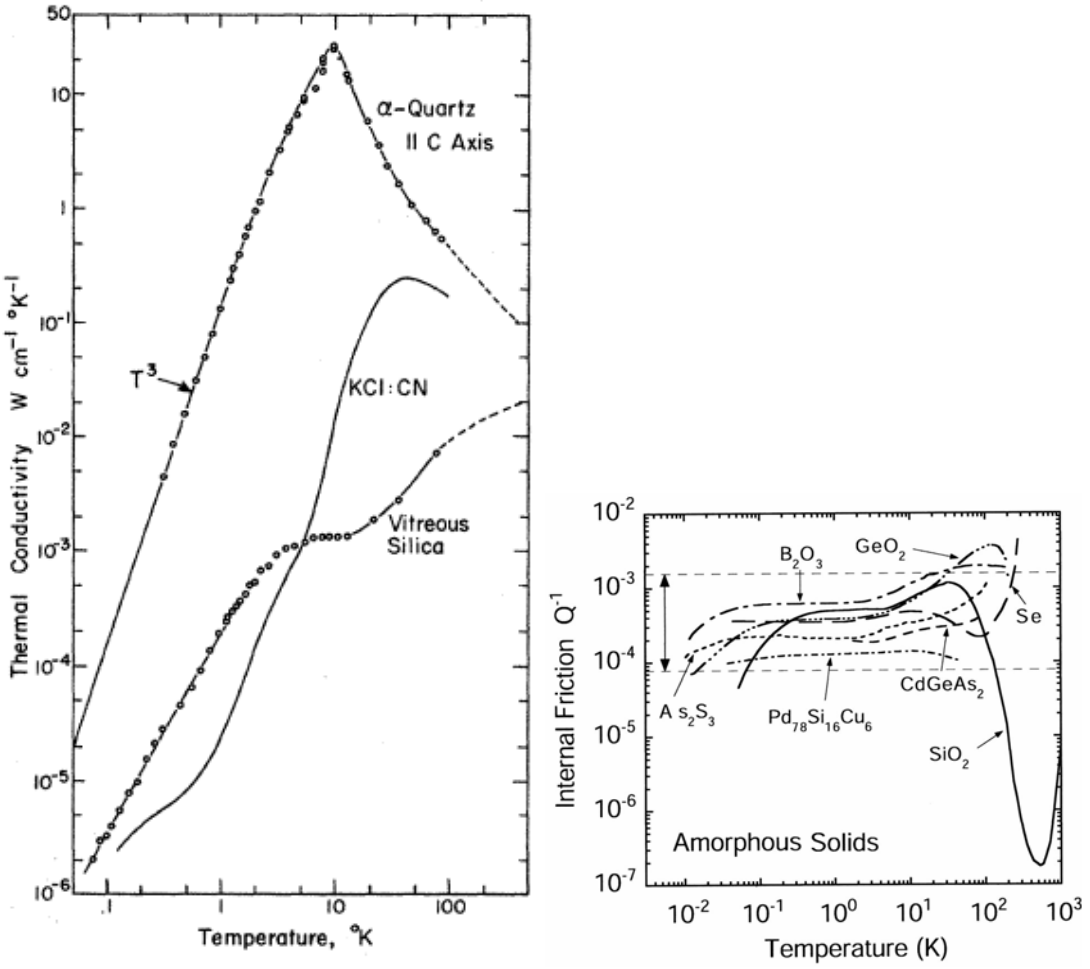

Figure. 5.2(a) Thermal conductivity of crystalline and amorphous silicon dioxide and crystalline KCl with less than 0.1% impurities. Such a small fraction of defects cause KCl's thermal conductivity to be below that of glass (Pure KCl crystal has a thermal conductivity similar to that of crystalline quartz) [21]. (b) Internal friction in different glasses as a function of temperature. At low temperatures most of the amorphous and some crystalline materials with defects show a characteristic plateau which falls within the 10^{-3} and 10^{-4}.

phonons, and these phonons can be described by low frequency sound waves traveling through an elastic continuum. It was assumed that long wavelength sound waves will not able to 'see' the microstructure in the amorphous and polycrystalline materials. However, in glasses for T < 1K, κ has a T^2 dependence. At higher temperatures, it has a characteristic plateau, and then it again rises with temperature. This behavior is observed for many disordered solids; an example of vitreous silica is shown in Fig. 5.2 (a), where κ approaches the value for crystalline quartz at higher temperatures. Similarly, dissipation in various amorphous solids at low temperatures often rises steeply at the lowest temperatures, then reaches a characteristic plateau above 1 K.

Figure 5.2(b) shows the internal friction as a function of temperature in many amorphous materials which are characterized by the presence of a large number of defects. Interestingly, the intrinsic friction (Q^{-1}) plateau falls within a factor of 20 for most of the amorphous materials including some quasi crystals, polymers, and materials with significant proportion of defects [22]. Hence, the dissipation behavior is referred to as "universal". What is more puzzling is the observation of the plateau in both thermal conductivity and acoustic dissipation measurements starting at ~1 K. The dominant phonons which contribute to thermal conductivity at 1 K have frequencies in the THz range, whereas acoustic dissipation in glasses has been measured in low frequency resonators down to few hundred Hz. Hence, disorder in the material influences the measured properties up to 10 orders magnitude of frequency higher. Similarly, low temperature measurements of the specific heat of glasses (T < 1 K) showed a linear temperature dependence, and specific heat is approximately two orders of magnitude higher than crystalline quartz [21].

These puzzling measurements are successfully described by the phenomenological tunneling model [23] [20] which takes into account the presence of two level states (TLS) where transitions between the two states occurs via quantum mechanical tunneling. Detailed discussions of the tunneling model are given in [20, 23, 24]. Here, we summarize the main features. This model assumes the presence of atomic tunneling entities with a broad distribution of energy splittings. According to this model, lower frequency acoustic phonons are attenuated by the relaxation of tunneling defects, while higher frequency phonons that carry the heat are resonantly scattered by low energy excitations. The scattering cross section of the defects for phonons is a strong inverse function of phonon wavelength. Higher specific heat at lower temperatures can be explained by the presence of low energy excitations. For acoustic measurements in the temperature-independent plateau region, the tunneling states are relaxed via a relaxational process in the strain field of sound waves mediated by thermal phonons. In the plateau region ($\omega\tau \ll 1$, low frequency, high temperature regime (T>1K)), internal friction is given by

$$Q^{-1} = \frac{\pi}{2}\frac{P\bar{\gamma}^2}{\rho v^2} \tag{5.13}$$

where P is the spectral density of tunneling states, γ the energy with which they are coupled to the lattice vibrations, v the sound velocity and ρ the density. Below a characteristic temperature called the crossover temperature (typically ~1 K), the acoustic dissipation dramatically decreases with temperature because the two level systems can

not relax fast enough with the oscilating strain field. At low temperatures ($\omega\tau >> 1$, high frequency, low temperature regime) internal friction is given by[25]

$$Q^{-1} = \frac{\pi^4}{96}\frac{\bar{P\gamma}^2}{\rho v^2}\left(\frac{T}{T_{CO}}\right)^{\beta} \qquad (5.14)$$

where, T_{CO} is the cross over temperature corresponding to $\omega\tau$ =1. This corresponds to relaxation of the fastest tunneling state. This crossover temperature depends on material parameters and the resonant frequency of the oscillator. β is a scaling factor and depends strongly on the type of material, and the nature of the defects. For example, for the standard tunneling model (STM), β = 3, for the Phillips model β = 1, for the soft potential model β=0.75, and β is 0.33 for oscillators with high surface to volume ratio [26, 27]. These differences arise due to different assumptions on the distribution of energy splittings and the density of states [27].

In recent years it has been observed that internal friction in amorphous films of silicon (a-Si) and carbon (a-C) does not follow the universal behavior observed in other amorphous materials [22]. These films showed departures from the universal behavior depending on their deposition and annealing conditions, as shown in Figure 5.3 [19]. The measurements which showed departure from universality were conducted after depositing a-Si and a-C films on single crystal silicon double paddle oscillators (torsional oscillators) and measuring the dissipation of the torsional mode at low temperatures. Intrinsic dissipation in single crystal paddle oscillator as a function of temperature is also shown in Figure 5.3. For example, e-beam deposited a-Si shows an internal friction in the plateau region which is 10 times lower than observed value in glasses (Figure 5.3). It has been speculated that the high coordination number of tetrahedrally bonded atoms /

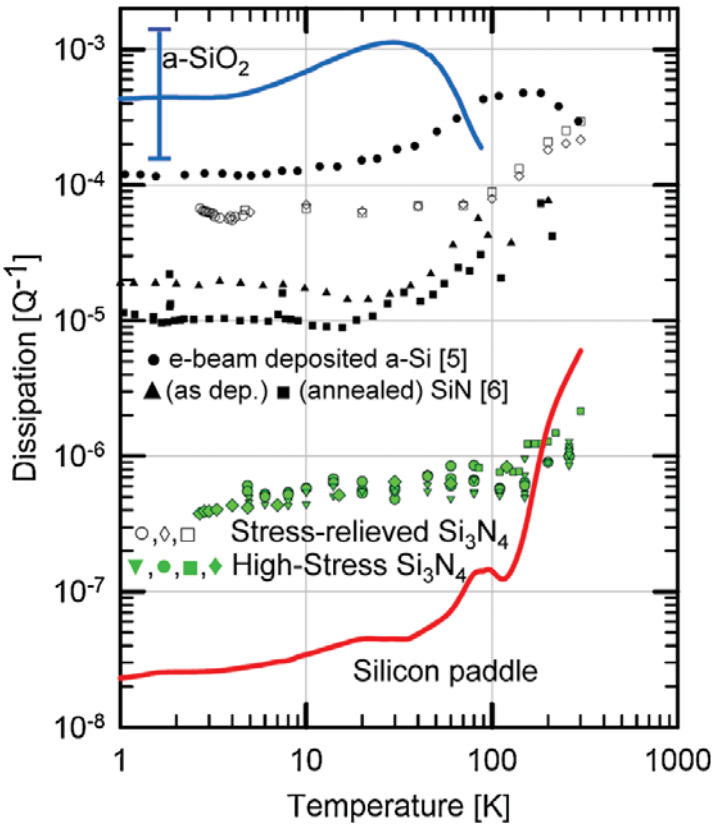

Figure 5.3 A comparison of intrinsic friction in amorphous silicon, silicon dioxide, polycrystalline SiN cantilevers (stress free), and high tensile stress SiN membranes. A tensile stress of 1 GPa in membranes causes the intrinsic friction to drop by 2 orders of magnitude.

materials (Si, Si_3N_4, C) inhibits the tunneling, and higher hydrogen content measured in some of these high Q (low dissipation) structures led many to believe that additional hydrogen results in more perfect fourfold coordination, thus reducing the tunneling states. However, the higher hydrogen content may also lead to changes in the residual stresses in the films. Similarly, there may be additional stresses due to thermal expansion mismatch with underlying silicon paddle oscillator. Craighead's group in Cornell University conclusively reported that quality factors of amorphous SiN beams

(flexural fixed-fixed beams[28]) and membranes[19] improved by 2 orders of magnitude in the presence of tensile stress as shown in Fig 5.3 (filled green data points). [19] While stress free SiN cantilevers followed universal behavior (empty data points). Both of these are flexural, monolithic resonators as opposed to torsional composite oscillators (which also showed departure from universal behavior). Stress alters either the density of tunneling states or the energy with which they are coupled to the lattice vibrations [19].

5.1.5.2 Characteristics of dissipation in diamond

The thermal conductivity of single crystal diamond is extremely high compared to most other materials: at room temperature, its value is 900- 2000W/mK compared to 401 W/mK for copper. At lower temperatures, its thermal conductivity further increases by 2 to 3 orders of magnitude. Even though diamond is a sp^3-bonded single element molecule, there is still scattering at low temperatures due to the presence of ^{13}C isotopic impurities as shown in Fig 5.4 (a), and from the boundaries of the sample. Since diamond has an extremely high Debye temperature, the thermal conductivity strongly depends on the reduction in phonon mean free path due to the scattering by imperfections (dopants, defects, isotopes) even at room temperature.

The thermal conductivity of polycrystalline diamond is significantly lower than that of single crystal diamond at room temperature. This is due to the scattering of thermal phonons by grain boundaries, and the defects and impurities in the grain boundaries, as shown in Fig 5.4 (b). Correspondingly, the reduction compared to single crystal diamond is larger the smaller the grain size. For UNCD, the thermal conductivity is approximately

2 orders of magnitude lower than that of single crystal diamond and is comparable to that of many glasses which follow universal behavior.

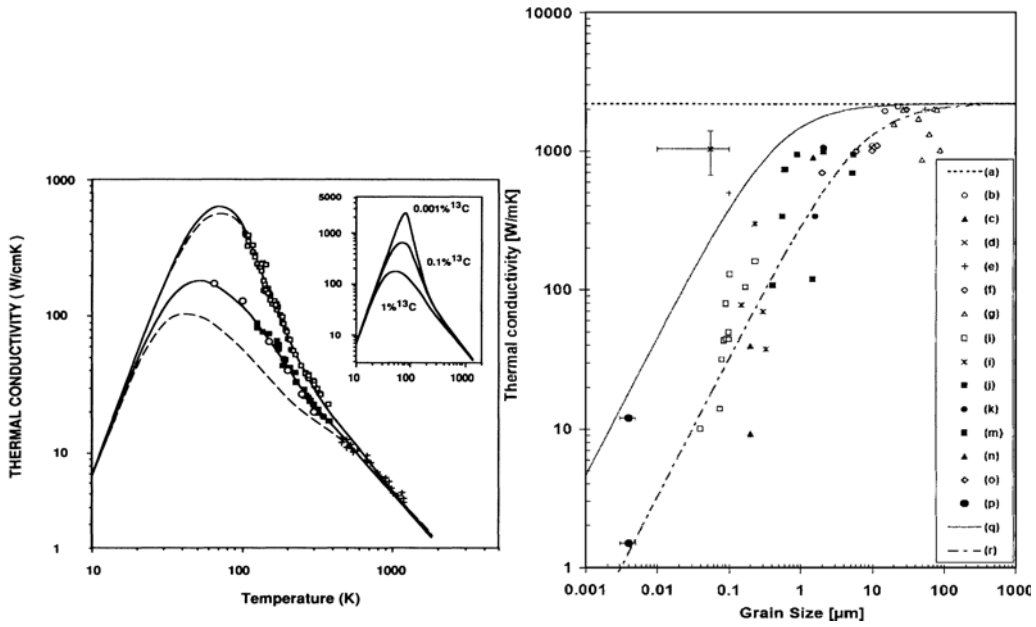

Figure 5.4 (a) Thermal conductivity of single crystal diamond as a function of temperature for natural diamond, which contains 1.1% C^{13} (empty circles, filled squares, and pluses) and isotopically enriched diamond containing 0.1% C^{13}. Theoretical prediction of thermal conductivity as a function of temperature and C^{13} isotope concentration is shown in inset. The thermal conductivity peak strongly depends on the isotope concentration [29]. (b) Thermal conductivity of polycrystalline diamond as a function of grain size. UNCD has a thermal conductivity of 1.5 - 10 W/mK which is comparable to glass [14].

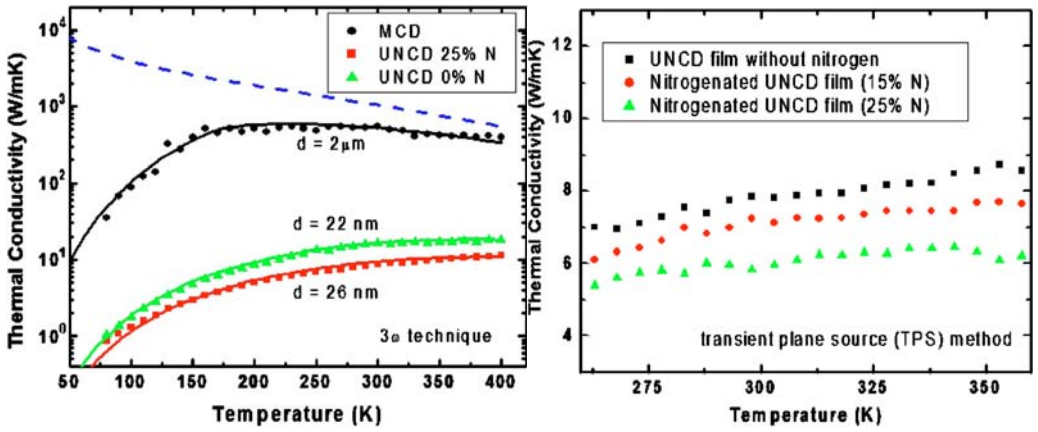

Figure 5.5. Comparison of thermal conductivity of polycrystalline diamond (grain size, 2 μm) and NCD films (a), and of NCD films grown with different nitrogen content in the plasma (b) as a function of temperature [30]. Authors measured a grain size of 17-26 nm for all of these films and hence these are NCD films and not UNCD films. Our UNCD films have a grain size in the range of 2-5 nm.

The temperature dependence of the thermal conductivity of polycrystalline diamond films has been studied recently [30]. For NCD films (grain size 17 nm – 26 nm), a reduction of thermal conductivity with temperature is seen at lower temperatures (Fig 5.5). Low temperature thermal conductivity measurements of UNCD films (grain size 2-5 nm) do not exist. Whether relaxation processes similar to the ones observed in amorphous glasses influence the thermal conductivity of UNCD is still an open question.

Internal friction of UNCD thin films has rarely been studied to date either; only one other study exists [27]. The low temperature measurements of intrinsic friction in UNCD, NCD, and other forms of carbon will be discussed later in this chapter in more detail, along with our experimental results on dissipation in stress free UNCD cantilevers as a function of temperature. As well, the influence of stress on the intrinsic dissipation in

diamond has never been discussed. This has been difficult to address experimentally because diamond films tend to have substantial residual compressive stresses which tend to buckle fixed-fixed beams and membranes which one would like to use as test structures. This makes it extremely difficult to actuate such devices either by electrostatic means or by magnetomotive force. Low temperature measurements (<10 K) of stress free cantilevers and stressed (tensile) resonators are necessary to fully understand the nature of defect transitions. A review of specific findings in the literature on the dissipation in diamond and amorphous carbon films will be discussed later in this chapter.

5.2 Dissipation in UNCD cantilevers at room temperature

In this thesis, the quality factor of stress-free UNCD cantilevers were measured at room temperature with the ring-down measurements or by measuring the full width at half maximum at their fundamental resonant frequencies under UHV conditions, using the technique described in Section 2.1.3. The curve fit to the damped oscillation yielded quality factors in the range of 5000-16000 for all the cantilevers measured, which had different dimensions and overhangs. Fig 5.6 (a) shows measured quality factors as a function of the fundamental flexural resonant frequency. There was no specific dependence of dissipation on the dimension of the cantilever and the overhang length, as shown in Fig. 5.6 (b). Furthermore, the quality factors were observed to be stable with time.

We measured quality factors up to 170,000 on single crystal silicon cantilevers of similar dimension using the same experimental setup. This indicates that extrinsic dissipation due to the measuring apparatus is negligible. Furthermore, the absence of any

metal coating on these cantilevers means that the observed dissipation can be attributed to clamping losses and/or intrinsic dissipation in the UNCD itself.

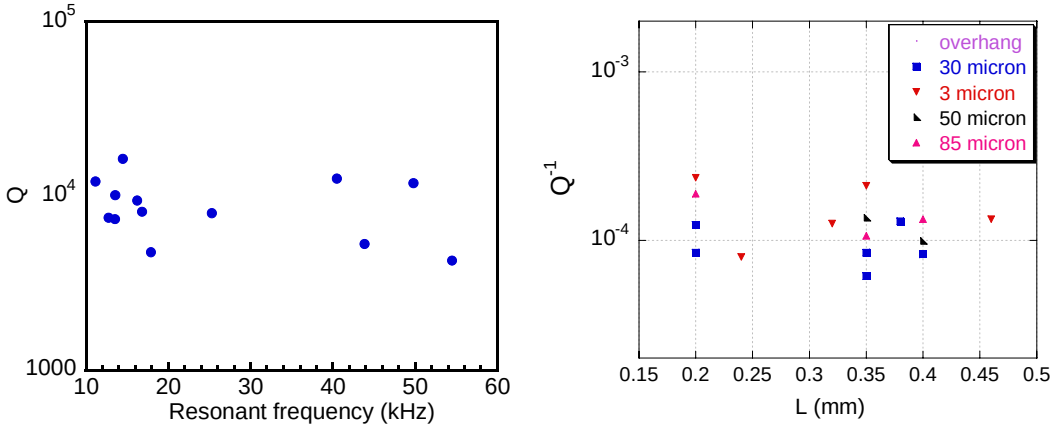

Figure 5.6. (a) Quality factor of UNCD cantilevers with different lengths. (b) Quality factors as a function of resonant frequency.

With reference to Section 5.1.1, the clamping losses for our cantilever beams with overhangs are difficult to model. Due to the low resonant frequencies of our beams (~10 kHz), the wavelength of the elastic wave in the base λ_b (acoustic velocity ~15,000 km/s, λ_b ~ 1 m) is much greater than the thickness of the base t_b. In our geometry, we have thickness-matching overhangs at the cantilever base (the wider UNCD overhang with $t=t_b$) and this thin overhanging membrane attaches to thick base (the UNCD on top of the Si die, Figure 5.1). No model for this situation has yet been developed. Therefore, we discuss reasonable approximations that may come close to describing the clamping losses. First, if we ignore the overhang and treat the base as one material instead of two layers (UNCD on top of Si), equation 5.5 yields dissipation values much less than the observed ones. Second, if we consider the overhang to be of infinite length and thus energy does not flow back to the resonator, then the equation predicts dissipation values 4

orders of magnitude higher than what we measured. A more elaborate approach which considers the finite extent of our overhang and the presence of different layers attached to this thin overhanging membrane is required to estimate the clamping losses.

However, as mentioned earlier, we did not see a systematic dependence of quality factors on either the dimension of the beam or the extant of the overhang. This strongly indicates that we can safely assume that clamping losses make a negligible contribution, and that the losses in our beams are dominated by intrinsic dissipation mechanisms, such as TED, internal friction due to defects, or dissipation due to interaction between thermal phonon and acoustic phonons.

The dissipation (Q^{-1}) vs. resonant frequency measured for UNCD cantilevers, and the predicted Q^{-1} calculated for possible intrinsic loss mechanisms (TED and phonon-phonon dissipation), are all shown in Fig. 5.7. These are the upper bounds for the achievable quality factor, higher quality factors are not possible due aforementioned dissipation mechanisms. Table 5.1 shows the constants used in the calculations for dissipation that are plotted in Fig. 5.7. The measured dissipation values are at least 1000 times higher than the theoretical predictions for TED and phonon-phonon dissipation put together. This indicates that TED and phonon-phonon dissipation are insufficient to explain the dissipation we measure. Having ruled out extrinsic loss mechanisms as well, we are left to conclude the observed dissipation is mainly due to the relaxation of defects in the bulk or the surface of the film.

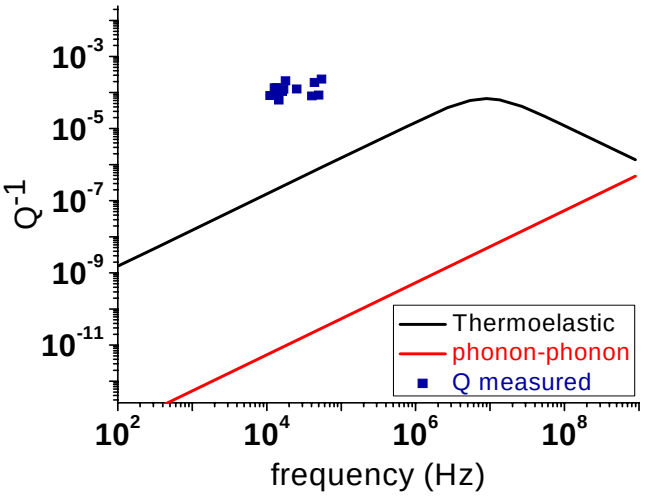

Parameter	Values used
C_p (J $Kg^{-1}K^{-1}$)	502*
α ($\times 10^{-6}K^{-1}$)	1*
γ	1*
T (°K)	300
C ($\times 10^{6}$ J $m^{-3}K^{-1}$)	1.767*
ρ (Kg/m^3)	3500*
E (GPa)	800
κ ($Wm^{-1}K^{-1}$)	10
v_D; v ($\times 10^{3}$ ms^{-1})	11.357, 15.33

Figure. 5.7. Solid lines: calculated dissipation in UNCD cantilevers (thickness = 1 μm) due to TED and phonon-phonon dissipation as a function of resonance frequency [31]. Data points: measured dissipation for the cantilevers used in this study. Since diamond remains an ideal Grüneisen's solid independent of the pressure [32], a Grüneisen's constant (γ) of 1 has been used in the models.

Table 5.1. Constants used for estimating dissipation due to clamping losses, phonon-phonon dissipation and thermoelastic dissipation. * Values used are for single crystal diamond.

We next consider these results in comparison to other measurements of dissipation in various forms of diamond or highly sp^3-bonded carbon films. Table 5.2 summarizes the results reported by other groups [5, 18, 25, 31-33] as compared to ours

Structure	Resonant frequency	Material	Q	Growth technique	Actuation method
Fixed-fixed[35]	17-66 MHz	NCD	600-2400	MPCVD	Magnetomotive
Fixed-free[5]	8-50 KHz	PCD	4000-100,000	MPCVD	Piezo-electric
Doubly clamped paddle[36]	6-30 MHz	NCD	2400-3500	MPCVD	Piezo-electric
Fixed-free (our work)	12-45 KHz	UNCD	5000-16000	HFCVD	Piezo-electric
Fixed-fixed[18]	14-157 MHz	NCD	~3000	MPCVD	Magneto motive
Fixed-free[34]	KHz	ta-C	3500	PLD	Piezo-electric

Table 5.2. Quality factor of flexural resonators from our work, as well as reported by other groups.

for different flexural beams fabricated using NCD, UNCD, or ta-C films. Sepúlveda *et al.* [5] reported Q values for polycrystalline diamond (PCD, grain size ~300 nm) micro-cantilevers of 4000-100,000 (Table 5.2). These include values higher than the Q's observed for UNCD cantilevers with comparable dimensions reported in this thesis. They suggested that as the percentage of the film composed of the initial nucleation layer, which contains finer-grained diamond, is increased, the quality factor of the resonators is reduced [33]. This is consistent with the idea that the higher dissipation in the UNCD resonators described here and in general is mainly due to the higher proportion of grain boundaries and defects. Cantilever resonator structures made from tetrahedral amorphous carbon (ta-C), which have a significant sp^3 content, (80% sp^3, 20 % sp^2) showed a lower Q of 3500 [34]. This value, being in the range of the "universal" values for amorphous

systems, indicates that dissipation in ta-C is dominated by the two-level tunneling states described above [25].

Hutchinson *et al.* [18] measured the dissipation of composite metal / nanocrystalline diamond (NCD) fixed-fixed beams (columnar grains, grain size 5-15 nm). These high frequency (MHz) resonators (dimensions ~0.8 μm × 0.5 μm × 10 μm) have a lower quality factor (~3000, at room temperature) than the low frequency UNCD cantilever resonators studied here. Higher dissipation in the NCD resonators can be attributed to the fact that as the resonator dimensions become smaller, dissipation due to surface effects plays a greater role [1, 13]. This argument is supported by the investigations of scaling of dissipation with the dimension of the NCD fixed-fixed resonators, as reported by Imboden *et al* [35]. Factors that contribute to the higher dissipation in these high frequency, metal-coated fixed-fixed flexural resonators may also include clamping losses, losses that occur at interface between metal-diamond interfaces, nucleation layer and the dissipation in the metal layer of the composite beams [1]. Similarly, as discussed earlier stress also plays an important role in the measured dissipation and these fixed-fixed beams are under compressive stress.

To consider the influence of surface as opposed to bulk defects, we terminated the surface with atomic hydrogen at 800°C in our HFCVD system. Details of this procedure are given in Chapter 3. This treatment removes contaminants, oxides, and non-diamond (sp^2) carbon bonds, leaving an ideal UNCD surface with a predominantly monohydride termination. We observed a slight improvement in the quality factor after H-terminating the UNCD cantilever surface (Fig. 5.8). This stable, inert surface results in the reproducible quality factors even after the exposure to air, unlike silicon resonators

whose Q degrades substantially upon air exposure which leads to oxidation and adsorption of water [37, 38]. The stability of the hydrogen terminated UNCD surface is likely due to the fact that it is relatively hydrophobic (contact angle ~99.6±1.7° [39]), and has a low surface energy. This stability upon air exposure has substantial practical benefits for device applications, where some ambient exposure will occur between processing and packaging steps.

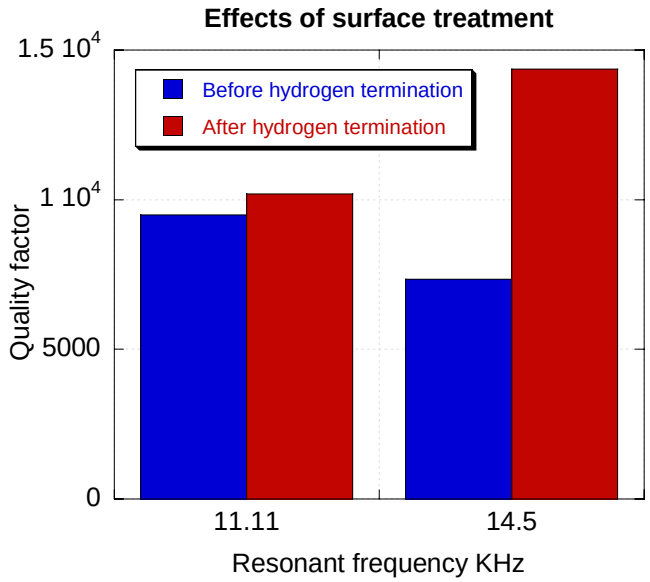

Figure 5.8: Quality factor of UNCD cantilever beams before and after hydrogen termination.

However, this improvement in Q may not be solely attributable to surface effects. The nucleation layer on the underside of the cantilevers tends to have more sp^2 carbon than the bulk of the resonator [40]. Hydrogen termination can remove this non-diamond carbon, and therefore produce an increased Q if the atomic hydrogen reaches the underside of the cantilevers during the H-termination process.

As well, the cantilevers' deflection after the hydrogen treatment generally increased, indicating an increase in the residual stress gradient. As mentioned earlier in this chapter, stresses can alter the defect motions and hence contribute to significant changes in dissipation. Therefore, it is difficult to attribute the observed change in quality factor solely to surface defects.

Even though these are limited measurements of the influence of surface effects, the increase in the Q is not significant, indicating that the influence of bulk defects on the dissipation is dominant. Further understanding the contribution of the defects requires temperature dependent (<300 K) measurements of dissipation. This was carried out and is discussed next.

5.3. Temperature dependence of the Quality factor

Figure 5.9 (a) shows the quality factor as a function of temperature in a 350 μm long UNCD cantilever beam with a large overhang (85 μm). We conducted similar low temperature dissipation measurements of three other cantilevers. Two had 85 μm overhang (with lengths of 400 μm and 250 μm respectively) and one with 30 μm overhang (with a length of 400μm) from room temperature to 138 K in the RHK 350 AFM in UHV conditions. The quality factors showed a weak temperature dependence from room temperature down to 138 K. We did not observe any characteristic Debye peaks in the measured temperature range, unlike observations by others of single crystal silicon cantilevers [16] and nanocrystalline diamond fixed-fixed beams [18]. A moderate improvement in quality factor can be seen.

The observed quality factors remained within a few percent during both heating and cooling cycles. To explore this behavior further, a much broader temperature range of measurements of dissipation was then used. Measurements were conducted from 450 K to 63 K, and then from 63 K to 450 K. Heating are cooling rates are approximately 1 K/min. The temperature was stabilized before each measurement. These measurements were conducted using a liquid helium-cooled stage in the RHK 750 UHV AFM described in Chapter 2. Successful measurements were obtained for two different UNCD cantilevers. Lever 1 has no overhang and lever 2 has an overhang of about 30 μm, with both of these levers being on the same die. The resonant frequency shifts of these cantilevers with temperature were reported in Chapter 4.

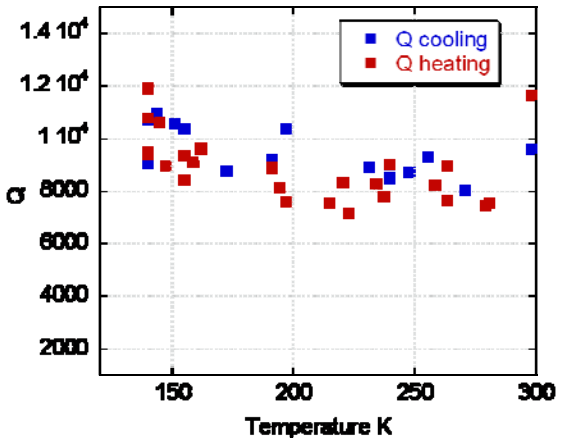

Figure 5.9. Quality factor of a 350 μm long cantilever as a function of temperature [41]. These measurements are performed under UHV conditions in a liquid nitrogen cooled RHK UHV 350 AFM. The cantilever is attached to an 85 μm overhang at its base. The heating and cooling rates are about 1 K/min. The experiment was started at 300 K, then cooled to 138 K, then heated back to 300 K.

The dissipation measured for the two cantilevers are in remarkable agreement. As with the results shown in Fig. 5.10 the cantilevers also show a moderate reduction in the dissipation Q^{-1} from 450 K to 180 K, below which it tapers off to a value of ~10^{-4}, which is near the lower bound value for the so-called "universal behavior". The dissipation measured for the two cantilevers are in remarkable agreement. There are a handful of results (on intrinsic friction in diamond or amorphous carbon films) in the literature that merit comparison to these. But all these results show an existence of a low temperature plateau confirming the presence of two level systems.

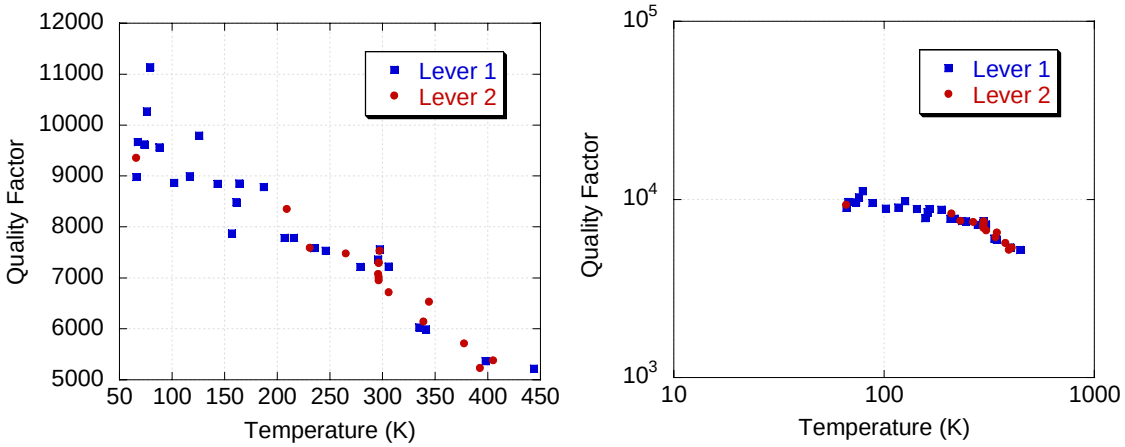

Figure 5.10. Quality factor of two UNCD cantilevers as a function of temperature. Lever 1 has no overhang and lever 2 has an overhang of approximately 30 μm. Data include both heating and cooling measurements. Below 150 K dissipation reaches a plateau characteristic of the amourphous materials and crystalline materials with defects. The value of Q^{-1} ~10^{-4} is in agreement with the so-called "universal behavior".

Recent investigation [27]of quality factor of metal-coated UNCD fixed-fixed beams at extremely low temperatures (<10 K) indicated a very weak temperature dependence (β=0.35 for T < 5K) followed by a plateau for a 5.1 MHz frequency

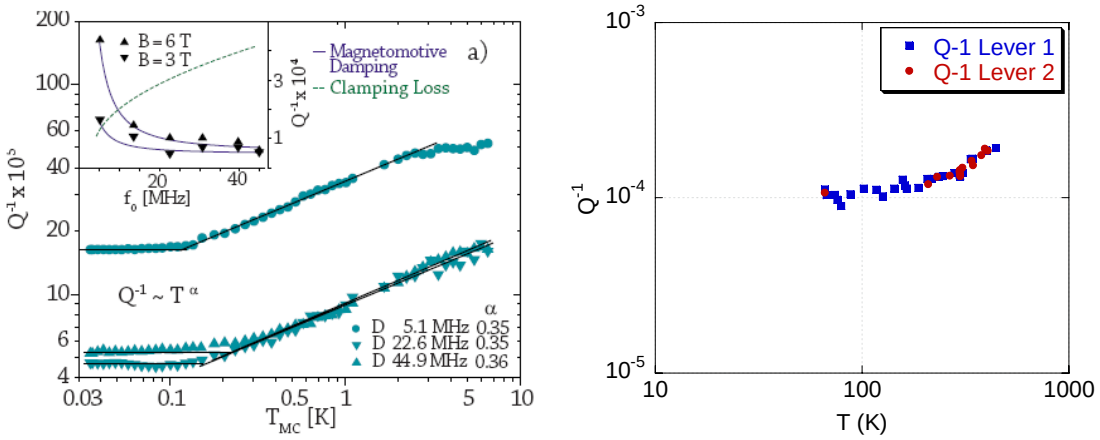

Figure 5.11(a) Dissipation in UNCD/metal composite fixed-fixed beam resonator structures from 5 K down to 0.03 K. [27] The Q values at 5 K for the resonators are ~2500-6600. Below ~5 K, dissipation reduced dramatically with temperature. Lower frequency resonator (5.1 MHz) shows a cross over temperature at 3 K. As discussed in section 5.1.5.1, the crossover temperature, T_{co}, is higher for higher resonant frequencies [22] which were not reached in this experiment due to experimental limitation. The authors do not discuss the low temperature plateau (below 0.2 K) The departure of the dissipation from the T^{β} dependence at lower temperatures (<0.2 K) has been observed before and has been attributed to interactions between different tunneling states or to thermal decoupling from the sample, *i.e.* where the sample is not actually being cooled to the desired temperature since thermal transfer is very challenging at this low temperature [42] (b) Dissipation as a function of temperature for our UNCD cantilevers. We have explored the intrinsic friction at higher temperatures, i.e. the transition from the dissipation plateau to gradually increasing values. As shown in Fig 5.2 (b), this transition temperature depends on the material.

resonator [42]. These fixed-fixed flexural beams, shown in Fig. 5.11 (a), exhibited quality factors ranging between 2500-6600 close to the dissipation plateau, which is only slightly lower than what we have measured. Figure 5.11 (b) is our experimental data from fixed-free coating free UNCD cantilevers at higher temperatures. Here, Fig. 5.10 (b) replotted as Q^{-1}.

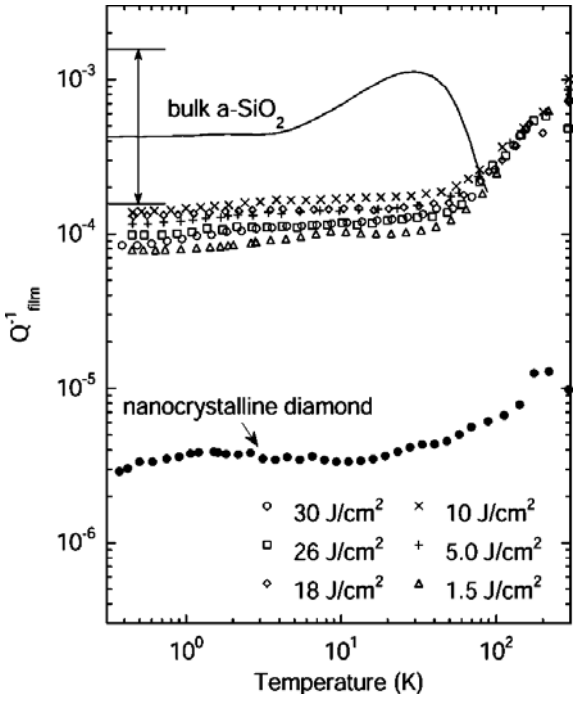

Figure 5.12. Temperature dependence of dissipation for NCD and tetrahedral amorphous carbon (ta-C) resonators. The ta-C films are deposited by pulsed laser deposition under different laser intensities which are indicated in the legend.[25, 43] These also show a plateau below 100 K. For NCD, the observed dissipation is ~2 orders of magnitude lower than many glasses (which show universal behavior) whereas for ta-C it is well within the range of universal behavior.

We emphasize that, unlike the data in Fig. 5.11 (a), these are for fixed-free, coating-free UNCD cantilevers, and the measurements are over a higher temperature range. Fixed-fixed beams suffer a serious disadvantage compared to cantilevers or torsional double paddle oscillators, namely, that the thermal stresses can bend the beams and influence the dissipation in ways are hard to gauge. Similarly presence of metal coating influences the observed dissipation.

Temperature dependent measurements of tetrahedral amorphous carbon and nanocrystalline diamond films deposited on silicon double paddle oscillators (torsional oscillators) are reported by Metcalf *et al [25, 43]*. The data also showed a plateau below 100 K, followed by a T^{β}(very weak power law dependence, $\beta < 1$) dependence below ~2 K shown in Figure 5.12. While nanocrystalline diamond (NCD) films showed dissipation in the plateau region less than what is observed for UNCD, ta-C showed values comparable to UNCD. As mentioned earlier in the discussion in section 5.1.5.1, the influence of residual and thermal stresses cannot be ignored in these composite resonator structures. Similarly two level systems couple differently to flexural and torsional modes [26]. What we have measured for our stress free, coating free cantilevers conclusively points to the presence of a dissipation plateau in UNCD which follows the universal behavior. The measurements are over a higher temperature range. The relative phonon mean free paths (λ/l) can be calculated from the dissipation plateau and is given by [22]

$$Q^{-1} = \frac{1}{2\pi}\frac{\lambda}{l} \tag{5.15}$$

From our measurements, the relative phonon mean free path for UNCD is approximately 6×10^{-4}, which is slightly higher than that of other amorphous materials but

well within the universal behavior. Further studies are needed to understand the role of residual stresses, grain boundary structure, and impurities on the observed dissipation in UNCD films. Measurements of internal friction below 10 K on stress free cantilevers are key to understanding the nature of dissipation in UNCD due to the presence of TLS, mainly at grain boundaries, and to understand their structure. This also suggests that altering the grain boundaries and the stresses is the key to controlling and increasing the Q of UNCD resonators at room temperature.

To conclude, we observed a very weak temperature dependence of dissipation from 450 K down to 63 K. Dissipation in UNCD shows a characteristic plateau observed in many amorphous solids and falls within the limits of universal behavior. This suggests that dissipation is dominated by defects in the bulk of the film. Controlling the residual stresses and the grain boundary structure are key to achieving high frequency, high Q UNCD resonators for RF-MEMS applications and resonant mass sensing applications.

References:

[1] C. Seoanez, F. Guinea, and A. H. C. Neto, "Surface dissipation in nanoelectromechanical systems: Unified description with the standard tunneling model and effects of metallic electrodes," *Physical Review B (Condensed Matter and Materials Physics),* vol. 77, p. 125107, 2008.

[2] C. Zener, "Internal Friction in Solids II. General Theory of Thermoelastic Internal Friction," *Physical Review,* vol. 53, p. 90, 1938.

[3] R. Lifshitz and M. L. Roukes, "Thermoelastic damping in micro- and nanomechanical systems," *Physical Review B,* vol. 61, p. 5600, 2000.

[4] V. T. Srikar and S. D. Senturia, "Thermoelastic damping in fine-grained polysilicon flexural beam resonators," *Microelectromechanical Systems, Journal of,* vol. 11, pp. 499-504, 2002.

[5] N. Sepulveda, L. Jing, D. M. Aslam, and J. P. Sullivan, "High-Performance Polycrystalline Diamond Micro- and Nanoresonators," *Microelectromechanical Systems, Journal of,* vol. 17, pp. 473-482, 2008.

[6] M. V. P. Braginsky V. B., Panov V.I., *Systems with small Dissipation*. Chicago: University of Chicago Press, 1985.

[7] S. Bianco, M. Cocuzza, S. Ferrero, E. Giuri, G. Piacenza, C. F. Pirri, A. Ricci, L. Scaltrito, D. Bich, A. Merialdo, P. Schina, and R. Correale, "Silicon resonant microcantilevers for absolute pressure measurement," *Journal of Vacuum Science and Technology B: Microelectronics and Nanometer Structures,* vol. 24, pp. 1803-1809, 2006.

[8] J. E. Sader, J. W. M. Chon, and P. Mulvaney, "Calibration of rectangular atomic force microscope cantilevers," *Review of Scientific Instruments,* vol. 70, pp. 3967-3969, Oct 1999.

[9] J. E. Sader, I. Larson, P. Mulvaney, and L. R. White, "METHOD FOR THE CALIBRATION OF ATOMIC-FORCE MICROSCOPE CANTILEVERS," *Review of Scientific Instruments,* vol. 66, pp. 3789-3798, Jul 1995.

[10] M. C. Cross and R. Lifshitz, "Elastic wave transmission at an abrupt junction in a thin plate with application to heat transport and vibrations in mesoscopic systems," *Physical Review B,* vol. 64, p. 085324, 2001.

[11] D. M. Photiadis and J. A. Judge, "Attachment losses of high Q oscillators," *Applied Physics Letters,* vol. 85, pp. 482-484, 2004.

[12] Y. Jimbo and K. Itao, "Energy loss of a cantilever vibrator," *J. Horolog. Inst. Jpn,* vol. 47, pp. 1–15, 1968.

[13] P. Mohanty, D. A. Harrington, K. L. Ekinci, Y. T. Yang, M. J. Murphy, and M. L. Roukes, "Intrinsic dissipation in high-frequency micromechanical resonators," *Physical Review B,* vol. 66, p. 085416, 2002.

[14] M. A. Angadi, T. Watanabe, A. Bodapati, X. C. Xiao, O. Auciello, J. A. Carlisle, J. A. Eastman, P. Keblinski, P. K. Schelling, and S. R. Phillpot, "Thermal transport and grain boundary conductance in ultrananocrystalline diamond thin films," *Journal of Applied Physics,* vol. 99, p. 6, Jun 2006.

[15] A. N. Cleland, *Foundations of Nanomechanics*. Heidelberg, New York: Springer Verlag, 2003.

[16] U. Gysin, S. Rast, P. Ruff, E. Meyer, D. W. Lee, P. Vettiger, and C. Gerber, "Temperature dependence of the force sensitivity of silicon cantilevers," *Physical Review B,* vol. 69, p. 045403, 2004.

[17] D. A. Czaplewski, J. P. Sullivan, T. A. Friedmann, and J. R. Wendt, "Temperature dependence of the mechanical properties of tetrahedrally coordinated amorphous carbon thin films," *Applied Physics Letters,* vol. 87, p. 161915, 2005.

[18] A. B. Hutchinson, P. A. Truitt, K. C. Schwab, L. Sekaric, J. M. Parpia, H. G. Craighead, and J. E. Butler, "Dissipation in nanocrystalline-diamond nanomechanical resonators," *Applied Physics Letters,* vol. 84, pp. 972-974, 2004.

[19] D. R. Southworth, R. A. Barton, S. S. Verbridge, B. Ilic, A. D. Fefferman, H. G. Craighead, and J. M. Parpia, "Stress and Silicon Nitride: A Crack in the Universal Dissipation of Glasses," *Physical Review Letters,* vol. 102, p. 4, Jun 2009.

[20] R. O. Pohl, X. Liu, and E. Thompson, "Low-temperature thermal conductivity and acoustic attenuation in amorphous solids," *Reviews of Modern Physics,* vol. 74, pp. 991-1013, Oct 2002.

[21] R. C. Zeller and R. O. Pohl, "Thermal Conductivity and Specific Heat of Noncrystalline Solids," *Physical Review B,* vol. 4, p. 2029, 1971.

[22] Pohl and et al., "Low-temperature thermal conductivity and acoustic attenuation in amorphous solids," *Reviews of Modern Physics,* vol. 74, p. 991, 2002.

[23] W. A. Phillips, "Two-level states in glasses," *Reports on Progress in Physics,* vol. 50, p. 1657, 1987.

[24] J. Jackle, "ULTRASONIC ATTENUATION IN GLASSES AT LOW-TEMPERATURES," *Zeitschrift Fur Physik,* vol. 257, pp. 212-223, 1972.

[25] T. H. Metcalf, X. Liu, B. H. Houston, J. W. Baldwin, J. E. Butler, and T. Feygelson, "Low temperature internal friction in nanocrystalline diamond films," *Applied Physics Letters,* vol. 86, pp. 081910-3, 2005.

[26] C. Seoanez, F. Guinea, and A. H. C. Neto, "Dissipation due to two-level systems in nano-mechanical devices," *Epl,* vol. 78, p. 6, Jun 2007.

[27] M. Imboden and P. Mohanty, "Evidence of universality in the dynamical response of micromechanical diamond resonators at millikelvin temperatures," *Physical Review B (Condensed Matter and Materials Physics),* vol. 79, pp. 125424-5, 2009.

[28] S. S. Verbridge, D. F. Shapiro, H. G. Craighead, and J. M. Parpia, "Macroscopic tuning of nanomechanics: Substrate bending for reversible control of frequency and quality factor of nanostring resonators," *Nano Letters,* vol. 7, pp. 1728-1735, Jun 2007.

[29] L. Wei, P. K. Kuo, R. L. Thomas, T. R. Anthony, and W. F. Banholzer, "Thermal conductivity of isotopically modified single crystal diamond," *Physical Review Letters,* vol. 70, p. 3764, 1993.

[30] M. Shamsa, S. Ghosh, I. Calizo, V. Ralchenko, A. Popovich, and A. A. Balandin, "Thermal conductivity of nitrogenated ultrananocrystalline diamond films on silicon," *Journal of Applied Physics,* vol. 103, pp. 083538-8, 2008.

[31] V. P. Adiga, A. V. Sumant, S. Suresh, C. Gudeman, O. Auciello, J. A. Carlisle, and R. W. Carpick, "Mechanical stiffness and dissipation in ultrananocrystalline diamond microresonators," *Physical Review B (Condensed Matter and Materials Physics),* vol. 79, pp. 245403-8, 2009.

[32] F. Occelli, P. Loubeyre, and R. LeToullec, "Properties of diamond under hydrostatic pressures up to 140 GPa," *Nat Mater,* vol. 2, pp. 151-154, 2003.

[33] N. Sepulveda, D. M. Aslam, and J. P. Sullivan, "Polycrystalline Diamond RFMEMS Resonators with the Highest Quality Factors," in *Micro Electro Mechanical Systems, 2006. MEMS 2006 Istanbul. 19th IEEE International Conference on*, 2006, pp. 238-241.

[34] D. A. Czaplewski, J. P. Sullivan, T. A. Friedmann, and J. R. Wendt, "Mechanical dissipation at elevated temperatures in tetrahedral amorphous carbon oscillators," *Diamond and Related Materials,* vol. 15, pp. 309-312, 2006.

[35] M. Imboden, P. Mohanty, A. Gaidarzhy, J. Rankin, and B. W. Sheldon, "Scaling of dissipation in megahertz-range micromechanical diamond oscillators," *Applied Physics Letters,* vol. 90, p. 3, Apr 2007.

[36] L. Sekaric, J. M. Parpia, H. G. Craighead, T. Feygelson, B. H. Houston, and J. E. Butler, "Nanomechanical resonant structures in nanocrystalline diamond," *Applied Physics Letters,* vol. 81, pp. 4455-4457, 2002.

[37] F. W. Dong and et al., "Thermal treatments and gas adsorption influences on nanomechanics of ultra-thin silicon resonators for ultimate sensing," *Nanotechnology,* vol. 15, p. 1851, 2004.

[38] J. Yang, T. Ono, and M. Esashi, "Surface effects and high quality factors in ultrathin single-crystal silicon cantilevers," *Applied Physics Letters,* vol. 77, pp. 3860-3862, 2000.

[39] W. Jian, M. A. Firestone, O. Auciello, and J. A. Carlisle, "Surface functionalization of ultrananocrystalline diamond films by electrochemical reduction of aryldiazonium salts," *Langmuir,* vol. 20, pp. 11450-11456, Dec 2004.

[40] A. V. Sumant, D. S. Grierson, J. E. Gerbi, J. A. Carlisle, O. Auciello, and R. W. Carpick, "Surface chemistry and bonding configuration of ultrananocrystalline diamond surfaces and their effects on nanotribological properties," *Physical Review B (Condensed Matter and Materials Physics),* vol. 76, p. 235429, 2007.

[41] V. P. Adiga, A. V. Sumant, S. Suresh, C. Gudeman, O. Auciello, J. A. Carlisle, and R. W. Carpick, "Temperature dependence of mechanical stiffness and dissipation in ultrananocrystalline diamond," in *Micro- and Nanotechnology Sensors, Systems, and Applications*, Orlando, FL, USA, 2009, pp. 731818-9.

[42] A. D. Fefferman, R. O. Pohl, A. T. Zehnder, and J. M. Parpia, "Acoustic Properties of Amorphous Silica between 1 and 500 mK," *Physical Review Letters,* vol. 100, p. 195501, 2008.

[43] T. H. M. Xiao Liu and, "Microstructure dependence of low-temperature elastic properties in amorphous diamondlike carbon films," *Physical Review B,* vol. 71, p. 155419, 2005.

6. Conclusion:

We have demonstrated through this work that the elastic properties and mechanical dissipation in nanocrystalline diamond is significantly influenced by the nature of interfaces at grain boundaries. The results are important for application to high performance resonant mass sensors and high frequency RF-MEMS devices. A summary of the achievements of thesis is presented below.

6.1 Summary of results:

- *Development of instrumentation for the studies of nanomechanical properties:*

  An ultrahigh vacuum atomic force microscope was assembled and tested for normal mode operation of AFM and characterization of UNCD cantilevers. The instrument allows variable temperature operation and surface science analysis (High pressure XPS, Auger, LEED) of sample properties. We also developed a novel custom-built UHV AFM compatible stage for measuring the temperature dependent mechanical response of microcantilever beams.

- *Characterization of HFCVD-grown UNCD films and fabrication of UNCD devices:* Conformal uniform UNCD films were grown on 6" silicon wafers using the HFCVD technique at 680 °C by our collaborators Advanced Diamond Technologies, Inc. These medium temperature films represent an important step toward growing diamond at temperatures that are compatible with the important CMOS semiconductor process. These films exhibited a residual compressive stress of 370 MPa. The films show characteristic diamond features in NEXAFS

spectra with a very low fraction of sp^2 content (< 5%) at the surface. The films contained 1-1.5% hydrogen content in the bulk (measured by FRES). We designed and fabricated UNCD cantilever devices using conventional lithographic techniques. Fabrication of wafer scale devices shows the maturity of UNCD device fabrication methods.

- *Elastic properties of ultrananocrystalline diamond films:* The Young's modulus of the 680 °C HFCVD-grown UNCD films is measured to be 790 ± 30 GPa. This value is approximately 25-30% lower than the theoretically predicted value for the Young's modulus of randomly oriented polycrystalline diamond having much larger grains, and ~15% lower than the experimentally determined value for the Young's modulus of traditional UNCD films. However, it is significantly higher than values measured for metal-coated UNCD beams grown at lower temperature. Non-diamond imperfections in the carbon atom bonding disordered carbon, dangling bonds, hydrogen, and increased sp^2 bonding at the grain boundaries is the likely cause of the reduction in the modulus in UNCD films. The biaxial Young's modulus of the films was determined to be 838 ± 2 GPa by measuring the amplitude and wavelength of fully relaxed substrate-free overhangs of the compressively stressed films. Based on these measurements, the Poisson's ratio was estimated for the first time for any UNCD film to be 0.057 ± 0.038, which is comparable to that of single crystal diamond and, like single crystal diamond, is much lower than amorphous diamond like carbon films.

- *Temperature dependence of Young's modulus of UNCD films:* UNCD films have shown remarkable thermomechanical stability despite the presence of a large fraction of under-coordinated atoms, defects, and disorder at the grain boundaries. The temperature dependence of Young's modulus is slightly greater than that of single crystal diamond (averaged over all directions) but is much lower than that observed in microcrystalline diamond films, nanocrystalline diamond films, and tetrahedral amorphous carbon films and many other MEMS materials including SiN, Si, SiC and AlN. Reduction in modulus is less than 0.25% from 63 K to room temperature. This has important implications for resonator devices fabricated from UNCD, as they can have extremely stable resonant frequencies relative to changes in temperature. Understanding this temperature dependence requires understanding the nature and contribution of grain boundaries to the temperature dependence. MD simulations on temperature dependent mechanical response of the UNCD films will be helpful in this regard.

- *Dissipation in the ultrananocrystalline diamond resonators at room temperature:* Dissipation in UNCD cantilevers ranged from 2×10^{-4}–6×10^{-5} at ~kHz resonance frequencies. The UNCD cantilever resonators exhibited higher dissipation compared to PCD cantilevers with comparable resonant frequencies, but less dissipation than amorphous carbon cantilever resonators. By quantitative comparison to established and new models for various dissipation mechanisms, we attribute dissipation in the UNCD resonators mainly to the presence of defects including nondiamond bonding at grain boundaries, and surfaces.

- *Temperature dependence of mechanical dissipation:* Dissipation in UNCD reduced with temperature and reached a characteristic universal plateau below 160 K. A "universal" low temperature dissipation plateau ($10^{-4} < Q^{-1} < 10^{-3}$) has been observed before in amorphous solids, polymers, and crystals with significant fraction of defects. Ultrananocrystalline diamond, which has significant fraction of defects at the grain boundaries, yielded dissipation values similar to those observed in defective solids in the plateau region. This indicates the presence of two level tunneling states in UNCD which couple low frequency acoustic phonons to other modes. Dissipation measurements at extremely low temperatures (<1K) are necessary to further quantify the nature of these transitions. In recent years it has been discovered that residual stress in the films strongly influences measured quality factors in amorphous films. Stress either alters the distribution of the tunneling states or the energy with which they are coupled to the lattice. The influence of stress on dissipation in UNCD resonator devices will be helpful in achieving resonators with extremely high quality factors. Further studies should elucidate the nature of these transitions and influence of stress on these transitions.

6.2: Future directions

There are many unresolved issues in understanding the temperature dependence of mechanical properties and mechanical dissipation of nanocrystalline materials. While understanding the influence of grain boundaries on elastic properties and dissipation is crucial for achieving thermally stable, high frequency, high Q resonators, the physical

origin of the temperature-dependent mechanical softening and dissipation (which is possibly explained by the so-called “two level system” model) are still not clear. In fact, the lack of a clear model for the structural and dynamic features of the two level system model is a significant hindrance in further interpreting these results. In this regard, experiments aimed at manipulating the growth conditions to modify the grain boundary structure will be helpful and potentially highly useful for applications. This could involve growing UNCD films under different temperature and gas chemistry to alter the grain size, grain boundary structure and impurities. Structural and compositional characterization as well as temperature-dependent measurements of modulus and dissipation will help to determine the structure-property relationship. Similarly, determining the specific heat of the UNCD films as a function of temperature will help us to understand the temperature dependence of mechanical properties.

As mentioned earlier, theoretical modeling of the specific heat of this structure is being attempted using MD simulations. This will be helpful in understanding the structure and influence of disorder at grain boundaries. Understanding the dissipation of flexural or torsional modes of vibration of MEMS devices by the disorder in the materials is still a challenge. Extremely low temperature (<10K) measurements are necessary to understand the nature of the tunneling-based energy dissipation mechanisms fully. Similarly influencing the growth chemistry to achieve high residual tensile stresses and grain boundary structure is necessary to understand the nature of coupling between excitations (such as those postulated in the two level systems model) and lattice strain fields. Temperature-dependent measurements of dissipation of devices made from UNCD films grown under different conditions will therefore be useful to both understand these

tunneling processes and to achieve high quality factors in UNCD-based devices. The overall impact will be to put the science of dissipation in solids on a firmer and more deterministic foot that is based on known structural and dynamic properties, and to exploit this knowledge for the design and development of high performance micro- and nano-mechanical devices.